THE UNIVERSITY OF ADELAIDE

DEPARTMENT OF MECHANICAL ENGINEERING

A NEW LOOK AT THE DESCRIPTION OF REVERBERANT SPACES

submitted by

Pan Jie, B. Sc.(Hons)

Thesis for the Degree of Doctor of Philosophy

September 1988

Summary

The traditional description of the sound field in an enclosure begins with the assumption that the walls are locally reactive. This assumption allows a formalism which is intended to adequately predict the acoustical response of an enclosure. The work described in this thesis is concerned with a reconsideration of the classical description of the interaction between the sound field and its boundaries and with the effect of this interaction on the sound wave behavior in an enclosure. An experimental investigation in a standard reverberation room shows that the walls of the room are not locally reactive, and that the coupling between the room modes and the wall structural modes affects the reverberation times in the room. These results reveal a limitation of the locally reactive boundary assumption. They indicate that to understand the behavior of reverberant spaces, it is necessary to understand the nature of the modal interaction between the sound field and the wall vibration.

This research is an experimental and theoretical study of the characteristics of a panel-cavity system. The acoustical properties of the system at low frequencies, such as the resonance frequencies, decay times and mode shapes, are predicted by a modal coupling analysis. These predictions have been verified experimentally for conditions where the classical sound absorption theory does not apply. The effects of the boundary characteristics on the sound field are discussed in some detail.

The study is extended to higher frequencies in a reverberation room, where the very large number of cavity modes makes modal coupling analysis too difficult. In this frequency range, the modal coupling between a sound field and the panels still controls the acoustical behavior of the room. Acoustical decays are described in terms of average modal coupling, damping and density parameters using a Statistical Energy Analysis format.

Another extension of the research is to study the sound field behavior in an enclosure with a complicated boundary. A two dimensional Finite Element Method is used to calculate the resonance frequencies and shapes of cavity modes which have been altered by the presence of a semicircular diffuser. These results suggest that large variations in the cavity modal distribution caused by changing the diffuser orientation are responsible for the dependence of the boundary sound absorption upon the diffuser orientation.

Contents

Statement of Originality

This thesis contains no material which has been accepted for the award of any other degree or diploma in any University. To the best of the author's knowledge, this thesis contains no material previously published or written by another person, except where due reference is made in the text.

Pan Jie

September 21, 1988

Acknowledgements

I wish to express my sincere thanks and gratitude to my supervisor Dr. D.A. Bies for his constant encouragement and his original ideas for the opening of this research. I appreciate his hard work in the proof-reading of this thesis. He has become a good friend and by his guidance he has given me confidence and enjoyment in this project. His attitude to work and life will be taken as an example in my future life.

To the Departmental staff, thanks are due for their assistance in the preparation the experimental facilities used for this work, in particular to Don Kerr, Eric Browne, Ron Jager, Craig Price and Malcolm Bethune of the Engineering workshop and Herwig Bode and George Osborne of the Acoustical Laboratory.

Special thanks are due to my fellow post-graduate students in this Department and in the Applied Math Department for their comments in our discussions, and particularly to Peter Lanspeary for his help with my English and computer software and to Laurence Campbell for the use of his plotting package.

Thanks are due to my mother and sister for their patience and encouragement, to my friend Xu Zhuande for his constant care of my family in China and to J. Wang for her help with my computer programming.

I am indebted to my Chinese friends Mr. Zhong and Mr. Ding for their help with my work.

The work described in this thesis was carried out in the Department of Mechanical Engineering of the University of Adelaide under the aegis of Professor R.E. Luxton. The author is indebted to Professor Luxton for the opportunity to carry out this research and his interest in this work.

Finally, I acknowledge the financial support from the Chinese Ministry of Education for the first two years and the scholarship award of the Adelaide University Postgraduate Research Grants for the rest of the research.

List of symbols

A	total cavity internal surface
$< \bar{a}^2 >$	time and spatial averaged squared acceleration
A_f	panel surface
A_l	locally reactive surface
A_p	particle board panel surface area
$B_{M,N}$	coupling coefficient
$B(M,N)$	panel-cavity modal coupling factor
C_o	speed of sound in air
C_L	speed of longitudinal waves in panel
E	Young's modulus
E	total energy stored in a subsystem
E_A	sound energy in room
E_P	energy in panel
E_{aN}/E_{pN}	sound field to panel energy ratio of the Nth mode
f_i	resonance frequency of the ith acoustical mode, $= \frac{Im(\lambda_i)C_o}{2\pi}$
$f_{l,m}$	resonance frequency of a two dimensional cavity mode
$f_{l,m,n}$	resonance frequency of the rigid wall cavity mode
$F_{M,N}$	transfer factor
f_r	resonance frequency
$f_{u,v}$	resonance frequency of a simply supported panel mode
$f_{u,v}(0)$	resonace frequency of the panel mode (u,v) without sand
$f_{u,v}(s)$	resonace frequency of the panel mode (u,v) with sand
$G_A(\vec{r},\vec{r}_o,\omega)$	Green's function in the cavity
$G_P(\vec{x},\vec{x}_o,\omega)$	Green's function in the panel
h	panel thickness
$\vec{i},\vec{j}$	unit vectors in X and Y directions
I	unit matrix
$\bar{I}$	average sound intensity
k	wave number of the sound field, $= \frac{\omega}{C_o}$
k_{a1}	damping constant of an acoustical mode with panels, $= \frac{6.91}{T'_{60}}$

k_{a2}	damping constant of an acoustical mode without panels, $= \frac{6.91}{T_{60}}$
k_m	damping constant of a mode
k_p	average panel damping constant, $= \frac{6.91}{T_p}$
k_{aN}	cavity mode wave number, $= \frac{\omega_{aN}}{C_o}$
k_{pM}	panel mode "wave number", $= \frac{\omega_{pM}}{C_o}$
L, S, V	total edge length, surface area and volume of the room
L_x, L_y, L_z	length,width and hight of the room (cavity)
$\mathbf{L}, \mathbf{M}, \mathbf{S}$	coupling, inertial and stiffness matrices
$M(u, v)$	panel modal (or floor) index and indexes in X and Y directions
$M(v, w)$	back wall modal index and indexes in Y and Z directions
m_p	mass of piston
M_p	panel mass
n_A	cavity modal density
n_P	panel modal density
$N(l, m, n)$	cavity modal index and indexes in X, Y and Z directions
P	sound pressure
P	energy dissipated per radian cycle
P_A	sound power flow into boundaries
$< \bar{p}^2 >$	time and spatial averaged squared sound pressure
Q	quality factor, $= \frac{f_r T_{60}}{13.8}$
$\vec{r}, \vec{r}_o$	observation and source points in sound field
S_M	the Mth panel eigenfunction
T	room temperature
T_{60}	reverberation time of the empty room (without panels)
T'_{60}	reverberation time (with panels)
T_{i60}	decay time of the ith acoustical mode, $= \frac{6.91}{Re(\lambda_i) C_o}$
T_{m60}	60 dB modal decay time
T'_{m60}	60 dB modal decay time, with panel influence
T_{aN}	modal decay time of the Nth cavity mode
T_{pM}	modal decay time of the Mth panel mode
T_p	average reverberation time of the panel
$\vec{V}$	air particle velocity

W	panel displacement
W_N	panel displacement of the Nth acoustical mode
$\vec{x}, \vec{x}_o$	observation and source points on panel
Z_A	specific acoustical impedance
Z_{apN}	specific acoustical transfer impedance of the Nth acoustical mode
α	sound absorption coefficient
α_{Sab}	Sabine absorption coefficient
β	specific acoustic admittance ratio, $= \frac{\rho_o C_o}{Z_A}$
$\delta(\vec{r} - \vec{r}_o)$	Dirac delta function for sound field
$\delta(\vec{x} - \vec{x}_o)$	Dirac delta function for panel vibration
Δf_{3dB}	half power frequency band
Δ_N^{Pd}	panel internal damping term for the Nth eigenvalue
Δ_N^{Pr}	radiation term for the Nth eigenvalue
$\Delta\omega_{aN}$	the Nth cavity modal bandwidth
$\Delta\omega_{pM}$	the Mth panel modal bandwidth
ζ_m	damping factor of a mode
ζ_{aN}	damping factor of the Nth cavity mode, $= 6.91/C_o T_{aN}$
ζ_{pM}	damping factor of the Mth panel mode, $= 6.91/C_o T_{pM}$
η	loss factor, $= \frac{13.8}{\omega T_{60}}$
η_A	loss factor of the room
η_P	loss factor of the panel
η_{AP}	coupling loss factor from room to panel
η_{PA}	coupling loss factor from panel to room
θ	diffuser orientation
λ	eigenvalue of the coupled system, $=-ik$
Λ_N	normalizing factor of the cavity mode
Λ_M	normalizing factor of the panel mode
μ	poission's ratio
ξ	eigenvalue of the coupled system
ξ_N	eigenvalue of the Nth cavity controlled mode
ξ_M	eigenvalue of the Mth panel controlled mode
ρ_o	air density

ρ	panel density
σ_{Rad}	panel radiation efficiency
$\sigma_{Re}(M,N)$	radiation efficiency of the Mth panel mode
$\sigma_{Im}(M,N)$	virtual mass term of the Mth panel mode
Φ_N	cavity eigenfunction
Ψ	acoustical velocity potential in the cavity
Ψ_N	acoustical velocity potential of the Nth acoustical mode
Ψ_E	acoustical velocity potential outside the cavity
ω_{aN}	angular resonance frequency of the Nth cavity mode
ω_{pM}	angular resonance frequency of the Mth panel mode
ω	angular frequency

All physical quantities in this thesis are expressed in SI (MKS) units.

List of Figures

List of Tables

Chapter 1

General introduction

1.1 Introduction

The traditional description of the sound field in an enclosure begins with the assumption that the walls are locally reactive and that they may be characterised by a normal acoustical impedance (Morse 1939). This assumption allows the introduction of sound absorption coefficients and a formalism which is intended to predict adequately the acoustical response of an enclosure. The assumption of locally reactive walls and the concepts which follow from it have been applied to architectural acoustics, apparently without question, for several decades. The theoretical principles arising from this assumption have been used for room acoustical design and have provided a conceptual framework for studying the transient and steady-state behavior of sound waves in an enclosure (Morse and Bolt 1944).

Describing the boundaries of a cavity as locally reactive is a satisfactory approximation only in some cases, however the interiors of aircraft and motor vehicles are examples where this description is useless. Even in a standard reverberation room, the locally reactive assumption for the wall surfaces can be violated (Munro 1982, Pan and Bies 1988). In the latter case the interaction between the sound field in the room and the wall structure is shown to depend upon modal coupling. This modal coupling has been recognized and used in the heuristic design of theatres (Beranek *et al.* 1964 and Bliven 1976), but when observed in laboratory measurements, this modal coupling has often been regarded as an irritation to be suppressed (Bhatt 1939, Hunt 1939b and Knudsen *et al.* 1967).

Where modal coupling exists, the sound wave behavior cannot be predicted by using the locally reactive boundary assumption. In this case it is necessary to take account of the fluid-structural coupling when formulating the boundary conditions of the sound field. Since the sound wave behavior is directly related to the nature of the interaction between the sound field and its boundaries, it is necessary to explore whether this behavior can be significantly altered by this coupling, and if so, what useful information can be obtained from a study of it.

In discussion of the mode coupling problem in the following Chapters, the terminology "fluid-structural coupling" is used to describe the modal interaction between a sound field and its boundary structures. The sound field and the structural (i.e. test panel) vibration resulting from this coupling are described by acoustical modes. An acoustical mode is a mode of the entire panel-cavity system. An acoustical mode can be interpreted as the result of combining the uncoupled cavity modes (called "cavity modes") and the uncoupled panel modes (called "panel modes").

If we measure the relative amounts of energy contained in the two parts of the acoustical mode (i.e. in the cavity sound field and in the panel vibration), we can identify two types of acoustical modes as either "cavity controlled" or "panel controlled". A cavity controlled mode has most of its energy stored in the cavity sound field, while a panel controlled mode has most of its energy stored as panel vibrational energy.

In following Chapters, the decay behavior of the sound field and structural vibration is the major item of interest. The decay behavior can be expressed in a number of different ways. The expression to be chosen in any particular case is determined almost entirely by conceptual convenience. However, all of these expressions are directly interrelated. The most often used quantity is *decay time*, which is defined as the time required for the sound pressure or panel acceleration to decay by 60 dB after an excitation is removed. For a single mode, such as a cavity, panel or acoustical mode, the decay time is called *modal decay time* (T_{m60}), or *60 dB modal decay time.* When the excitation is over a band of frequencies, the term *reverberation time* (T_{60}) is used.

Quality factor Q, damping factor ζ_m and damping constant k_m provide alternative descriptions of the decay behavior of a single mode. They are related to the modal decay time

by,

$$Q = \frac{f_r T_{m60}}{13.8}, \tag{1.1}$$

$$\zeta_m = \frac{6.91}{C_o T_{m60}}, \tag{1.2}$$

$$k_m = \frac{6.91}{T_{m60}}, \tag{1.3}$$

where f_r is the resonance frequency and C_o is the speed of sound in air.

Similarly, loss factor η can be used to describe the average damping of the sound field or the panel vibration (over a frequency band) ;

$$\eta = \frac{13.8}{\omega T_{60}}. \tag{1.4}$$

The contribution of modal coupling to sound field absorption in an enclosure is strongly dependent upon the coupling parameters (e.g. coupling coefficients, panel modal density, panel internal damping and radiation loss). As will be shown, the classical room acoustics problem is closely related to previous research in the field of fluid-structural coupling. The results from this latter research provide a sound starting point for the work presented here. In return, the results presented here from this investigation into room acoustics can also improve the understanding of the coupling mechanism.

The modal coupling between a sound field and its boundaries will also affect the room acoustical behavior at middle and high frequencies. However participation of large numbers of coupled modes in these frequency ranges suggests that a statistical description of the coupling should be used, and the effect of coupling on the average sound wave behavior must be considered. Using Statistical Energy Analysis (SEA), a simple average description can be obtained for a sound field with an extensively reactive boundary. The sound field decay and the decay of structural vibration can be derived from a few SEA parameters. This analysis clarifies the physical meaning of the measured sound absorption coefficient of an extensively reactive panel.

When a semi-circular diffuser is present in a rectangular cavity, the complicated boundaries of the sound field distort the mode shapes and the resonance frequencies from

those predicted and measured in the cavity without the diffuser. The modal properties of the sound field in the cavity are calculated as a function of diffuser orientation. As will be shown, large variations in the cavity modal distribution caused by changing the diffuser orientation are responsible for the dependence of the boundary sound absorption upon the diffuser orientation.

1.2 Objectives

The objectives of this thesis are as follows:

1. Investigate the adequacy of the locally reactive assumption and the alternative modal coupling assumption. Show that the modal coupling model properly describes the interaction between a sound field in a reverberation room and the walls, and that the locally reactive description is inadequate.

2. Describe the sound wave behavior in a simple and representative model of the panel-cavity system. Show that the acoustical properties of the individual modes can be predicted from the fundamental parameters of the panel and the cavity.

3. Consider the effect of fluid-structural coupling on the acoustical decays in a reverberation room in the high frequency range where the mode by mode method, which is suitable for the low frequency analysis, is inadequate. Verify both theoretically and experimentally a description for the average behavior of the coupled system.

4. Estimate the effect of a semi-circular diffuser on the sound waves in a room. Evaluate the influence of irregularity in the cavity shape on the sound field behavior. Show a possible numerical interpretation for the dependence of the sound absorption of panels upon orientation of a diffuser.

1.3 Layout of the thesis

Chapter 2 begins with some quantitative experimental evidence which suggests that the mechanism of the interaction between the sound field and its boundaries should be re-examined.

This evidence suggests the criteria which should be satisfied by a solution for the sound field and boundary response when the interaction between them is not locally reactive.

In Chapter 3, a coupled panel cavity system is chosen as an analytical model for the interaction between a sound field and its boundaries. A theoretical investigation into the effect of this interaction upon the characteristics of the sound waves in an enclosure is presented. This analysis is presented as a fluid-structural coupling problem. When this approach is taken, the long established knowledge of coupling suddenly becomes useful in the prediction of the acoustical decay in an enclosure. In return, some of the results clarify the nature of the coupling mechanism.

Chapter 4 provides a description of experimental arrangements. In this chapter, the acoustical properties of individual normal modes in a rectangular panel-cavity system are investigated experimentally. These experiments verify the earlier predictions of Chapter 3.

The effect of the fluid-structural coupling on acoustical decays is reviewed in Chapter 5 for the high frequency range. Quasi-transient Statistical Energy Analysis (SEA) solutions are used for the calculation of the reverberation time in a reverberation room containing test panels.

Chapter 6 deals with the influence of a semi-circular diffuser on the sound field in a rectangular room. Response for an essentially two dimensional room is calculated by a two dimensional Finite Element Method. Experimental verification is provided for the calculation in a three dimensional cavity in which the influence of the third dimension is suppressed by design.

Where appropriate, each Chapter contains its own literature review and conclusions. The scope for future work is also discussed independently in each Chapter.

Chapter 2

The interaction between a sound field and its boundaries

2.1 Introduction

The nature of the interaction between a sound field in a reverberation room and its boundaries is fundamental in the study of room acoustics. Both the steady state distribution and the transient behavior of the sound field in an enclosure depend upon the sound reflection and absorption at the boundaries, but the sound reflection and absorption are actually controlled by this interaction and cannot be separately defined except as a crude approximation.

In geometrical acoustics based on the diffuse sound field assumption, this interaction is described by the concept of the sound absorption coefficient. This coefficient α is defined as the average ratio of absorbed sound energy to incident sound energy at the boundary surfaces. Physically, it represents part of the mechanism of sound energy exchange over the boundaries.

Sabine (1922) first employed this concept in his empirical development of reverberation theory. The well-known Sabine formula

$$T_{60} = \frac{0.161V}{\alpha_{Sab}S} \tag{2.1}$$

provides a relationship between the Sabine absorption coefficient α_{Sab} of the boundaries and the reverberation time T_{60} of a room, where V and S are the total volume and surface area of the room. The reverberation time is the time interval taken for the sound pressure level to

decrease 60 dB from a steady state level. Sabine absorption coefficient is laboratory measured. The differences between α and α_{Sab} have long been the topic of discussion (Embleton 1971) and they are equal when the incident sound field is diffuse. Although many modifications of the Sabine formula have been made (Eyring 1930 and Millington 1932), the basic relationship has always been used as a guide in architectural acoustic design.

As the laboratory equipment used in acoustical measurements has been gradually improved, it has become apparent that in many enclosures, large discrepancies exist between the predictions of the Sabine formula and the experimental measurements and efforts were made to explain them (Morris *et al.* 1938, Norris 1932 and Hunt 1939b). The main results of the efforts were to show that the Sabine formula and the related concept of sound absorption coefficient are only meaningful when the sound field is diffuse. They also showed that a detailed physical picture can only be obtained by taking the wave nature of sound into account.

The concept of specific acoustic impedance Z_A is traditionally introduced to assist understanding of sound wave behavior in a room. The boundaries are described in terms of this normal specific acoustic impedance which is defined as the complex ratio of the sound pressure to the normal particle velocity at the surface of the boundary. This normal velocity may be due to induced motion of the boundary or to motion of air into pores in the boundary (Morse and Bolt 1944).

Morse and Ingard (1968) considered the possible response of a boundary surface to sound pressure excitation, and classified surfaces according to their response either as locally reactive surfaces or as surfaces of extended reaction. The locally reactive surface is defined as one for which, on each portion of the surface, the response is only dependent on the local sound pressure and is independent of the response at any other part of the boundary. When the parts of the surface are coupled together, (i.e. when the surface behavior at one point not only depends upon the local sound pressure, but also upon the motion of the coupled parts), this surface is defined as a surface of extended reaction.

A surface of extended reaction may be changed to have the approximate behavior of a locally reactive surface if some physical characteristic of the boundary is suitably altered. For example, a thin panel is generally best described as a surface of extended reaction. However, the spatial correlation between different parts of a panel decreases as the damping of the panel increases (Vyalyshev *et al.* 1977) and the panel response then tends to that of a locally reactive

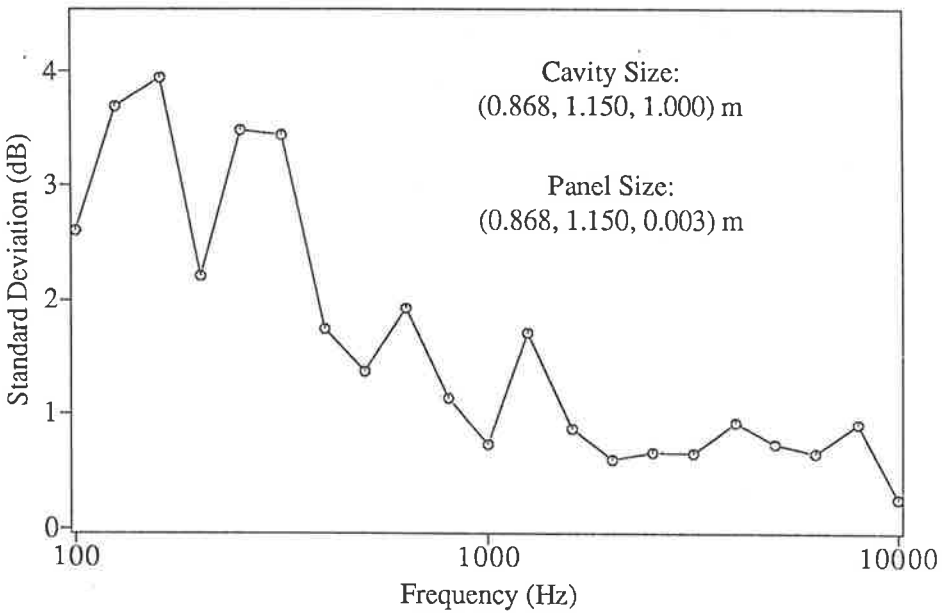

Figure 2.1: Standard deviation of panel acceleration level.

surface.

In another example, the response of a panel tends to uniformity as the driving sound field tends to be more and more diffuse. Experimental investigation of a panel-cavity system shows that the average variation of the panel vibration decreases as the sound field frequency increases, and the acoustic field tends to complete diffusivity. In consequence, the panel vibration is proportional to sound pressure at high frequencies and the panel may be approximated as locally reactive. To illustrate this point, the standard deviation of the measured acceleration level at a panel surface (of a panel-cavity system) is shown in Figure 2.1, against the driving frequency of the sound field in the cavity. The panel-cavity system will be described in Chapter 4.

As a further example, if a layer of sound absorptive material is placed upon the surface of a rigid wall, the material's acoustic impedance may be dependent upon the angle of the incidence of the sound wave. Usually this sort of surface can be described by two sound velocities, one being for sound traveling tangential to the surface through the material, while the other is for sound traveling normal to the surface (Morse 1939). When the tangential velocity is much smaller than the speed of sound in air, the boundary can be described by a normal specific acoustic impedance, independent of the angle of the incident waves.

In the development of the wave theory of room acoustics, many workers have been involved in pioneering research since 1930's. The paper by Morse and Bolt (1944) provides an excellent review of the history of room acoustics. In this introduction, only the immediately relevant works will be mentioned.

To investigate the wave behavior of sound in an enclosure, Morse obtained a solution for a sound field in a rectangular room by solving the sound wave equation (Morse 1939, Morse and Bolt 1944). For his solution, each wall was assumed to be uniformly covered with sound absorptive material and the normal specific acoustic impedance of the material was assumed independent of the incidence angle of the sound waves. Morse introduced the locally reactive assumption and used it to define his boundary conditions.

There are probably two justifications for Morse's assumptions. Firstly, at the time of his investigation most available sound absorptive materials were well described as locally reactive, although not many materials had been tested. In many practical cases, the walls of enclosures were covered by such materials. In addition there was a reliable experimental method by which to measure the normal specific acoustic impedance of materials. Secondly, when the boundaries are not rigid, the solution of the eigenvalue problem of a sound field in a reverberant enclosure, is very difficult. Even for the uniform locally reactive surface, which may be the simplest case besides that of the rigid boundary condition, the analysis is so complicated that the general physical picture is often lost among the obtruding details.

From the assumption of locally reactive boundaries, a quantitative relationship has been established between the normal acoustic impedance of the boundaries and the modal decay rates of the sound field in a rectangular room. One of the interesting results from Morse's solution is that the acoustic modes in a rectangular room can be classified into seven groups. Three groups are axial modes, three are tangential modes and one group is oblique modes. If the impedance of the boundaries varies little over the frequency range of interest, then every mode in a given group should decay at the same rate.

Since Morse's solution, it has become clear that the acoustical absorption coefficient has no meaning if the sound field is not diffuse. Alternatively when the sound field is diffuse, the acoustical absorption coefficient can be written as a function of local acoustical impedance and has meaning (Morse 1948a). The vital difference is the diffusivity of the sound field.

Morse's solution was verified by Bhatt's experimental investigation into the decay

properties of acoustic modes in a room (1939). The normal acoustic impedance of absorbing materials on a wall was calculated by measuring the resonant response and the modal decay rates of the room, and using Morse's theoretical solution. These results were compared with the measurements by the standing wave tube method. Since then Morse's solution has been used to predict the decay rates in rooms where the Sabine formula is not valid, and where the sound absorption coefficient loses its meaning. It is also regularly taken as a starting point for further investigation (Bodlund 1980 and Jacobsen 1982). For example, it has been used as the explanation of the discrepancies between the Sabine formula prediction and the experimental measurements and so on, without question. However, Morse's solution can only be used when the boundaries of the room are locally reactive. Therefore, before this solution can be used, this boundary condition should be verified.

Munro (1982) examined two theoretical models for predicting the decay rate of individual modes. The first was Morse's solution for a very lightly damped room. The second was based on a combination of the modal approach and the ray tracing approach as applied to a rectangular room. Both models relied upon the assumptions that the walls can be accurately modelled as locally reactive and that the wall impedance can be modelled as constant over the wall surfaces and slowly varying throughout the frequency range investigated. The resonance frequencies and modal decay rates of the sound field in a reverberation room were measured for comparison with each model. It was shown that neither model accurately predicts the relative rates of decay of the measured modes. For example, where the measured modal decay times were expected to be constant within each group, in fact they varied substantially. Large differences in the measured decay times were observed in every group. The calculated values of the decay time from Munro's second model varied by as much as a factor of eight from the measured values. The most probable reason for the failure of the models to predict the modal decay rate is that the locally reactive assumption is not satisfied in the reverberation room used in Munro's experiments although the latter room was constructed according to accepted standards.

The remainder of this Chapter reviews experimental evidence which shows that the walls of the reverberation room used by Munro are not locally reactive. In this room, typical of such reverberation rooms, modal coupling determines the interaction between the sound field in the room and vibration of the walls. The coupling between the room modes and the wall structural modes affects the reverberation time in the room at low frequencies.

2.2 The reverberation room

The test facility, used by Munro and in most of the experiments to be discussed, was a rectangular parallelopiped room with inside dimensions of 6.84 m length, 5.57 m width and 4.72 m height as illustrated in Figure 2.2.

The acoustic modes in the room are described by mode (l, m, n), where l, m and n are integers indicating the number of nodes in the pressure field in X, Y and Z directions respectively. The room is supported on soft springs and is otherwise structurally isolated from the surrounding building. The steel reinforced concrete walls (including the floor and ceiling) are 0.280 m thick.

A rotating diffuser is mounted in the ceiling of the reverberation room on a vertical shaft. It consists of a counter balanced aluminum semi-circular cylinder of 3.5 m diameter and 2.4 m height. The definition of the orientation of the diffuser can be found in Figure 2.3.

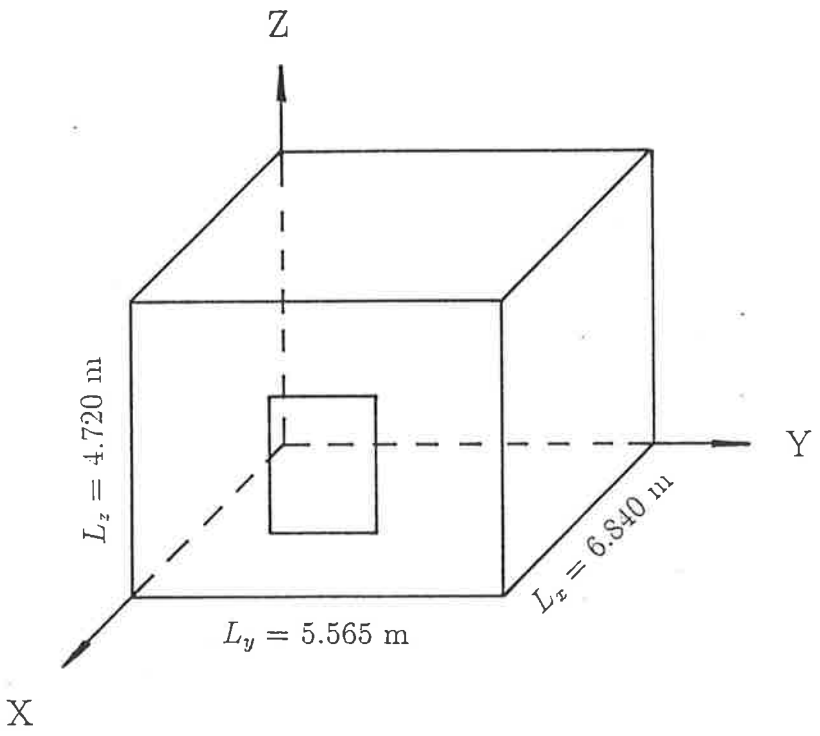

Figure 2.2: The inside surfaces of the reverberation room.

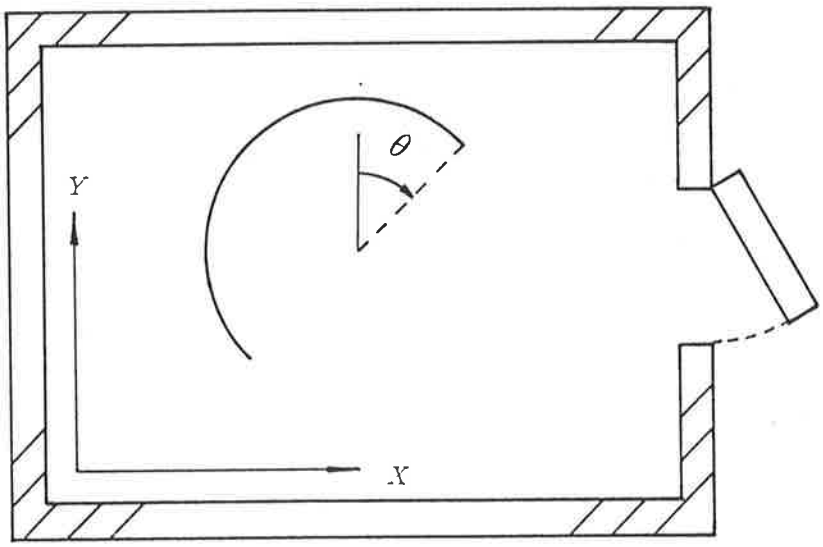

Figure 2.3: A plan view of the diffuser in the reverberation room.

2.3 Measurement of standing wave patterns in the floor

The frequency responses of the floor to the excitation of an electrical shaker were obtained by measuring the vibration spectrum from the output of an accelerometer at various points on the floor. Although the spectra, as shown in Figure 2.4, depend on the positions of the shaker and the accelerometer, as well as the damping of the floor, the modal response of the floor is easily recognized by the peaks in the spectra.

Standing wave patterns in the floor corresponding to peak frequencies in a spectrum were readily identified by measuring the phase difference between selected points and changes in amplitude of response, since on either side of a nodal line of a standing wave the phase of the vibration amplitude will differ by 180 degrees and the amplitude will decrease to a minimum at the node.

The first few resonant modes of the floor were identified as shown in Table 2.1. The modal shapes are similar to those of a simply supported rectangular panel.

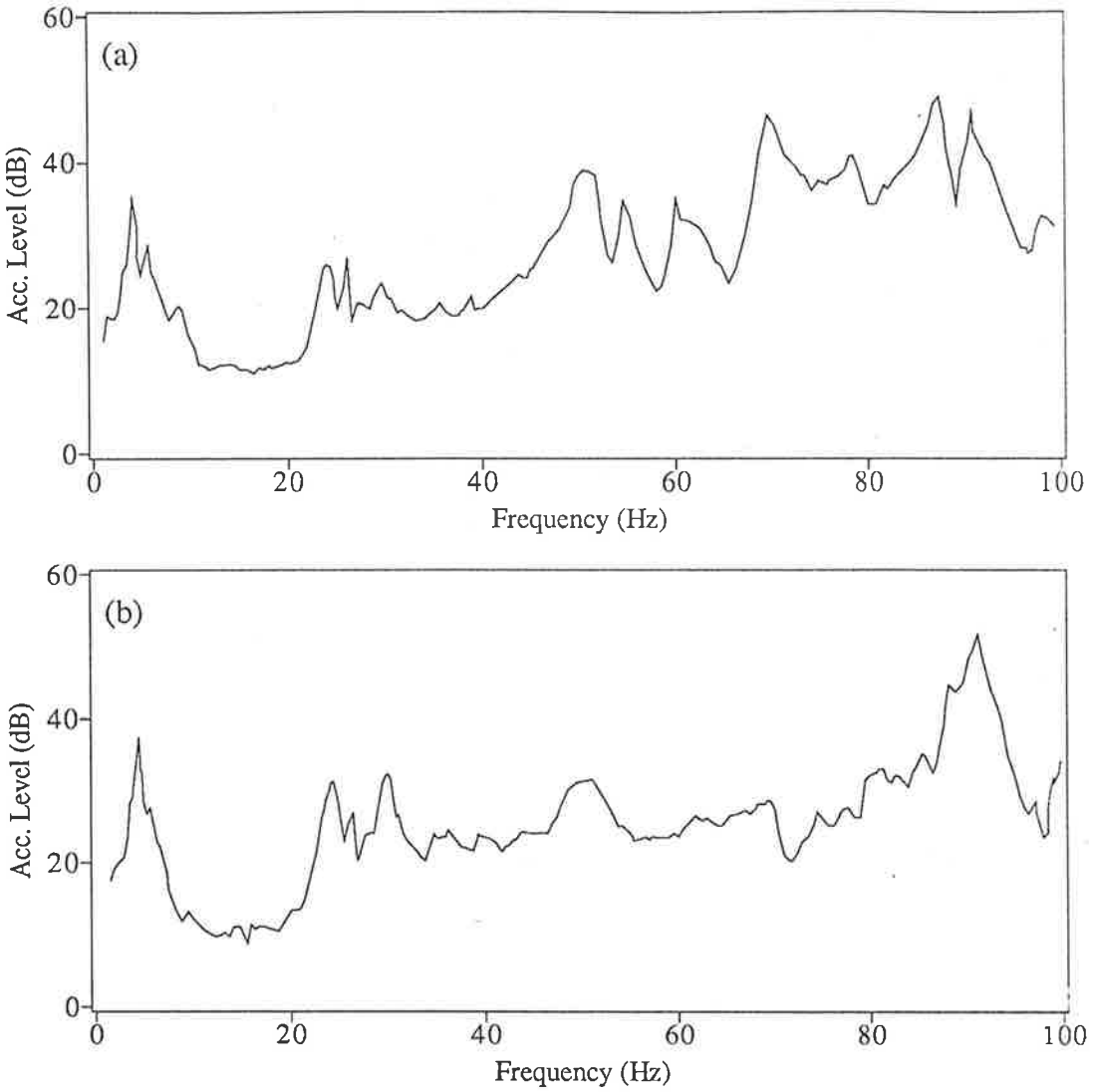

Figure 2:4: Frequency response of the floor to shaker excitation, accelerometer located at (X, Y) = (5.13 m, 1.39 m); (a) shaker at (X, Y) = (1.71 m, 4.08 m); (b) shaker at the centre of the floor.

Table 2.1: First few modes in the floor of a reverberation room

mode(u, v)	1,1	2,1	1,2	3,1
$f_{u,v}$ (Hz)	30.	52.	71.	91.

Using the same method, the standing wave patterns of the back wall were also identified. The floor modes are described by mode(u, v), where u and v are integers indicating the number of displacement antinodes in X and Y directions. In the case of the back wall, the modes can be represented as mode(v, w) where v and w are integers indicating the number of the antinodes in Y and Z directions.

The identification of the modal characteristics of the wall structure of the room shows that the walls of the reverberation room are not locally reactive boundaries, though the steel reinforced concrete walls are very massive. Similar to any other structures, the response of the walls is not only determined by the forces acting on the wall surfaces but also by their own resonances and mode shapes. Those modal properties of the walls can be determined by a wave equation, which describes the relationship between the motion of one part of the wall and the motion of any other part of the wall, and the edge boundary conditions. Consequently, those parameters which describe the global character of the walls, such as the dimensions, mechanical damping and the sound velocity in the walls, become more important than the local details of the boundary materials.

2.4 The coupling between room and structural modes

Since the walls of the reverberation room are extensively reactive, their modal behavior should be displayed when they are exposed to a sound field. The next experiments demonstrate this.

The steady-state response of the sound field in a reverberation room to a sound source can be considered as a collection of acoustical modes vibrating at the frequency of the source. At low frequencies, the resonance frequencies of the modes are often well separated. If the frequency of a well placed source in the room matches the resonance frequency of an acoustic mode, the sound field will be dominated by this mode. Therefore, this acoustic mode may be studied in some detail, although the near sound field effect of the sound source, the damping and nearby acoustic modes may distort the mode slightly from the eigenmode which is theoretically predicted by neglecting such perturbations.

Experimentally, an room mode was generated by a loudspeaker placed at a corner of the room and driven at the modal resonance frequency. The sound field distribution near the

surface of the boundaries was determined by using a sound level meter to measure the sound pressure level at the surface. The same method, as used in the investigation of section 2.3 was used to measure the responses of the floor and walls.

Three kinds of coupling mechanisms of sound field and floor have been identified. The first coupling mechanism (Figure 2.5) is the result of interaction of one room mode and one floor mode.

The second coupling mechanism (Figure 2.6) is due to interaction between one room mode and a vibration pattern of the floor which is the combination of two fundamental floor modes.

The third coupling mechanism (Figure 2.7) is the result of one room mode which excites a distorted vibration pattern in the floor, which cannot be regarded as the combination of a few fundamental modes of the floor. Since the floor is not really a simply supported panel, it is actually supported by springs, the floor may vibrate like a piston so that the vibration of the edges is non-zero. Moreover, the coupling between the floor and the side walls sometimes cannot be neglected. These observations may provide explanations for the third case.

The distribution of the sound field on the surface of the floor and the floor acceleration response were also measured quantitatively. The sound pressure level and the phase difference between the measuring microphone signal and the output of a reference microphone were measured at the points formed by a uniform 11×11 rectangular grid covering the whole floor. This procedure was repeated but with the microphone being replaced by an accelerometer which was fixed to the floor at the grid points. The distributions of the sound pressure level and the relative phase (which are plotted in Figure 2.8) are close to those of the (2,1,1) mode. In this measurement, the loudspeaker and reference microphone were located at $(X, Y, Z) =$ (6.84, 5.57, 0.00) m and the room was driven at the frequency of 69.01 Hz. The diffuser was at 180^o. The distributions of the acceleration level and relative phase in the floor (as shown in Figure 2.9) are close to those of the (1,2) mode.

The identification of the coupling models shows that the interaction between the distributed sound field and the extensively reactive walls is by modal coupling. The complexity of this interaction shows that it is not suitable to determine the vibration of the walls by a uniformly distributed locally reactive specific acoustic impedance.

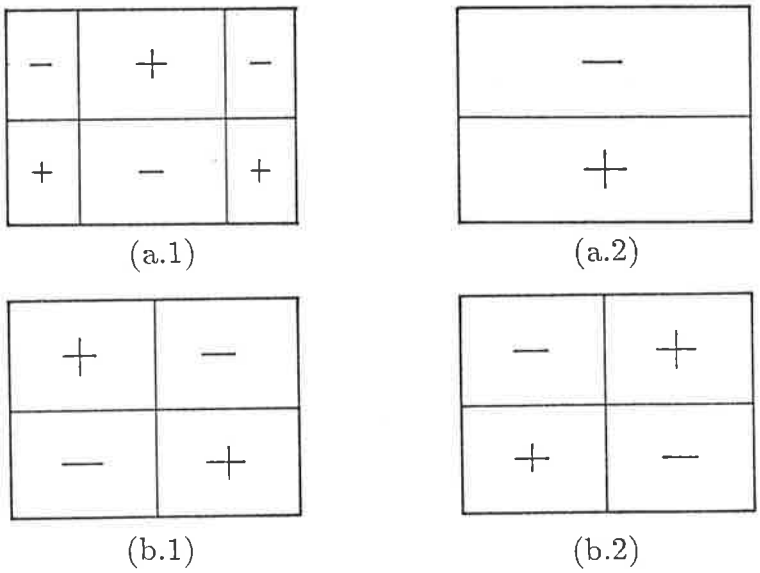

Figure 2.5: A room mode coupling with a floor mode. (a.1) room mode (2,1,1); ($f_{2,1,1}$ = 69.09 Hz,θ = 210°); (a.2) induced floor mode (1,2); (b.1) room mode (1,1,1); ($f_{1,1,1}$ = 53.49 Hz, θ = 0°); (b.2) induced floor mode (2,2).

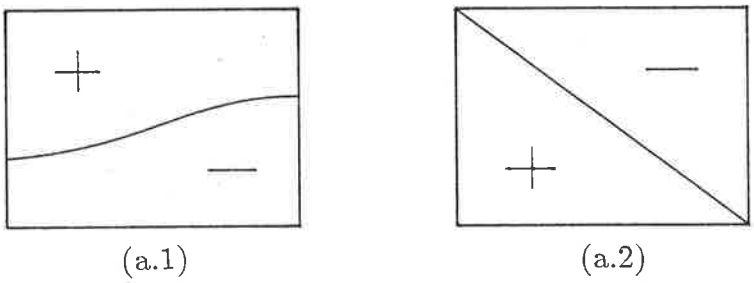

Figure 2.6: A room mode coupling with two floor modes. (a.1) room mode (0,1,1), ($f_{0,1,1}$ = 47.33 Hz, θ = 0°) (a.2) floor response ((2,1) mode and (1,2) mode combination).

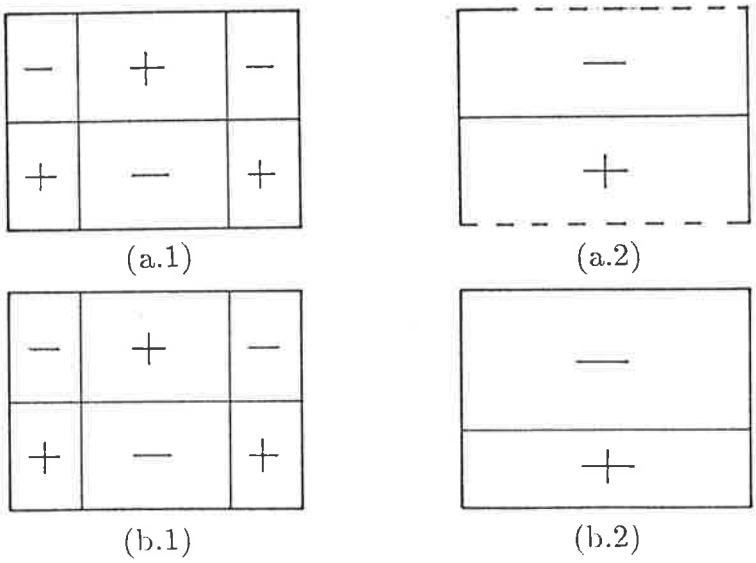

Figure 2.7: A room mode coupling with an unidentified floor mode. (a.1) room mode (2,1,0), ($f_{2,1,0}$ = 58.69 Hz, θ = 0°); (a.2) corresponding floor response, A dashed line on a boundary indicates that the acceleration at that boundary is not zero; (b.1) room mode (2,1,1); ($f_{2,1,1}$ = 69.01 Hz, θ = 60°); (b.2) corresponding floor response.

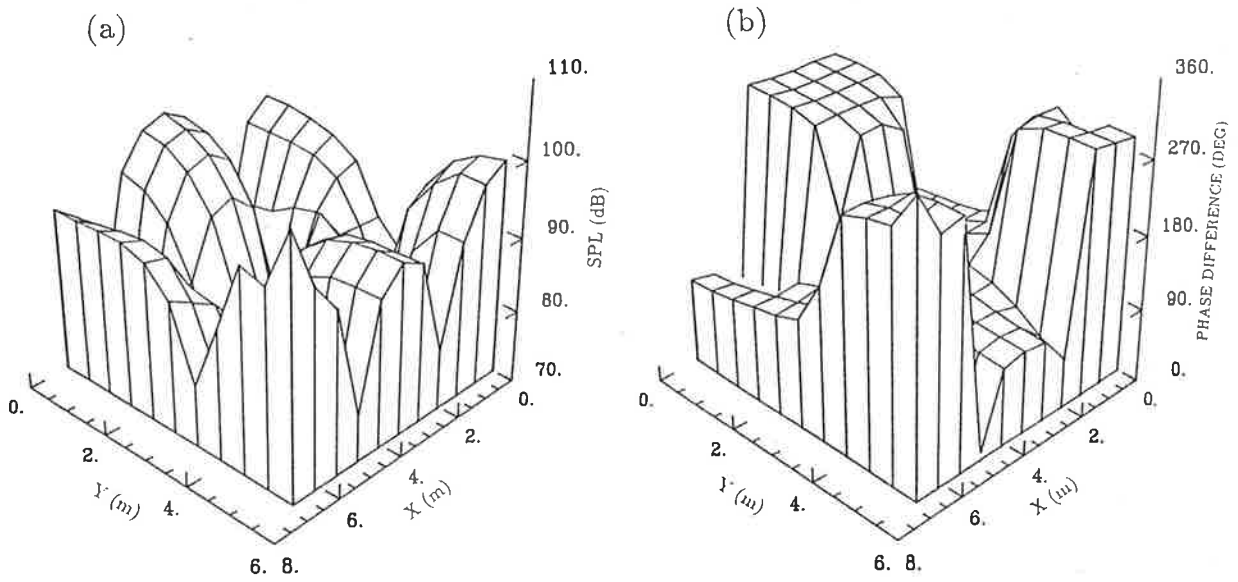

Figure 2.8: Sound field distribution on the floor. (a) Measured sound pressure level (the driving frequency is 69.01 Hz); (b) Phase difference between the outputs of the measuring microphone and a reference microphone near the loudspeaker.

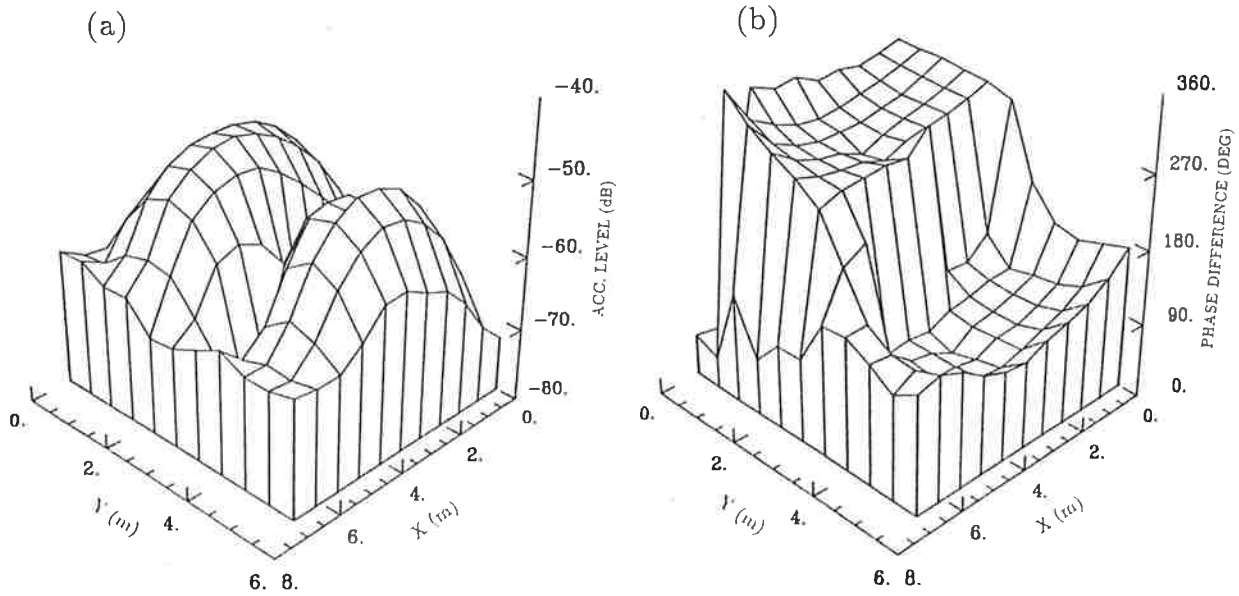

Figure 2.9: Distribution of floor acceleration. (a) Measured floor acceleration level re. 1 g (g = 9.8 m/s^2); (b) Phase difference between the outputs of the measuring accelerometer and a reference microphone near the loudspeaker.

2.5 Extensively reactive acoustic impedance

The normal impedance at a point on a surface of extended reaction can not be uniquely defined, because the induced velocity response will not only depend upon the local sound pressure, but also upon the total distribution of the sound pressure forcing field over the entire surface. As an example, an electro-magnetic driver was used to drive a simply supported aluminum panel (0.8 m in length, 0.5 m in width and 0.001 m in thickness) and the frequency response at the driving point was measured while the voltage across the magnet was kept constant. For comparison another magnet was placed at a second position. A large variation in the measured response was observed at the first position when the second force was applied to the panel.

A panel vibration damper, as illustrated in Figure 2.10 was constructed using a set of rubber capped screws mounted on a steel frame. By increasing the tension between the screws and the surface of the panel, large damping can be achieved near the attachment points, so that the vibration of the panel may be reduced.

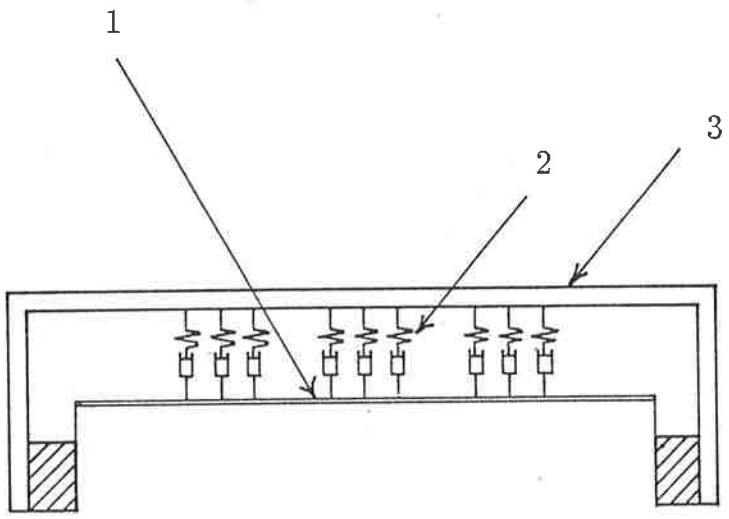

Figure 2.10: Panel vibration damper. The panel dimensions are $L_x = 0.8$ m and $L_y = 0.5$ m. 1. simply supported panel; 2. rubber capped screw; 3. steel frame.

It is found that when the panel is driven only by a point force, the average vibration at certain frequencies can be greatly reduced by the vibration damper (Figure 2.11). However, if the driving force is distributed, as provided by a sound field when the panel is tested in a reverberation room, the average vibration level over the panel will show less change no matter what the damping and whether the damper is present or not (Figure 2.11).

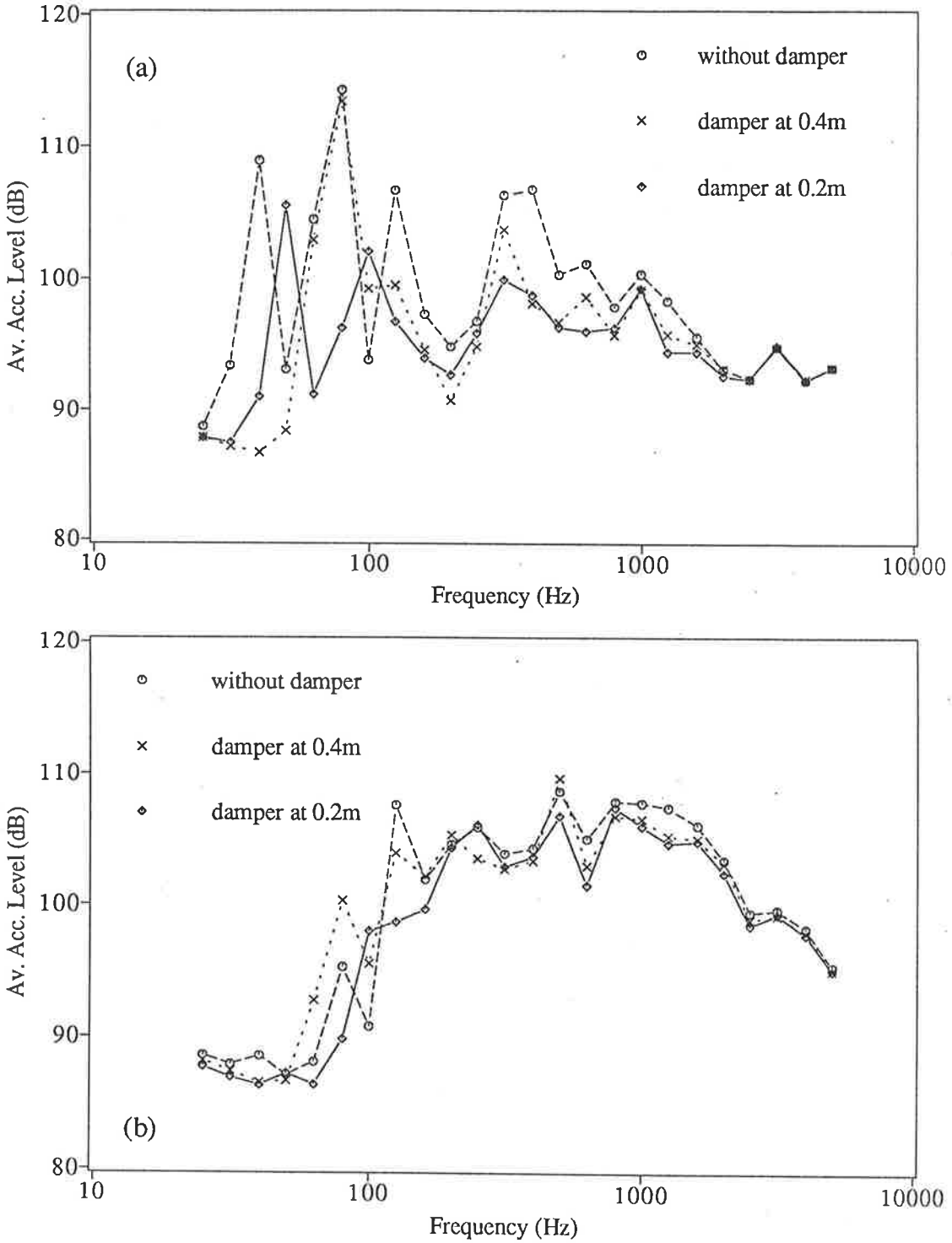

Figure 2.11: Average acceleration level of panel. (a) excited by magnetic driver; (b) exposed to a reverberant field. The damper is located at two different distances ($x = 0.2$m & $x = 0.4$m) from the side of the panel.

The following interpretation of the experiment is offered. For a point force, there is always some critical position of the damper which will make the driving point impedance very large so that little energy can be transmitted into the panel. However, if the panel is submerged in a sound field there is no position for the damper which ensures that the impedance at every point of the surface is very large. The distributed force of the sound field can always find places to inject energy at the panel surface where the acoustic impedance is not large and thus the panel vibration level is less affected by the presence of the damper.

The complexity of the extensively reactive surface shows that it is not possible to find a simple quantity such as the normal specific acoustic impedance for a locally reactive surface to describe an extensively reactive boundary. To find the acoustic impedance of a surface of extended reaction, the sound pressure distribution on the surface and the vibration distribution of the boundary must be determined before hand by considering their modal coupling. However, the purpose of employing the acoustic impedance is to enable estimation of the sound field distribution and the response of the boundaries. It is not necessary to calculate the acoustic impedance if information about the sound field and the boundaries is known. Therefore it is felt that a suitable description of the interaction between a sound field and its boundaries must be in terms of modal coupling when the boundaries are extensively reactive.

2.6 Effect of the modal coupling on decay rate of acoustic modes

During the decay of a sound field, sound energy is mainly dissipated over the boundaries of a room if the frequency is not too high. Part of it is transmitted through the walls to the outside, and part of it is dissipated in the walls as heat. The sound energy loss at the boundaries is related to the nature of the interaction between the sound field and its boundaries. In the reverberation room, for instance, the energy loss over the walls is related to the coupling between room modes and wall structural modes.

The rotating diffuser in the reverberation room is normally used to increase the diffuseness of the sound field. Experimental investigation at low frequencies showed that the spatial distributions, the resonance frequencies and the decay times of the acoustic modes varied with different orientations of the diffuser (Munro 1982).

The response of the walls was measured while the orientation of the diffuser was changing periodically and the driving frequency of the sound field was tuned to one of the resonance frequencies of the room corresponding to a fixed position of the diffuser. The measured response changed periodically with the periodical motion of the diffuser (Figure 2.12).

As the diffuser is moved to a new position, the resonance frequency corresponding to that position may be shifted away from the driving frequency of the sound source, so that the amplitude of the sound pressure may become smaller, which will result in a smaller response of the walls. Since the spatial coupling between the sound field and the walls is associated with the sound field distribution over the wall surfaces, the response of the walls may also be changed by changing the distribution of the sound field, which is related to the orientation of the diffuser. A close look has been taken at the acoustic mode (2,1,1) and the response

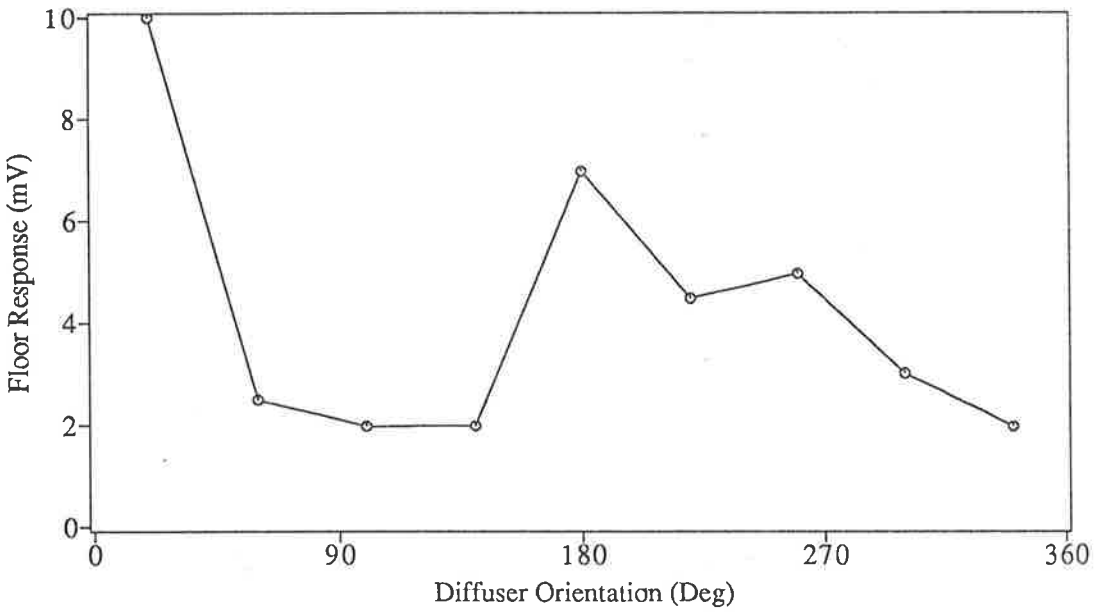

Figure 2:12: Response of the floor at (X = 1.9 m, Y = 1.7 m) as a function of diffuser orientation. Driving frequency of the sound field is 70 Hz.

of the floor vibration under the influence of the diffuser. The sound field distribution on the surface of the floor, the response of the floor and the modal decay rates of the modes were measured for 12 positions of the diffuser. In Figure 2.13, the modal decay times (T_{m60}) were transformed into modal quality factors Q, which are related to the modal decay times T_{m60} by $Q = f_r T_{m60}/13.8$ where f_r is the resonance frequency of the mode.

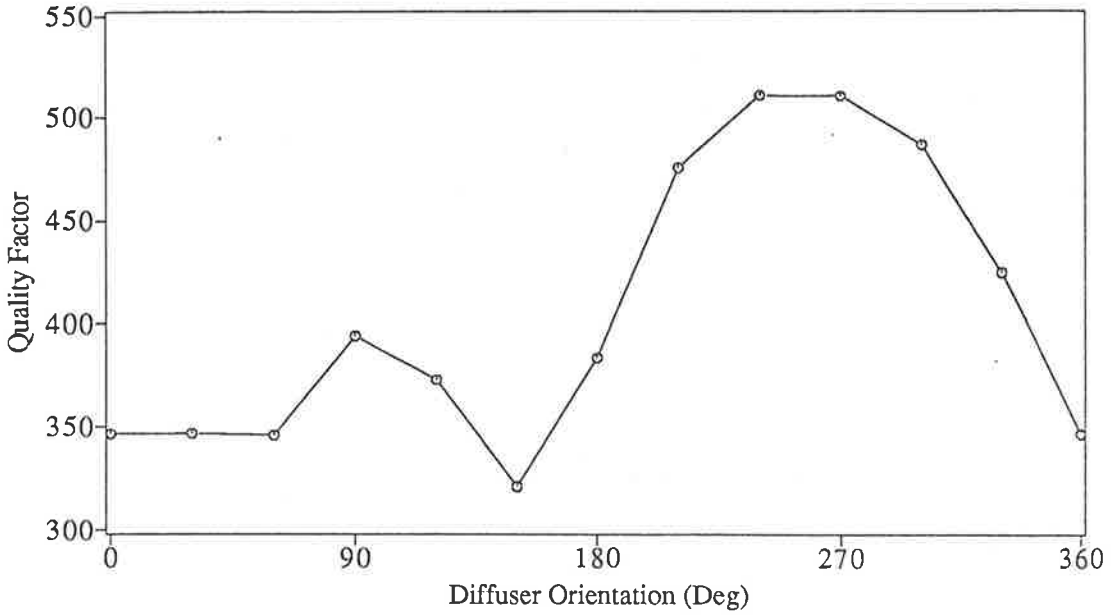

Figure 2:13: Quality factor of (2,1,1) mode as a function of diffuser orientation.

The sound field distributions for the positions of the diffuser at 60 degrees and 150 degrees are similar, and the resulting response of the floor is similar too (see Figure 2.14). This means that the coupling coefficients of the sound field and the floor at these two positions are similar. Mathematically the coupling coefficient is defined as the integral of the product of local sound pressure and structural response over the surface of the structure. As is shown in Figure 2.14, the modal distributions at these diffuser orientations are close and reference to Figure 2.13 shows that the corresponding values of quality factor Q for these positions are also close. Similar results were also obtained for two other positions of the diffuser, at 210 and 270 degrees (Figure 2.15). At the latter two positions the coupling factors and quality factors are similar although they are different from those of the first two positions.

Similar coupling coefficients give rise to similar quality factors while different coupling coefficients give rise to different quality factors. The experimental results strongly suggest that the change of the coupling between the sound field and the floor may be the reason why the decay rate of the acoustic mode changes with the orientation of the diffuser. Furthermore, a rotating diffuser continuously changes the coupling between the sound field and the boundaries, and so the energy loss over the boundaries varies with the rotation of the diffuser.

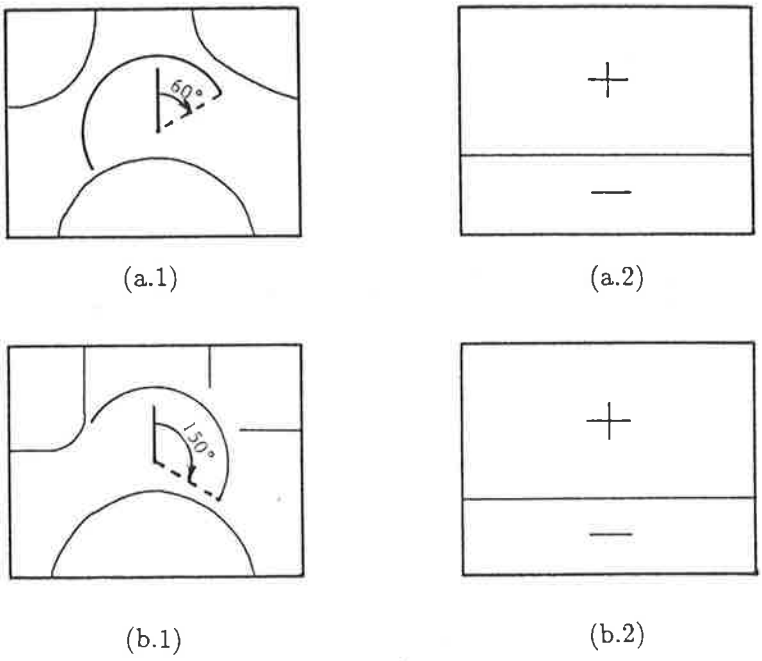

(a.1) (a.2)

(b.1) (b.2)

Figure 2.14: Modal distributions of the acoustic field near the floor and the floor responses with the diffuser at $\theta = 60^o$ and $\theta = 150^o$.
(a.1) $Q = 346.0$, ($f = 69.16$ Hz, $\theta = 60^o$); (a.2) corresponding floor response;
(b.1) $Q = 321.0$, ($f = 69.01$ Hz, $\theta = 150^o$); (b.2) corresponding floor response.

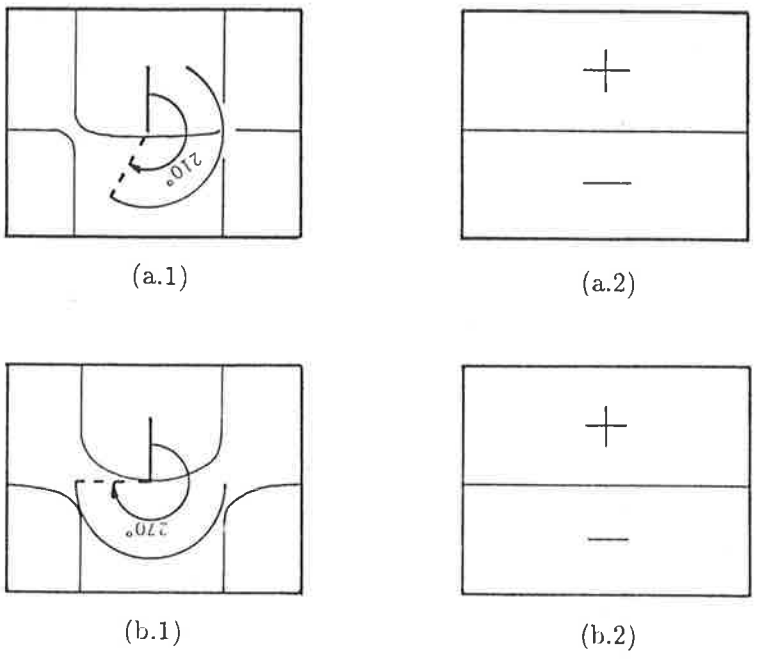

(a.1) (a.2)

(b.1) (b.2)

Figure 2.15: Modal distribution of the acoustic field near the floor and the floor responses for the diffuser at $\theta = 210^o$ and $\theta = 270^o$.
(a.1) $Q = 475.6$, ($f = 68.96$ Hz, $\theta = 210^o$); (a.2) corresponding floor response;
(b.1) $Q = 510.7$, ($f = 68.95$ Hz, $\theta = 270^o$); (b.2) corresponding floor response.

During measurement of the frequency response of the walls of the reverberation room, it was found that when the diffuser was at 180 degrees and the driving frequency was at 84.6 Hz, the response of the back wall was maximal. This suggested that the coupling between the sound field and the back wall might be stronger than any other coupling. The back wall mode and the acoustic mode were investigated. They were found to be mode(1,2) and mode(2,2,1) respectively.

The coupling between two sub-systems is dependent on their modal characteristics such as their resonance frequencies, modal damping and mode shapes. Therefore when these characteristics are changed, the coupling of these two sub-systems will also change. If the decay of the acoustic mode is really related to the coupling, the decay time will change when the modal characteristics of the back wall are changed.

To investigate this possibility, some wooden blocks were wedged tightly between the back wall of the reverberation room at the mode antinodes and the building wall which is about half a meter away (Figure 2.16).

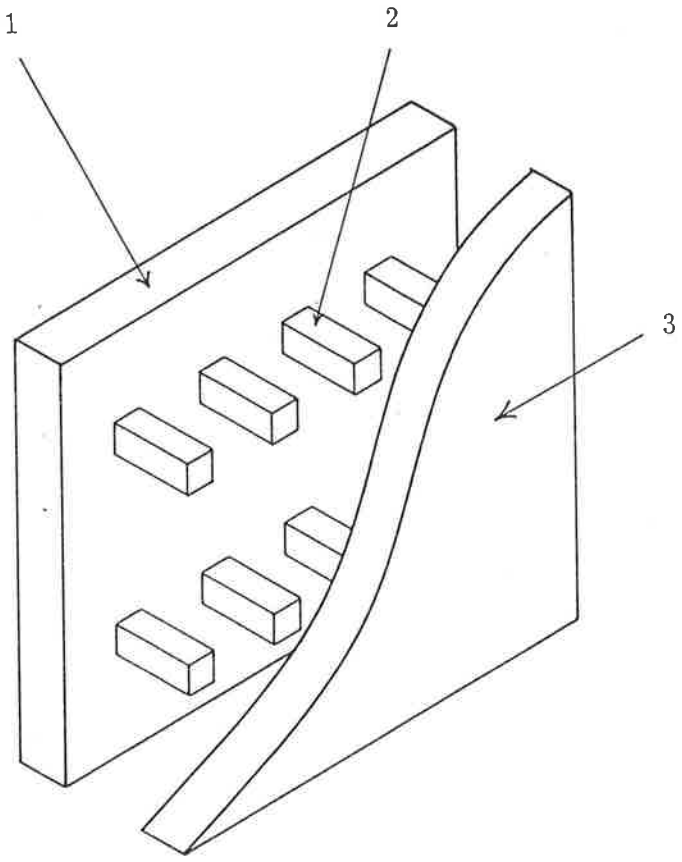

Figure 2.16 Experimental arrangement for varying the quality factor of the back wall of the reverberation room. 1. back wall of the reverberation room; 2. wooden block; 3. outside building.

As the number of the blocks was increased, the modal decay time in the room and the quality factor of the back wall were measured. The result is shown in Figure 2.17. In this case, the modal decay time decreases as the quality factor of the back wall decreases.

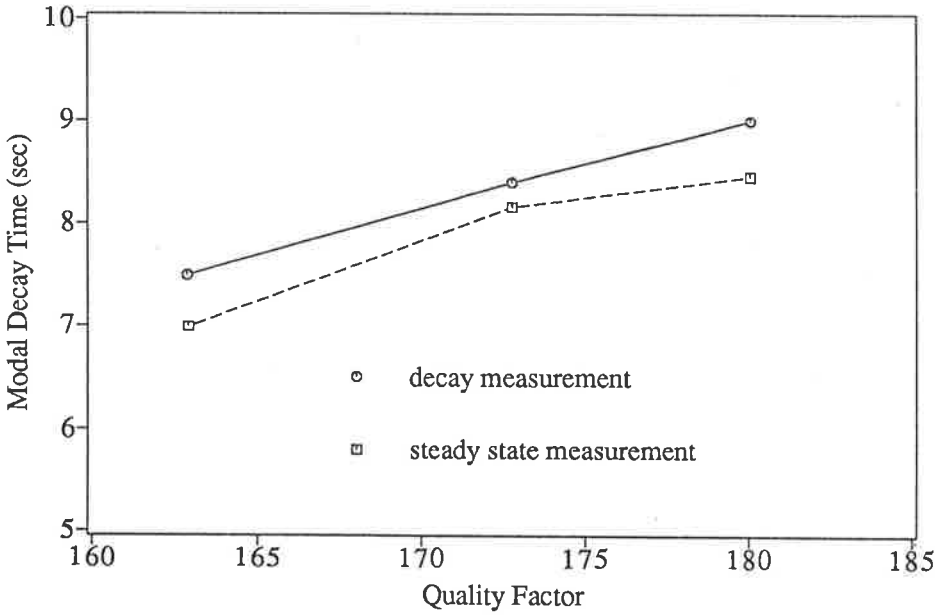

Figure 2:17: Decay time of (2,2,1) mode as a function of the quality factor of the (1,2) back wall mode.

2.7 Discussion and conclusions

Although the above experiments were undertaken in a reverberation room, their results have provided a close look at sound fields in enclosures in a very general sense. Most boundaries of enclosures, such as those of theaters and studios and those of aircraft or motor vehicles, are acoustically similar to the walls of the reverberation room in that they are extensively reactive boundaries, though they may be different in shape, dimension and material construction. Even with a layer of sound absorptive material on the surface, the extensive properties may not be totally neglected in all cases.

In some factories, it has been found that the measured reverberation time can be correlated with the sound absorptive properties of the ceiling panels implying modal coupling (Hodgson 1983) and in the construction of a very famous theater, the influence of the modally responsive floor, stage and walls on the interior acoustics has been taken into consideration

(Bliven 1976). Even in the experiment to verify the reverberation theory based on the locally reactive assumption, the modal vibration of the boundaries was observed, and sand was used to damp it (Bhatt 1939). All these examples provide evidence to show that the coupling between acoustical and structural modes plays an important part in practice.

The conclusions of this Chapter are

1. The reverberation theory based on the locally reactive boundary assumption is not correct when it is applied to enclosures with boundaries which are extensively reactive.

2. Modal coupling determines the interaction between a sound field and boundary surfaces of extended reaction.

3. Instead of normal specific acoustic impedance, modal coupling provides a proper description for the interaction.

4. In the case of extensively reactive boundaries the behaviour of the sound field and the response of the boundaries is certainly related to the coupling.

About fifty years ago, in his remarkable paper (Morse 1939) *Some Aspects of the Theory of Room Acoustics*, and as he was introducing the locally reactive acoustic impedance concept for his calculation, Morse pointed out that

> "Of course further detailed experiments, with other materials, may show that even the normal impedance varies with angle of incidence of the wave: in which case we will have to use another, more deep-seated, physical quality to measure the material's absorption. Until such time as experiment forces us to complicate the picture, ..."

Now indeed, all of these qualitative results suggest a requirement exists for a solution for the sound field and boundary response when the interaction between them is determined by modal coupling, particularly for the solution of the decay behavior of the sound field. Further investigations towards this goal will be reviewed in the next two Chapters.

Chapter 3

Effect of fluid-structural coupling — theory

3.1 Introduction

3.1.1 Statement of the problem

Forty nine years ago, Morse (1939) developed a theory of sound absorption for a rectangular room in terms of the locally reactive normal acoustic impedance. This theory is not only useful for predicting sound behavior in enclosures where the geometrical acoustic method does not apply, but it also suggests an entirely new way of looking at this problem. The significance of this pioneering work can be judged from the rapid progress which followed it in the field of room acoustics.

The assumption of locally reactive boundaries decreased the complexity of Morse's analysis, and enabled the understanding of some basic physical properties of the acoustical modes in the room. Although most of the sound absorption material tested at the time behaved in a locally reactive manner, Morse hypothesized that future experiments might expose inadequacies in the locally reactive boundary assumption.

Experiments described in Chapter 2 on the interaction between a sound field and its boundaries have demonstrated that the walls of a reverberation room are modally reactive,

rather than locally reactive. Experimental evidence has also demonstrated that the modal coupling of the sound field and walls affects the decay times in the room. In this case, the sound absorption is associated with the more complicated mechanism (modal coupling) and Morse's solution cannot provide an explanation for these experimental results, because the simplified locally reactive boundary assumption is not satisfied.

However the significance of the fluid-structural coupling on sound absorption in a room and the relationship between the coupling properties and the sound field decay remain unknown until the mechanism of sound absorption by modally reactive boundaries is understood. The original question was associated with an architectural acoustics problem, but very soon it was recognized that the research stands on the new ground of fluid-structural coupling. Knowledge of modal coupling is certainly fundamental for solving the room acoustics problem and such knowledge may provide its own insights for architectural acoustics purposes.

3.1.2 Literature review

A literature survey of the fluid-structural coupling problem shows that a large amount of work has been done in the study of fluid and structural responses due to mutual coupling, but very little has been published on the effect of this coupling upon the decay behavior of the coupled system. However, in the case of architectural acoustics the transient response is of fundamental importance.

Previous investigations into fluid-structural coupling have been motivated by the need to understand the effects of the vibrating boundaries on the fluid response, and a need to understand the acoustical loading of boundary structures by a cavity. Examples of the former are sound transmission into an enclosure from a vibrating boundary structure and sound radiation from a structure into the surrounding medium. These previous investigations cover a wide range of research and applications, but the underlying mechanism of the fluid-structural coupling remains the same. In the last twenty years, workers in a variety of fields have achieved a great deal of understanding of this mechanism.

The study of the effect of an underlying cavity on a plate originated from an interest in panel stability and panel excitation by aerodynamic noise. The modal response of a cavity backed plate was first investigated by Dowell and Voss (1963). Further investigations by Pret-

love (1965a) (1965b) (1969) and Guy(1979b) have progressively improved theoretical methods and physical insight. At about the same time as Dowell, Lyon (1963) published his research on sound transmission into a rectangular enclosure through a panel. Since then, there has been a continuous effort (by Pretlove (1966), Khilman (1967), Bhattacharya *et al.* (1969) (1970), Dowell *et al.* (1977), Guy *et al.* (1973) (1979a), Naryannan and Shanbhag (1981a) (1981b)) directed at improving the understanding of sound transmission through panels.

In addition to investigations of the simple rectangular panel-cavity system in Cartesian coordinates, the fluid-structural coupling problem has been studied in complex shaped cavities and structures, (particularly cylindrical shapes) which are closely related to the noise control problem in aircraft, piping systems and water borne structures. For example, the recent work by Fuller *et al.* (1982),(1986) and Pope *et al.* (1982),(1983) indicates the trends of aircraft noise control, and the work by Junger and Feit (1986) presents a general treatment of the coupling problem (for cylindrical structures) in underwater acoustics.

Recently developed numerical techniques have made possible detailed investigation into the coupling in irregularly shaped cavities. After the energy formulation of the fluid-structural coupled system was developed by Gladwell and Zimmermann (1966), Craggs *et al.* (1971,1972) used a finite element method to calculate the acoustical modes and resonance frequencies of a system. Since then this approach and other similar numerical methods (e.g. integral equation (Sestieri *et al.* 1984)) have been used for control of noise inside a moving vehicle (Sung *et al.* 1984) and sound transmission calculations. The paper by Nefske *et al.* (1982) briefly reviewed the relevant research.

One particular aspect which is very often put aside is the effect of the fluid-structural coupling on the decay behavior of the coupled system. In the analysis of the coupling problem, the modal damping in the uncoupled sub-systems is difficult to determine theoretically and is generally considered as an experimental parameter. Therefore, like other conventional approaches, the damping effect was normally neglected at first and if necessary, the undamped system was modified later.

In the field of room acoustics, the decay behavior of an enclosure has been taken as an important measure of its acoustical quality, but the dependence of the decay on the fluid-structure coupling is still unknown. Under this circumstance, it is clear that an investigation into sound decay due to the coupling effect is necessary. The only paper to be found which

attempted such analysis was published by Rogers in 1939. This is a study of the effect of the coupling between the sound field and moving pistons. In his paper, Rogers studied the absorption of sound due to the coupling between a one dimensional sound field and piston-like panels backed by a cavity. By comparing his result with the Sabine formula, he linked the sound absorption coefficient of the piston to the mechanical properties of the pistons and the cavity. He then discussed the extension of his results to the three dimensional diffuse sound field. However, the response of boundary structures to a sound field is more complicated than that of a piston as the three dimensional modal distribution of the sound field and the modal response of the boundary structure must also be taken into account.

Today, by using previous studies of the fluid-structural coupling problem as a basis, we are able to use "the modal coupling method" to analyse the sound absorption of modally reactive boundaries.

This Chapter contains a theoretical investigation into the free vibration behavior of a panel-cavity system. The behavior of the system is described in terms of acoustical modes. A solution for the decay time and resonance frequency of each acoustical mode is obtained by a modal coupling analysis. In this analysis, the characteristics of each mode can be determined in terms of the modal parameters of the uncoupled panel and cavity. By varying the properties of the test panel, the resonance frequency and the decay time of each acoustical mode can be changed. Relative maximum panel absorptions of the cavity controlled modes are identified when the participating panel and cavity modes are well coupled. The effect of the panel damping and radiation loss to the outside space upon the decay time of the cavity controlled modes is also discussed.

3.2 Theoretical model

3.2.1 Description of the model

A panel-cavity coupled system is chosen as the theoretical model. This system consists of a rectangular box with slightly absorptive walls and a simply supported panel on the top. The coordinates of the system are shown in Figure 3.1.

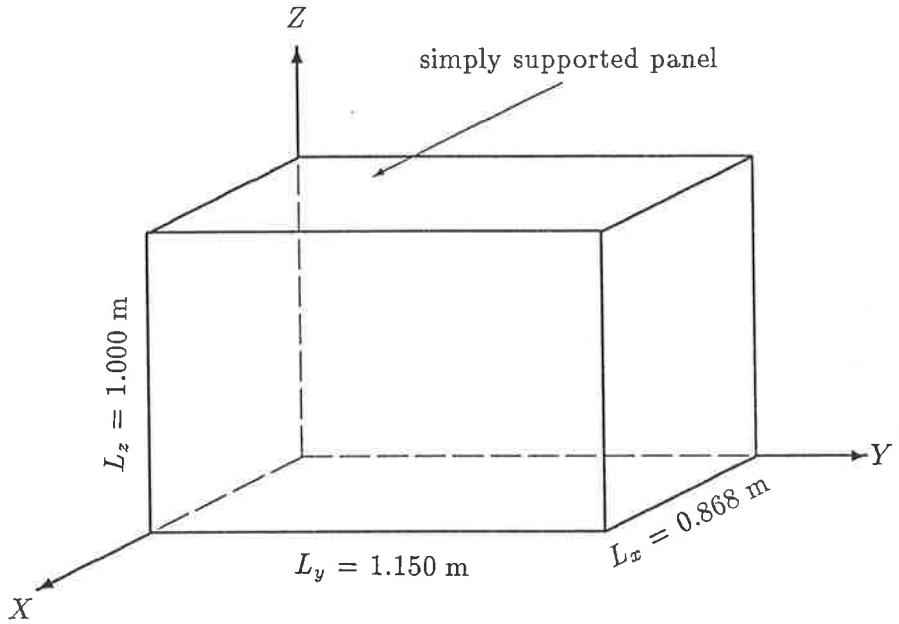

Figure 3.1: Coordinate system of the panel-cavity model.

3.2.2 General mathematical description

The properties of the coupled system can be obtained from the its free vibration solution, because the solution will give rise to modal properties, which are fundamental to the system. Once these modal properties are obtained, any response of the system to external excitation can be described in terms of the modal properties and the nature of the excitation.

In general, the the free vibration problem of the system is described either in differential form with explicit specification of the interaction over the contacting boundaries of the fluid and the structure, or in integral form which automatically includes the boundary conditions. The energy description (Hamiltonian) of the system will result in an integral equation and other integral forms can be derived directly from the differential form by the Green's function method. The physical meaning of the differential equations is straightforward, while the integral equations provide a convenient form for various numerical approximations.

3.2.3 Differential expressions

The free vibration of the panel-cavity system of Figure 3.1, can be classified in three parts as follows:

1. The sound field in the cavity is governed by a wave equation and its boundary conditions.

   In terms of an acoustic velocity potential Ψ, the wave equation for the free vibration problem is

   $$\nabla^2\Psi - \frac{1}{C_o^2}\frac{\partial^2\Psi}{\partial t^2} = 0 \ , \tag{3.1}$$

   where C_o is the speed of sound in the air. The air particle velocity $\vec{V}$ and sound pressure P are related to the velocity potential by $\vec{V} = \nabla\Psi$ and $P = -\rho_o\frac{\partial\Psi}{\partial t}$ respectively.

   The five walls of the cavity are assumed to be locally reactive and the boundary condition over the walls is described by the relation between the velocity potential and the specific acoustical impedance Z_A on the surfaces as follows.

   $$\frac{\partial\Psi}{\partial n} = -\frac{\rho_o}{Z_A}\frac{\partial\Psi}{\partial t} \ . \tag{3.2}$$

   In this equation, n indicates the normal direction on the surface of the boundary (positive outwards) and ρ_o is the air density. If the boundaries are rigid, then $\frac{\partial\Psi}{\partial n} = 0$.

   The boundary condition over the flexible panel is determined by continuity of the normal air particle velocity and the normal panel velocity on the surface:

   $$\frac{\partial\Psi}{\partial n} = \frac{\partial W}{\partial t} \ , \tag{3.3}$$

   where W is the panel normal displacement.

2. Different wave forms may exist in the panel, but only flexural waves have motions perpendicular to the surface which can cause radiation of sound into an adjacent medium. The behavior of the panel flexural motion is determined by the differential equation of motion, the boundary conditions along the panel edges and the forces acting on the panel surfaces. The forces on the panel are due to the interior and the external sound pressure. For a thin isotropic panel, the equation for flexural vibration is

   $$\rho h\frac{\partial^2 W}{\partial t^2} + \frac{Eh^3}{12(1-\mu^2)}\nabla^4 W = \rho_o\left(\frac{\partial\Psi_E}{\partial t} - \frac{\partial\Psi}{\partial t}\right) \ , \tag{3.4}$$

   where ρ, E, μ, h and Ψ_E are the density, Young's modulus, Poisson's ratio, thickness of the panel and the acoustic velocity potential on the outside surface of the panel

respectively. The positive direction for panel displacement is outward. The panel edges are simply supported for this analysis. This means that the displacement and the bending moment are zero along the all edges.

3. The velocity potential on the external surface of the panel is evaluated by the Rayleigh integral (Rayleigh 1896) for sound waves radiating from a baffled panel,

$$\Psi_E = -\frac{1}{2\pi}\int_{A_f} \frac{\partial W}{\partial t}\frac{\exp(-i\vec{k}\cdot\vec{r})}{r} ds_o \ , \tag{3.5}$$

where k is the wavenumber of the sound field and r is the distance from the source point (x_o, y_o) on the panel surface to the observation point (x, y). The time dependence term $\exp(i\omega t)$ has been suppressed in all expressions.

Many authors used transformation methods to solve the above equations (Pretlove 1965a, Khilman 1967, Bhattacharya 1970, Guy 1979b). Guy (1979b) finally presented a general analysis for the behavior of a cavity backed panel. The transformation method (Fourier transformations to remove the spatial parameters and Laplace Transformation to remove the time dependence) provides an exact solution to the non-dissipative panel-cavity system. The properties of the system can be determined by searching the singularities (the poles) of the modal coefficients of the panel displacement. The response of the system to the external excitation can be obtained by additional investigation of the poles of the external force in the frequency domain. However, it is difficult to find the solution when damping of the system is present because the background modal damping is difficult to introduce in those cavity modes with non-zero modal index on the Z axis (see Figure 3.1). These modes are implicitly represented in the solution.

3.2.4 Integral expressions

Equations (3.1) and (3.4) can be reduced to their corresponding integral equations by means of the Green's function method(Feshbach 1944). The integral equations for the acoustical velocity potential in an enclosure, and the panel displacement are equivalent to the original differential equations and automatically include the boundary conditions. This procedure requires a Green's function which satisfies the inhomogeneous equations (the original partial differential equations with a Dirac delta function as a point source). The Green's function can also be chosen to satisfy convenient boundary conditions to reduce the difficulties in the

resulting boundary integral. The constructed Green's function is a transfer function from a point source to the velocity potential at an observation point in the cavity. By Gauss's theorem, the vibrating boundaries are mathematically taken as sources and the total contribution of these sources to the velocity potential is described by the summation (integration for the continuous source distribution) of the sources through their transfer functions over the whole of the boundaries. A sound field Green's function in the cavity , which satisfies the Neumann boundary condition, can be obtained by normal mode expansion,

$$G_A(\vec{r},\vec{r}_o;\omega) = \sum_N \frac{C_o^2}{\Lambda_N}\frac{\Phi_N(\vec{r})\Phi_N(\vec{r}_o)}{(\omega^2-\omega_{aN}^2)} , \tag{3.6}$$

$$\Lambda_N = \int_V \Phi_N(\vec{r})\Phi_N(\vec{r})dv . \tag{3.7}$$

For the rectangular cavity, each normal mode can be written as

$$\Phi_N(\vec{r}) = \cos(\frac{l\pi x}{L_x})\cos(\frac{m\pi y}{L_y})\cos(\frac{n\pi z}{L_z}) , \tag{3.8}$$

where (l,m,n) are the modal indices of the Nth cavity mode and ω_{aN} is the angular frequency of the Nth cavity mode.

The acoustical velocity potential in the cavity can be predicted by integrating the distributed velocity contribution on the boundaries (Appendix A):

$$\begin{aligned}\Psi &= -\int_A G_A\frac{\partial\Psi}{\partial n}ds_o \\ &= -\int_{A_f}\frac{\partial W}{\partial t}G_A ds_o + i\frac{\omega}{C_o}\int_{A_l}\beta\Psi G_A ds_o ,\end{aligned} \tag{3.9}$$

where $\beta = \frac{\rho_o C_o}{Z_A}$ is the specific acoustic admittance ratio on the wall surfaces A_l.

Similarly, the Green's function for a simply supported panel is

$$G_p(\vec{x},\vec{x}_o;\omega) = -\sum_M \frac{S_M(\vec{x})S_M(\vec{x}_o)}{\Lambda_M(\omega^2-\omega_{pM}^2)} , \tag{3.10}$$

$$\Lambda_M = \int_{A_f} S_M(\vec{x})S_M(\vec{x})ds . \tag{3.11}$$

For a rectangular panel, each normal mode can be written as

$$S_M = \sin(\frac{u\pi x}{L_x})\sin(\frac{v\pi y}{L_y}) . \tag{3.12}$$

ω_{pM} is the angular frequency of the Mth panel mode and (u,v) are the modal indices of the Mth panel mode. $\vec{x}$ and $\vec{x}_o$ are the observation and source points on the panel surface

respectively. Therefore the displacement of the panel due to the distributed sound pressures on the panel surfaces can be represented by

$$W = -i\frac{\rho_o \omega}{\rho h}\int_{A_f} G_p(\vec{x},\vec{x}_o;\omega)(\Psi - \Psi_E)ds_o \ . \tag{3.13}$$

3.3 Solution of the integral equations

The general mathematical methods for solving integral equations have been discussed by Morse and Feshbach (1953). To solve Eqs. (3.9) and (3.13) in the following sections, the methods of orthogonal expansion and of successive substitutions will be used. Dowell *et al.* (1977) used the orthogonal expansion method to study the sound transmission problem between two rooms through a panel partition and the response of a panel-cavity system. The agreement of their measured and predicted panel resonance frequencies for various cavity depths demonstrates the success of the method for the coupling problem.

3.3.1 Method of orthogonal expansion

In this method, the acoustical velocity potential in the cavity $\Psi(\vec{r})$ is expanded in orthogonal functions Φ_N (rigid wall mode expression) and the panel displacement W is expanded in orthogonal panel mode functions S_M. These orthogonal cavity and panel modes are identical to those in the Green's functions for the cavity and the panel.

$$\Psi = \sum_N C_N \Phi_N \ , \tag{3.14}$$

$$W = \sum_M D_M S_M \ . \tag{3.15}$$

Substituting Eqs.(3.14) and (3.15) into Eqs. (3.9) and (3.13) and neglecting the panel radiation term, a series algebraic equations for each cavity mode N and for each panel mode M are obtained as follows:

$$(\lambda^2 - 2\zeta_{aN}\lambda + k_{aN}^2)M_N^a C_N + \lambda C_o \sum_I B_{I,N} D_I = 0 \ , \tag{3.16}$$

$$(\lambda^2 - 2\zeta_{pM}\lambda + k_{pM}^2)M_M^p D_M - \lambda C_o \sum_J B_{J,M} C_J = 0 \ , \tag{3.17}$$

where $M_N^a = \Lambda_N$ and $M_M^p = \frac{\rho h C_o'^2}{\rho_o}\Lambda_M$. $k_{aN} = \frac{\omega_{aN}}{C_o}$ is the wavenumber of the Nth cavity mode, $k_{pM} = \frac{\omega_{pM}}{C_o}$ is the "wavenumber" of the Nth panel mode and $\lambda = -ik$. In the panel

wavenumber expression, the speed of sound in the denominator of the expression is for air rather than for the panel.

The damping of the Nth cavity modes is described by the specific acoustic admittance ratio β in Eq. (3.9). The boundary integral associated with β (i.e. $\Lambda_N^{-1} \int_{A_l} \beta \Phi_N \Phi_N ds$) becomes the modification term for the wavenumber of the Nth mode (Morse and Bolt 1944). The integral can be split into two parts associated with the real and imaginary parts of β. As a result, the integral with conductance (real part of β) is associated with the damping constant ζ_{aN} of the Nth cavity mode.

Each damping constant is used to represent the background absorption of each cavity mode and the Nth modal damping factor ζ_{aN} is related to the 60 dB decay time T_{aN} of the Nth cavity mode by $\zeta_{aN} = \dfrac{6.91}{C_o T_{aN}}$. The integral with susceptance (imaginary part of β) is related to the resonance frequency correction of the Nth cavity mode.

The mechanical damping of the test panel is usually represented by the complex Young's modulus and complex Poisson's ratio (Snowdon 1970). This produces complex angular resonance frequencies for the uncoupled panel.

The damping factor of the Mth panel mode, which is represented by ζ_{pM} in a manner similar to the cavity modal damping constant, can also be determined from the modal decay time of the Mth panel mode using $\zeta_{pM} = \dfrac{6.91}{C_o T_{pM}}$.

$B_{M,N}$ is the modal coupling coefficient between the Mth panel mode and the Nth cavity mode,

$$B_{M,N} = \int_{A_f} S_M \Phi_N ds \; . \tag{3.18}$$

For the system of Figure 3.1, the coupling coefficient between the Mth panel mode(u, v) and the Nth cavity mode(l, m, n) is,

$$B_{M,N} = \begin{cases} (-1)^n \dfrac{A_f}{\pi^2} \dfrac{uv[(-1)^{l+u} - 1][(-1)^{m+v} - 1]}{(l^2 - u^2)(m^2 - v^2)} & \\ 0 & l = u \;\text{ and, or }\; m = v \end{cases} \; . \tag{3.19}$$

The modal coupling coefficient is a measure of the spatial match between panel and cavity modes. As noted by Pretlove (1965a) and Bhattacharya (1970), the coupling of the cavity modes and the panel modes is very selective. Table 3.1 shows the possible coupling modal pairs. Khilman (1967) also estimated the coupling coefficient of a panel mode with all

the possible cavity modes, he found that the coupling coefficient is large only for a very few cavity modes.

Table 3.1: Selection rule for panel-cavity modal interaction

(o: odd number, e: even number n: arbitrary cavity modes index in Z direction)

panel	cavity modes			
modes	(o,o,n)	(e,e,n)	(o,e,n)	(e,o,n)
(o,o)		√		
(e,e)	√			
(o,e)				√
(e,o)			√	

($\surd$: $B_{M,N} \neq 0$)

From Eqs.(3.16) and (3.17), a matrix form can be constructed for the solution of the eigenvalues λ

$$(\lambda^2\mathbf{M} + \lambda\mathbf{L} + \mathbf{S})\mathbf{X} = \mathbf{0} \ , \tag{3.20}$$

where $\mathbf{M}$ is the inertia matrix, $\mathbf{L}$ is the coupling matrix and $\mathbf{S}$ is the stiffness matrix. If only $N1$ cavity modes and $N2$ panel modes are used, then

$$\mathbf{M} = \begin{pmatrix} M_1^a & & & & & \\ & \ddots & & & 0 & \\ & & M_{N1}^a & & & \\ & & & M_1^p & & \\ & 0 & & & \ddots & \\ & & & & & M_{N2}^p \end{pmatrix} \tag{3.21}$$

$$\mathbf{L} = \begin{pmatrix} -2M_1^a\zeta_{a1} & & 0 & & C_oB_{1,1} & \cdots & C_oB_{1,N2} \\ & \ddots & & & \vdots & & \vdots \\ 0 & & -2M_{N1}^a\zeta_{aN1} & & C_oB_{N1,1} & \cdots & C_oB_{N1,N2} \\ -C_oB_{1,1} & \cdots & -C_oB_{N1,1} & & -2M_1^p\zeta_{p1} & & 0 \\ \vdots & & \vdots & & & \ddots & \\ & & & & 0 & & \\ -C_oB_{1,N2} & \cdots & -C_oB_{N1,N2} & & & & -2M_{N2}^p\zeta_{pN2} \end{pmatrix} \tag{3.22}$$

$$\mathbf{S} = \begin{pmatrix} M_1^a k_{a1}^2 & & & & & & \\ & \ddots & & & 0 & & \\ & & M_{N1}^a k_{aN1}^2 & & & & \\ & & & M_1^p k_{p1}^2 & & & \\ & 0 & & & \ddots & & \\ & & & & & \ddots & \\ & & & & & & M_{N2}^p k_{pN2}^2 \end{pmatrix} \tag{3.23}$$

and $\mathbf{X}$ is the eigenvector of the system with all the unknown coefficients $(C_1 ... C_{N1}; D_1 ... D_{N2})$ as its components.

By using $N1$ cavity modes and $N2$ panel modes, Eq.(3.20) becomes a $(N1 + N2)$ dimensional matrix equation which gives $(N1 + N2)$ eigenvalues $(\lambda_1, \lambda_2, \cdots, \lambda_{N1+N2})$. The imaginary part of the eigenvalue λ_i is related to the resonance frequency of the ith acoustic mode ($f_i = \frac{Im(\lambda_i)C_o}{2\pi}$) and the real part is related to the damping constant (or the modal decay time) of the mode ($T_{i60} = \frac{6.91}{Re(\lambda_i)C_o}$).

This solution shows that the sound field in the cavity and the response of the panel may be described in terms of the uncoupled cavity modes and panel modes with interactions between them. The interaction accounts for the structural vibration which disturbs the interior acoustical response, and also the acoustical pressure loadings which act on the panel. The coupling of the two sets of uncoupled modes is mathematically represented by matrix $\mathbf{L}$.

Since this expression only requires the modal parameters of the cavity and panel, various numerical technique can be employed to find these parameters first when the shapes of the cavity and the panel are complicated. Then coupling is introduced to obtain a new set of acoustical modes, which are represented in terms of the uncoupled modes.

By means of a matrix transformation (Anderson 1973), the non-standard eigenequation, Eq.(3.20), can be changed into a standard real eigenequation but at the expense of doubling the dimension of the matrix. By introducing $\mathbf{Y} = \lambda \mathbf{X}$, Eq. (3.20) becomes

$$\begin{bmatrix} \mathbf{0} & \mathbf{I} \\ -\mathbf{M}^{-1}\mathbf{S} & -\mathbf{M}^{-1}\mathbf{L} \end{bmatrix} \begin{bmatrix} \mathbf{X} \\ \mathbf{Y} \end{bmatrix} = \lambda \begin{bmatrix} \mathbf{X} \\ \mathbf{Y} \end{bmatrix}. \tag{3.24}$$

This standard eigenvalue problem is solved by an IMSL package (IMSL 1985) in the following calculation.

For each eigenvalue, an eigenvector can be obtained. The components of this eigenvector are used to describe the distribution of the corresponding acoustical mode. For example, eigenvalue λ_i corresponds to the eigenvector $(C_{i1}, \cdots C_{iN1}, D_{i1}, \cdots D_{iN2})$. The sound field part of the ith acoustical mode can be written in as

$$\Psi_i = \sum_N C_{iN} \Phi_N, \tag{3.25}$$

and panel vibration part can be written as

$$W_i = \sum_M D_{iM} S_M. \tag{3.26}$$

3.3.2 Method of successive substitutions

The eigenvalues and eigenfunctions of the cavity controlled modes of the coupled system can also be evaluated individually. For example, the complex wavenumber (eigenvalue) of the Nth cavity controlled mode ξ_N can be estimated using the following relation (see Appendix A),

$$\begin{aligned} \xi_N^2 &= k_{aN}^2 + i\frac{\int_{A_l} \beta \Psi \Phi_N ds}{\int_V \Psi \Phi_N dv} \xi_N - \frac{\rho_o C_o^2}{\rho h} \frac{\int_{A_f} \int_{A_f} \Psi G_p \Phi_N ds_o ds}{\int_V \Psi \Phi_N dv} \xi_N^2 \\ &\quad + \frac{\rho_o C_o^2}{\rho h} \frac{\int_{A_f} \int_{A_f} \Psi_E G_p \Phi_N ds_o ds}{\int_V \Psi \Phi_N dv} \xi_N^2. \end{aligned} \tag{3.27}$$

Equation (3.27) shows that the eigenvalue of each cavity controlled mode is represented by four terms. The first term is related to the eigenvalue of the corresponding cavity mode for the

rigid wall condition. The second term is the contribution of the locally reactive boundaries. Morse has investigated the effect of this term upon the eigenvalues of a rigid wall cavity. The third term is the contribution of the interaction of the interior sound field with the panel vibration and the last term is the contribution due to the panel radiation into the external space.

The eigenfunction for the sound field part of the Nth cavity controlled mode is

$$\Psi_N = \Phi_N - \int_{A_f} \frac{\partial W}{\partial t} G'_A ds_o + i\frac{\omega}{C_o} \int_{A_l} \beta \Psi G'_A ds_o, \tag{3.28}$$

where the prime on the cavity Green's function indicates that the term involving Φ_N in the sum is omitted.

By including the damping of the cavity and panel modes (and neglecting the panel modal radiation effect i.e. $\Psi_E = 0$), the approximate solution for the Nth eigenvalue ξ_N becomes :

$$\begin{aligned} \xi_N^2 &= k_{aN}^2 + 2i\zeta_{aN}\xi_N + \frac{1}{M_N^a} U_{N,N}\xi_N^2 \\ &\quad + \sum_{N' \neq N} \frac{U_{N',N}U_{N,N'}}{M_N^a M_{N'}^a [\xi_N^2 - (k_{aN'}^2 + 2i\zeta_{aN'}\xi_N)]} \xi_N^4 + ..., \end{aligned} \tag{3.29}$$

where

$$U_{N,N} = \sum_M \frac{C_o^2 B_{M,N}^2}{M_M^p [\xi_N^2 - (k_{pM}^2 + 2i\zeta_{pM}\xi_N)]}, \tag{3.30}$$

$$U_{N',N} = \sum_M \frac{C_o^2 B_{M,N'} B_{M,N}}{M_M^p [\xi_N^2 - (k_{pM}^2 + 2i\zeta_{pM}\xi_N)]}. \tag{3.31}$$

The third term on the right side of Eq. (3.29) is the contribution of the coupling of the examined cavity mode with all the panel modes. The fourth term is the contribution of the coupling of the examined cavity mode with other cavity modes through their interactions with panel modes.

The ξ_N^2 can be solved by successive approximation as follows:

$$\xi_{N(1)}^2 = k_{aN}^2 + 2i\zeta_{aN}k_{aN} \ , \tag{3.32}$$

$$\xi_{N(2)}^2 = k_{aN}^2 + 2i\zeta_{aN}\xi_{N(1)} + \frac{1}{M_N^a} U_{N,N}\xi_{N(1)}^2 \ , \tag{3.33}$$

$$\begin{aligned} \xi_{N(3)}^2 &= k_{aN}^2 + 2i\zeta_{aN}\xi_{N(2)} + \frac{1}{M_N^a} U_{N,N}\xi_{N(2)}^3 \\ &\quad + \sum_{N' \neq N} \frac{U_{N',N}U_{N,N'}}{M_N^a M_{N'}^a [\xi_{N(2)}^2 - (k_{aN'}^2 + 2i\zeta_{aN'}\xi_{N(2)})]} \xi_{N(2)}^4 \ . \end{aligned} \tag{3.34}$$

When the panel radiation term is taken into account, an extra term Δ_N^{Pr} should be added to the right side of Eq (3.29). The first order approximation of this term is obtained by using the first order approximate panel displacement and neglecting the panel cross modes interaction.

$$\Delta_N^{Pr} = -\frac{iA_f C_o^4}{4M_N^a}(\frac{\rho_o}{\rho h})^2 \sum_M \frac{B_{M,N}^2[\sigma_{Im}(M,N) - i\sigma_{Re}(M,N)]}{(M_M^p)^2[\xi_N^2 - (k_{pM}^2 + 2i\zeta_{pM}\xi_N)]^2}\xi_N^3 , \tag{3.35}$$

where $\sigma_{Re}(M,N)$ is the radiation efficiency of the Mth panel mode at the resonance frequency of the Nth cavity controlled mode:

$$\sigma_{Re}(M,N) = \frac{2\xi_N^2}{\pi A_f}\int_{A_f} S_M(\vec{x}_1)S_M(\vec{x}_2)\frac{\sin(\xi_N r)}{\xi_N r}ds_1 ds_2 . \tag{3.36}$$

The calculation of the modal radiation efficiency of a simply supported rectangular panel has been discussed by Wallace (1972) and Leppington *et al.* (1982). r is the distance between point $\vec{x}_1$ and point $\vec{x}_2$ on the panel. $\sigma_{Im}(M,N)$ is associated with the contribution of the "virtual mass" of the Mth panel mode:

$$\sigma_{Im}(M,N) = \frac{2\xi_N^2}{\pi A_f}\int_{A_f} S_M(\vec{x}_1)S_M(\vec{x}_2)\frac{\cos(\xi_N r)}{\xi_N r}ds_1 ds_2 . \tag{3.37}$$

Pretlove studied the "virtual mass" of a simply supported panel and pointed out that the effect of the virtual mass attached to the panel is negligibly small in all practical cases (1965b). When the panel radiation term is considered, a substitution method similar to that of Eqs. (3.31), (3.32) and (3.33) is used by including Δ_N^{Pr}.

3.4 Properties of the solutions

3.4.1 Convergence

The acoustical velocity potential Ψ (Eq. (3.9)) obtained by the Green's function integral on the internal boundaries has discontinuous slope at the panel surface, because the selected Green's function satisfies the second order homogeneous condition on the boundaries on the panel surface (i.e. $\frac{\partial G_A}{\partial n} = 0$). This prescribed boundary condition for the Green's function has the result that $\frac{\partial \Psi}{\partial n} = 0$ on the panel surface, but the boundary condition of the velocity potential Ψ at the panel surface has been defined by Eq.(3.3) as nonzero. Although only Ψ rather than $\frac{\partial \Psi}{\partial n}$ is used in the analysis, when the velocity potential is expanded as orthogonal functions (which are the same as those for the Green's function), this discontinuity may affect the speed of the convergence of the solution.

The acoustical velocity potential in the cavity can be represented by any set of orthogonal functions which are complete in the region of the cavity. However, when the chosen functions do not satisfy the boundary conditions (for example that the cosine functions which we have chosen do not satisfy the inhomogeneous Neumann condition on the panel surface), the speed of the convergence of the expansion (of the slope of the functions) to the exact value will depend upon the number of terms in the expansion and the position chosen for the evaluation. Near the boundary more terms may be needed to achieve the convergence, but away from the boundary, only a few terms may be needed to give a reasonable value.

Taking the sound field in a one dimensional tube (with length of $L_x = 1$ m) as an example, the first mode for the two rigid ends can be simply represented by one function $\cos(\frac{\pi x}{L_x})$ from the whole set of the cosine functions in the region $(0 \leq x \leq L_x)$. If one end of the tube is terminated by a resonant piston, the shape of the first mode changes [1] (see Figure 3.2). However, the mode shape can still be resolved into a set of cosine functions which are the normal modes for the rigid wall tube. Figure 3.3 shows the squared error of the approximated sound field distribution from the exact distribution in the tube. Increasing the number of the base functions improves the convergence of the calculation but the convergency rate is different for different positions in the tube. Convergence is problem dependent, and numerical tests may be a proper way to evaluate it. Nefske *et al.* (1982) estimated the convergence of the resonance frequencies of the sound modes in a piston terminated tube as a function of the number of the rigid wall modes. Dowell (1977) pointed out that the sound pressure can still be determined correctly anywhere including the surface of the panel, even though the normal derivative of the expression for the normal modes expansion does not converge uniformly at the panel surface. Feshbach (1944) also mentioned that the difficulty of the convergence will not exist for simple boundaries. A boundary is called simple if the geometrical dimension of the boundary which is used to calculate the Green's function is the same as that of the actual boundary. All of this previous work suggests that modal coupling approach can achieve good convergence.

[1] The exact solution for the resonance frequencies of the one dimensional sound field terminated by a resonant piston (resonance frequency is f_0) can be obtained from $[1 - (\frac{k_o}{k})^2] = \frac{V\rho_o}{m_p}\frac{\cot(kL_x)}{kL_x}$, where $k_o = \frac{2\pi f_o}{C_o}$, V is the volume of the tube and m_p is the mass of the piston. In the calculation of Figures 3.2 and 3.3, $f_o = \frac{340}{\pi}$ Hz, the radius of the tube is 0.05 m, $m_p = 0.05$ kg and $L_x = 1$m. The first resonance frequency of the tube with the piston is 106.3 Hz.

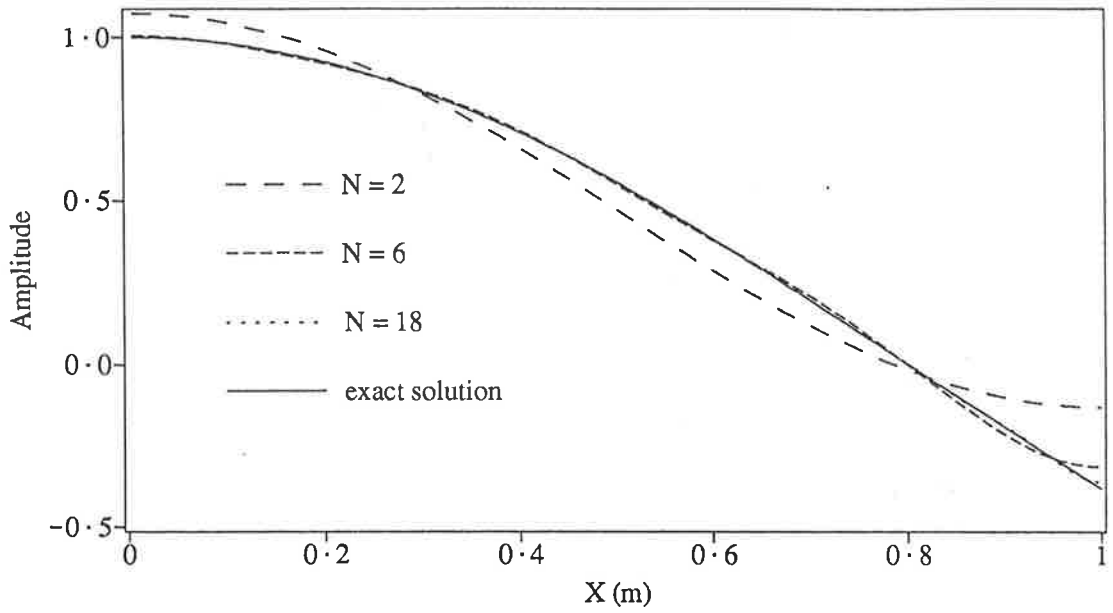

Figure 3.2: The sound field distribution of the first mode in a tube terminated by a resonant piston. Exact sound field distribution and the approximated distribution by the first N terms of the base function $cos(n\pi x/L_x)$, $(n = 0,\ 1,\ 2\ ...\ N-1)$.

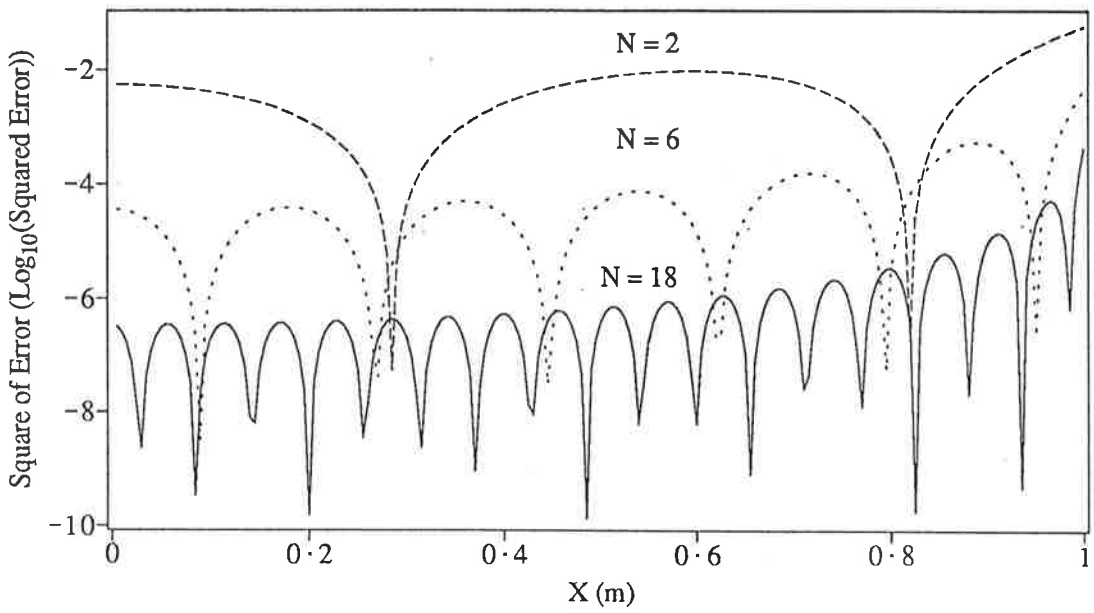

Figure 3.3: Square of the amplitude error between the approximate sound field distribution and exact sound field distribution of the first mode.

3.4.2 Weak coupling

Weak coupling has been commonly assumed in the analysis of air-structural interaction problems (Pope and Wilby 1977). It prescribes the state of the strength of the interaction of the subsystems in the coupled system. In general if the energy involved in the interaction is much smaller than the energies in the subsystems, the coupling is described as weak. The motion of each subsystem in a weakly coupled system will not be essentially different from that of the uncoupled systems. The coupling only perturbs the state of the motion of the uncoupled systems. Mathematically, the coupled modes will be sufficiently represented by a limited number of the uncoupled cavity and panel modes.

When the panel and cavity are coupled, the mode shapes and the resonance frequencies of the panel and cavity are only slightly disturbed. Because of the low density of the air and the high stiffness of the panel, the radiation loading generally has little effect upon the panel vibration and the actual motion of the panel normal to its surface is so small that the mode shapes of the sound field in the cavity will not be strongly affected. However, if the cavity in contact with the panel is very shallow and the panel is very light (Pretlove 1965a), or the density of the surrounding medium is more dense than air, such as water, (Fahy *et al.* 1970) the coupling may turn out to be strong and big deformation of the resulting modes from the uncoupled panel and the cavity modes may be expected. In this situation, mode coupling analysis may be inadequate.

3.4.3 Well coupled modes

When two subsystems are weakly coupled, it is usually expected that some modes in the uncoupled systems will play no important role in the coupling mechanism. In this case the problem will be greatly simplified by neglecting these unimportant modes. In statistical energy analysis, the well coupled modes concept has been used to select the modal pairs which dominate the coupling calculation of the two subsystems (Lyon 1962, Fahy 1969). The condition for the well-coupled mode has been obtained (Fahy 1969) and is as follows:

$$2|\omega_{aN} - \omega_{pM}| < (\Delta\omega_{aN} + \Delta\omega_{pM}) \,, \tag{3.38}$$

where $\Delta\omega_{aN}$ is the bandwidth of the Nth cavity mode and $\Delta\omega_{pM}$ is the bandwidth of the Mth panel mode. In this analysis, the power transfer between those modal pairs which do not satisfy

the condition given by Eq. (3.38) will be neglected, whatever their coupling coefficient might be. In the study of individual mode behavior, this criterion will also be useful for estimating the relative importance of the participating modal pairs. The modal coupling coefficient must also be taken into consideration, because there will be no energy transfer between two modes while their coupling factor is zero, even though their resonance frequencies are close. In this work, a transfer factor (Louisell 1960) which has been used in electrical coupling problems is used to decide the relative importance of different modes. The transfer factor of electrical coupling theory re-interpreted for the Nth cavity mode and Mth panel mode of the panel-cavity system may be written as

$$F_{M,N} = [1 + (\frac{\omega_{aN} - \omega_{pM}}{2})^2 \frac{1}{B(M,N)^2}]^{-1} , \tag{3.39}$$

where

$$B(M,N) = [\frac{\rho_o C_o^2}{\rho h \Lambda_N \Lambda_M}]^{1/2} \, B_{M,N} . \tag{3.40}$$

When $|F_{M,N}| \cong 1$ the coupling is very important, but if $|F_{M,N}| \ll 1$ the modes will be less affected by one another. In the analysis of two weakly coupled oscillators, the transfer factor is used to determine the maximum fraction of the energy transferred between the oscillators. Therefore, larger energy transfer is expected between the Nth cavity mode and the Mth panel mode when their transfer factor is large.

3.5 Coupling effect on the acoustical modes

The solution of Eq(3.24) or Eq(3.27) depends upon the parameters of the uncoupled test panel and the cavity. The purpose of this section is to discuss how these parameters relate to the coupling and to the behavior of the coupled system with emphasis on the resulting modal decay times.

3.5.1 Modal coupling coefficients

A coupling coefficient between a cavity and a panel mode is determined by the integral of their mode shapes on the contacting surface. The mode shapes of the panel in turn depend upon its dimensions and the boundary conditions. Different boundary conditions will give rise to different mode shapes and to different coupling factors. In order to obtain a basic physical

picture, we will confine the analysis to the simply supported edge condition for the panel, although similar analysis can be applied to more complicated boundary conditions.

3.5.2 Resonance distribution and panel modal density

It is well known that the energy transfer between two coupled oscillators depends upon the uncoupled resonance frequencies of each oscillator. The power flow from one oscillator to another increases as the difference of their resonance frequencies decreases (Morse and Ingard 1968b). The panel-cavity system is interpreted as a multi-mode coupled system. The relative resonance frequencies of the coupled cavity and panel modes will also affect the energy transfer between them just in the similar case of the two coupled oscillators. The modal density of the panel and the cavity at the examined frequencies will also affect the energy transfer, because the coupling is not only controlled by the two interacting panel and cavity modes, but is also affected by other modes of near resonance frequencies.

The resonance frequencies of the rigid wall cavity (Knudsen 1932) and of the simply supported panel are given by following equations,

$$f_{l,m,n} = \frac{C_o}{2}[(\frac{l}{L_x})^2 + (\frac{m}{L_y})^2 + (\frac{n}{L_z})^2]^{1/2} , \tag{3.41}$$

$$f_{u,v} = 0.458 C_L h[(\frac{u}{L_x})^2 + (\frac{v}{L_y})^2] , \tag{3.42}$$

where C_L is the longitudinal speed of sound in the panel.

In the panel-cavity system, the resonance frequencies of the uncoupled modes can be adjusted by altering the dimensions of the cavity or the panel, or by changing the panel material (changing the longitudinal speed of sound in the panel). For the model shown in Figure 3.1, the cavity dimensions are fixed but the test panel can be changed. In this analysis, the resonance frequencies of panel modes are altered by changing the panel thickness. The panel is aluminum.

The thickness h of a panel with fixed surface area A_f and longitudinal wave speed C_L is related to the modal density of the panel by

$$n_p = \frac{\sqrt{3} A_f}{C_L h} . \tag{3.43}$$

Panel modal density is used to characterize the test panel. The modal density not only gives the average number of panel modes in a particular frequency band, but also, together with the

shape and boundary conditions of the panel, specifies the resonance frequencies. The average number of the the panel modes in the region of a resonance frequency of a cavity mode governs the overall nature of the coupling behavior, while the distribution of panel resonance frequencies determines the details of the coupling effect. The modal densities of the cavity and of two aluminum panels of different thicknesses are plotted in Figure 3.4. The first few resonance frequencies of the cavity modes are within the frequency range from 150 Hz to 280 Hz. When the panel modal density is very small, very few or no panel modes will couple with the cavity modes. As panel modal density becomes higher, more panel modes may participate in the coupling with cavity modes.

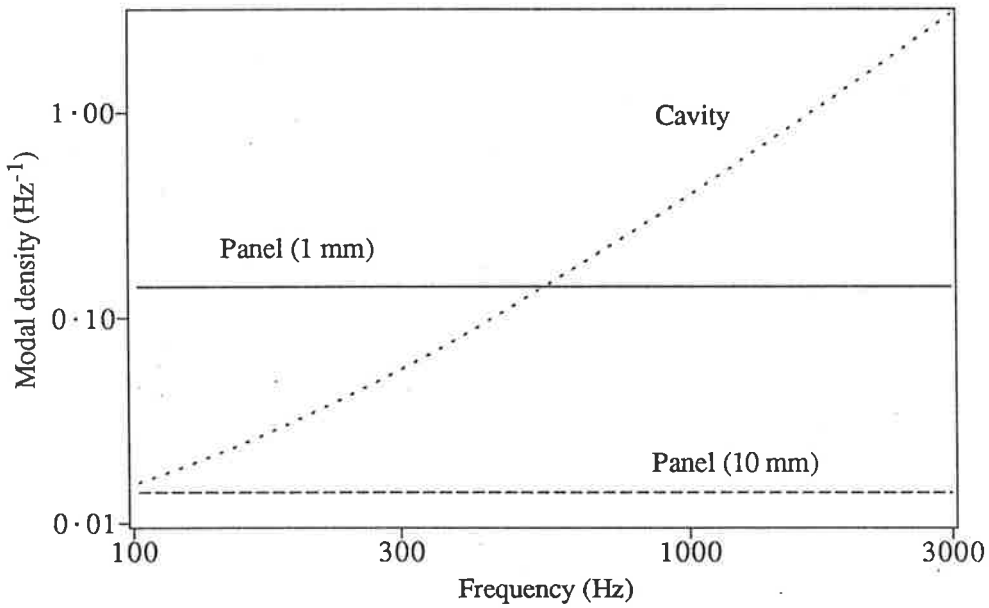

Figure 3.4: Modal densities of the cavity and of the panels (Aluminum panel $C_L = 5150$ m/s).

The properties of first six cavity controlled acoustical modes have been calculated as functions of panel modal density by the orthogonal expansion method (Eq. 3.24). Forty panel modes and forty cavity modes have been used. All cavity modes are assumed to have a 15 second decay time, and all panel modes are assumed to have a 0.5 second decay time. The panel radiation is neglected. Figure 3.5 shows the variation in the decay time of the acoustical modes with panel modal density. When the panel modal density is high, and particularly for those panel modal densities, where no panel modes are well coupled with the cavity mode, the accuracy of the results from this method is limited because of the limited number of modes used in the calculation.

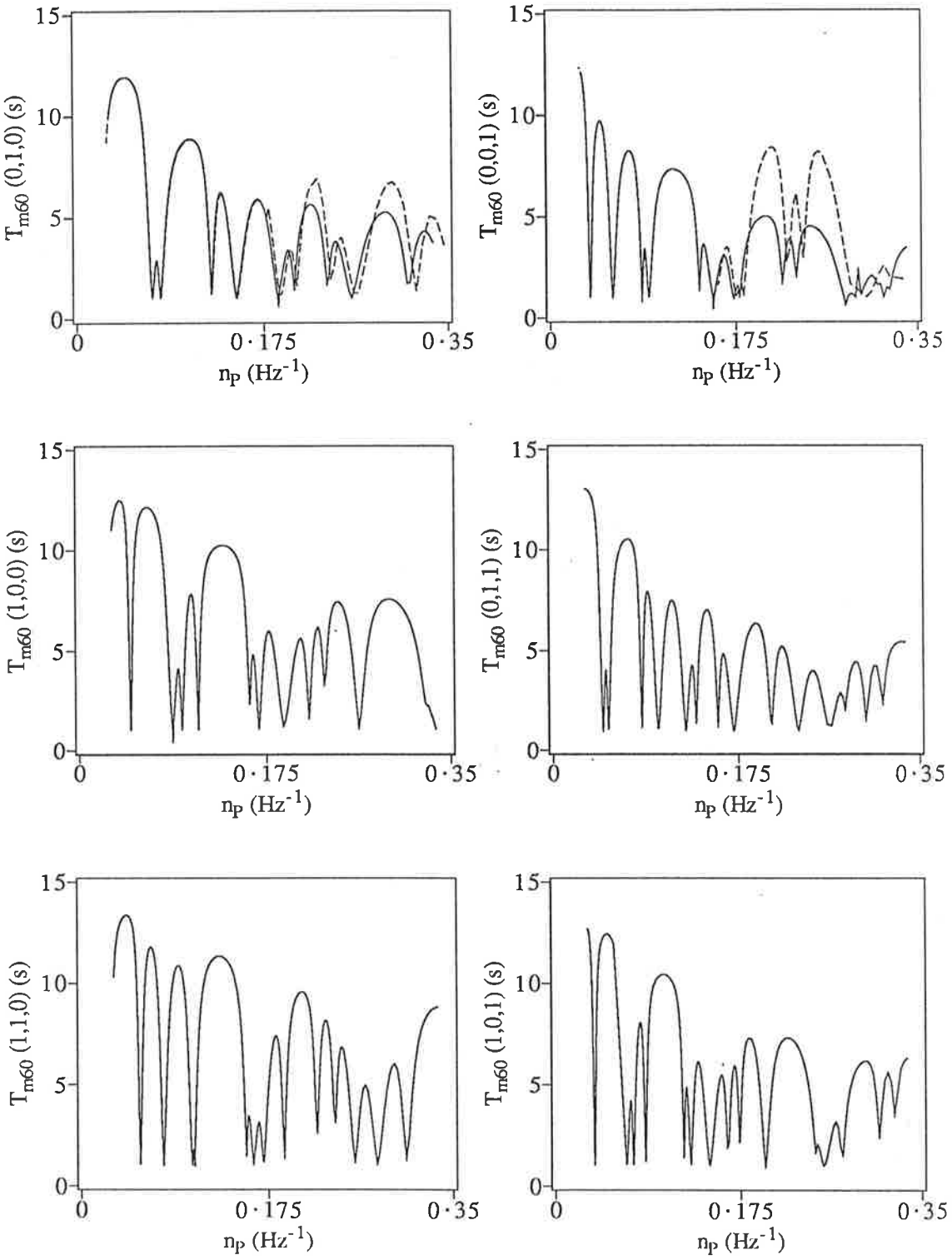

Figure 3.5: Decay times of the first few cavity controlled modes. (- - -) orthogonal expansion method; (——) successive iteration method (T_{aN} = 15.0 sec and T_{pM} = 0.5 sec).

There are two extreme conditions of cavity-panel mode coupling. The first one is where a panel mode and a cavity mode are well coupled. In this case, the energy transfer between the sound field and the panel is almost entirely between these two modes. The behavior of the resultant acoustic mode and the energy flows between different parts of the modes are well approximated by considering the coupling of a few modes even when only including those two well coupled modes. The second condition is where none of the panel modes are well coupled with the cavity mode. For this case, the energy transfer from the cavity mode is distributed over many panel modes, and the cavity controlled acoustical mode contains components from many panel and cavity modes of similar importance. Therefore, if only a small number of uncoupled modes is used in the analysis, some important modes may be excluded and errors may develop in the calculation of modal decay time. For these situations, the alternative method of successive iteration (Eq.(3.29)) has been used, because the number of panel modes is not limited by the computer memory capacity in this method. For example, in the calculation of Figure 3.5, 100 panel modes were used.

It is shown in Figure 3.5, that as the panel modal density is increased, the decay time of each mode has a relative minimum. On the average, the decay time is longer in the low panel density region, and it becomes shorter as the panel modal density is increased. Figure 3.6 shows the transfer factor between cavity mode (0,0,1) and the first 14 panel modes (with non zero coupling coefficients) as a function of panel modal density. In the region of the maximum values of the transfer factor, there is large energy transfer and maximum sound absorption by the panel. These peaks correspond to the decay time minima of cavity controlled mode (0,0,1) in Figure 3.5.

When the panel modal density is small, only very few panel modes lie in the effective frequency region of the examined cavity mode and the energy transfer of the cavity mode into the panel will usually be dominated by a single panel mode. The influence of the higher order panel modes upon the energy transfer is small. This is shown in Figure 3.6. Unless one panel mode happens to satisfy the well coupled condition with the examined cavity mode, the coupling between the cavity mode and the panel is generally very poor. Therefore, in this region of panel modal density, the modal decay time is long except for a few special regions where the well coupled condition is satisfied. When the panel density becomes high, Figure 3.6 shows that more panel modes (both low order and high order) participate in the coupling with the examined cavity mode. In this case, the cavity mode will have more panel modes to

couple with. Therefore on average the resulting cavity controlled modes have smaller decay times.

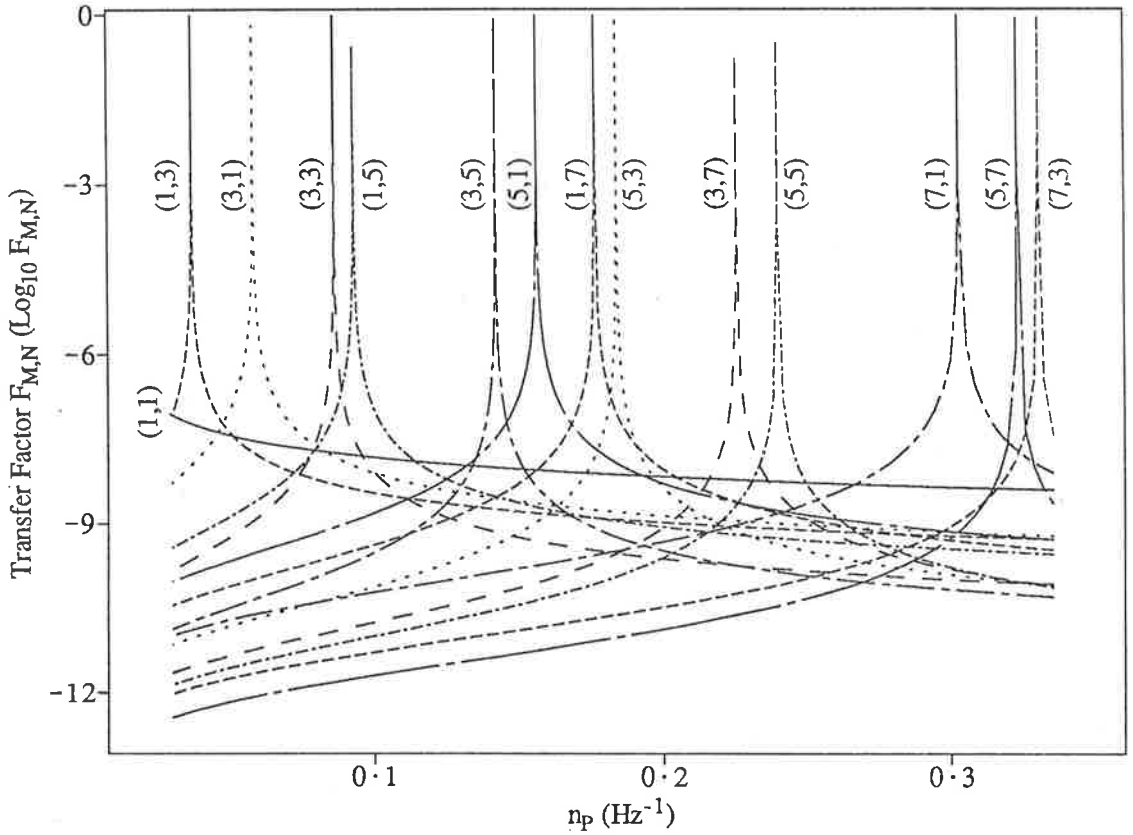

Figure 3.6: The transfer factor $F_{M,N}$ between (0,0,1) cavity mode and panel modes as a function of panel modal density.

The details of the calculated modal decay curves (Figure 3.5) in the region of minimum decay time are of special interest. The minimum modal decay time indicates maximum sound absorption by the panel. As panel modal density increases within this region, the resonance frequency of the cavity controlled mode "jumps" to a higher frequency (see Figure 3.7).

In order to explain the physical mechanism of this behaviour, we must compare the motion of the panel with the motion of the sound field and the panel energy with the energy in the sound field. A calculation of the eigenvector of an acoustical mode from Eq. (3.20) can provide some insight into this relative motion and this relative energy content. The eigenvector of an acoustical mode determines the distribution of the sound field and the distribution of the panel vibration for that mode according to Eqs. (3.25) and (3.26).

The relative motion of the sound field and panel vibration of the Nth acoustical mode is described by the specific acoustical transfer impedance Z_{apN}, which is sound pressure divided by panel velocity. In terms of the acoustical velocity potential Ψ_N and the displacement W_N of the Nth mode, Z_{apN} is written as

$$Z_{apN} = -\rho_o \frac{\Psi_N}{W_N}. \tag{3.44}$$

When Ψ_N is evaluated at the same point as W_N, Z_{apN} is the specific acoustical impedance at this point.

Similarly, the ratio of sound field energy to panel vibration energy E_{aN}/E_{pN} of the Nth mode is given by,

$$\frac{E_{aN}}{E_{pN}} = \frac{1}{C_o^2}\left(\frac{\rho_o V}{\rho h A_f}\right)\frac{<\overline{\Psi_N \Psi_N^*}>}{<\overline{W_N W_N^*}>}, \tag{3.45}$$

where Ψ_N^* and W_N^* are the complex conjugates of Ψ_N and W_N respectively.

The energy ratios of two selected acoustical modes are shown in Figure 3.8(a) as a function of panel modal density. The resonance frequencies and the 60 dB decay times of these two modes are shown in Figures 3.8(b)and (c). For comparison, the resonance frequencies of the corresponding cavity mode and panel mode are also shown in Figures 3.8(b).

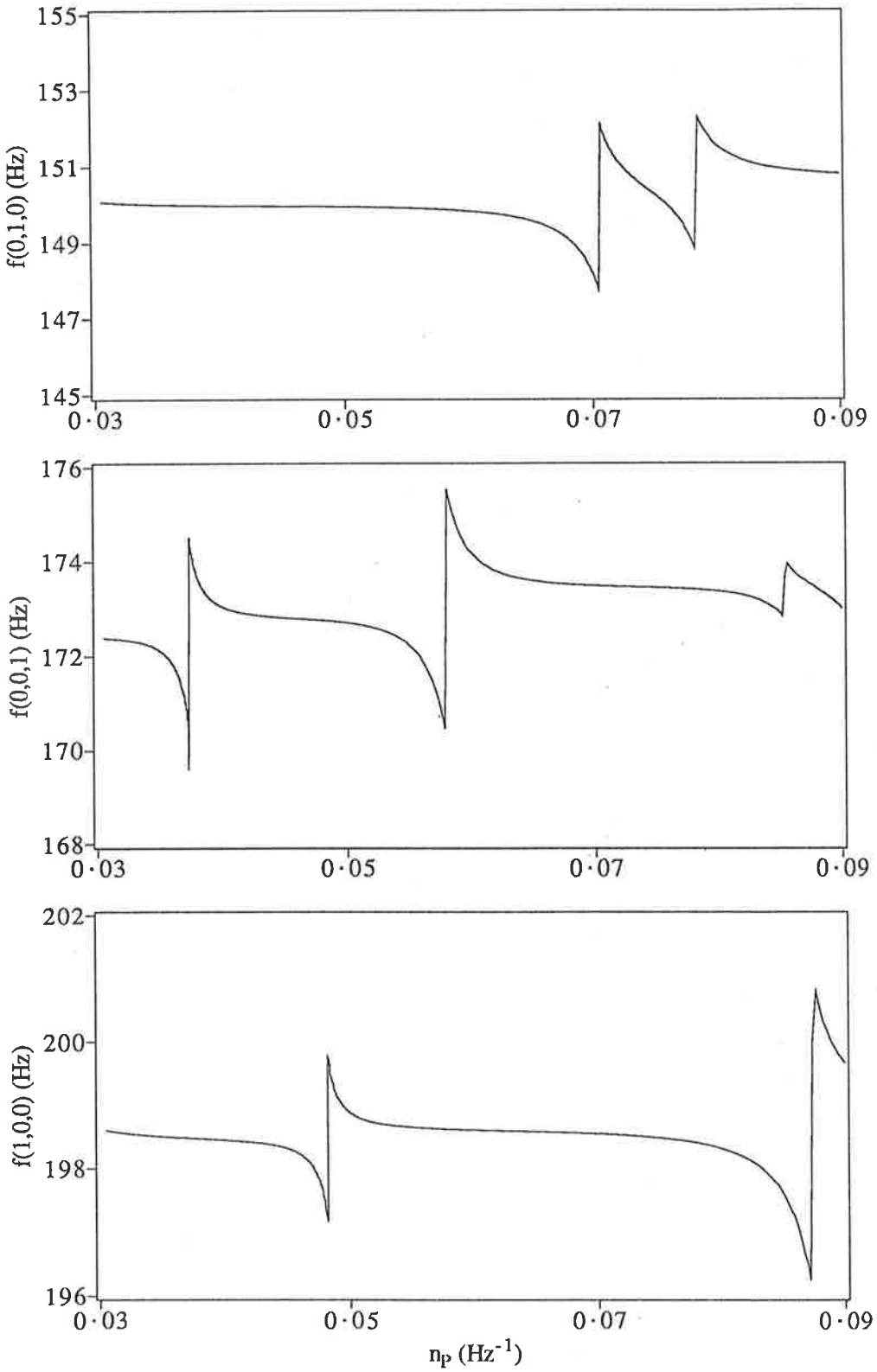

Figure 3.7: Resonance frequencies of the first few cavity controlled modes as a function of panel modal density; Calculated by successive iteration method ($T_{aN} = 15.0$ s and $T_{pM} = 0.5$ s).

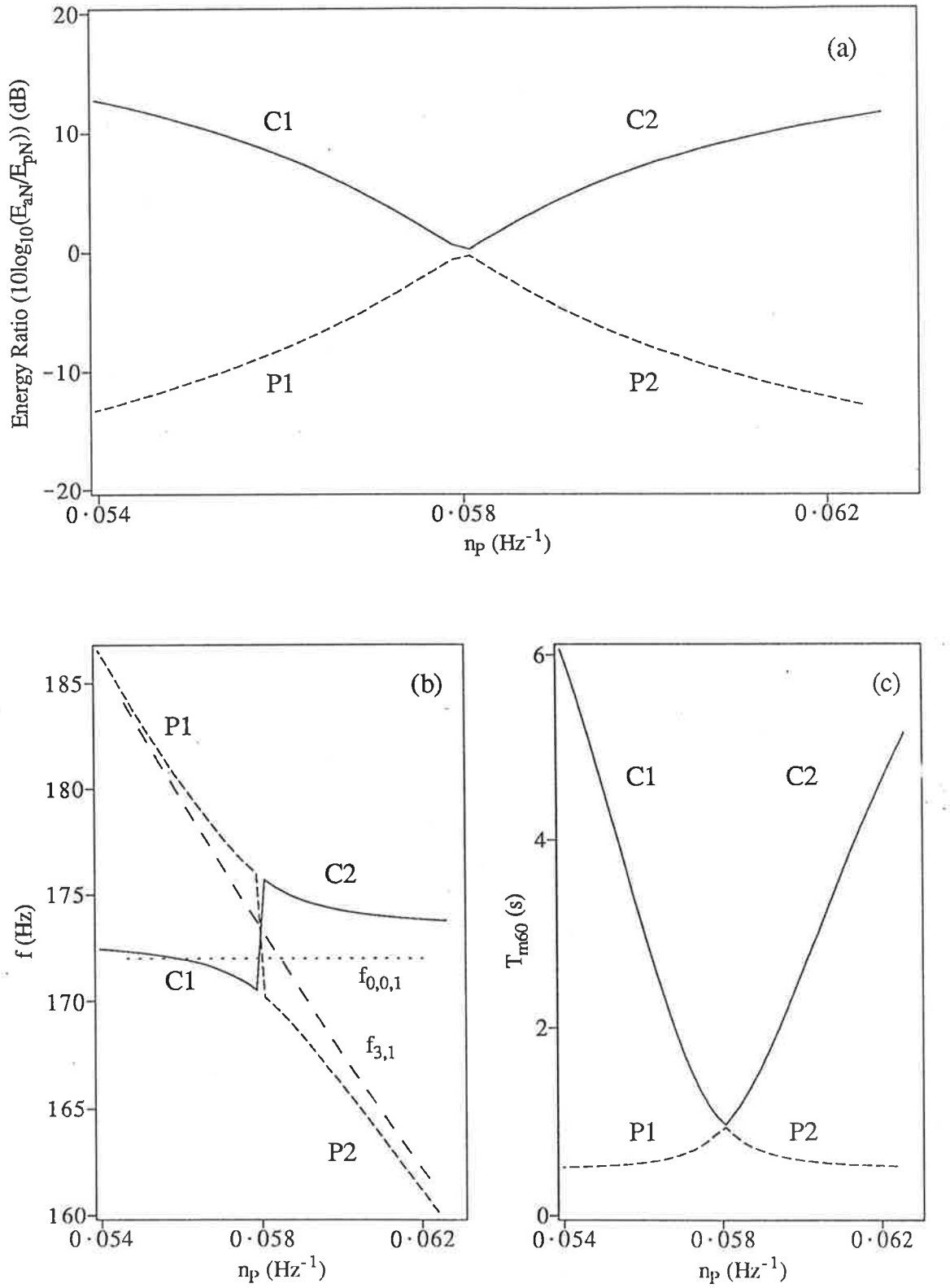

Figure 3.8: (a) Ratio of sound field energy to the panel vibration energy for two acoustical modes — (0,0,1) cavity controlled mode and (3,1) panel controlled mode; (b) Resonance frequencies of the two acoustical modes, and of the uncoupled (0,0,1) cavity mode $f_{0,0,1}$ and (3,1) panel mode $f_{3,1}$; (c) 60 dB modal decay times.

The solid curve in Figure 3.8 represents the cavity controlled mode and consists of two parts labelled C1 and C2. The dashed curve represents the panel controlled mode and is labelled P1 and P2. These two curves meet at a point where *sound* absorption of the cavity controlled mode is maximum. When not in the vicinity of the point of maximum sound absorption (which corresponds a peak in Figure 3.6, e.g. (3,1) in this case), the difference between a cavity controlled mode and a panel controlled mode can easily be distinguished from the energy ratio, but near this point, the energy ratios of the two types of modes are indistinguishable. Near the maximum sound absorption point, each part (panel and cavity) of the panel controlled mode has the same amount of energy, and each part of the cavity controlled mode has the same amount of energy.

Therefore, for white noise excitation in the cavity, we expect to find two spectral peaks in the sound field when the modal density of the panel is close to the value for maximum sound absorption and the amplitudes of these peaks will be approximately equal.

The curves in Figures 3.8 (a), (b) and (c), are obtained by considering forty cavity modes and forty panel modes. Table 3.2 lists the coefficient amplitudes of those uncoupled modes for a panel modal density of $n_p = 0.056\text{Hz}^{-1}$. It shows that the cavity part of the vibrating system is dominated by the (0,0,1) cavity mode, and the panel part is dominated by the (3,1) panel mode. Therefore it is convenient to call these acoustical modes the "(0,0,1) cavity controlled mode" and the "(3,1) panel controlled mode".

The curves in Figure 3.8(a) also show that the "P2" part of the panel controlled mode is a continuation of the "C1" part of the cavity controlled mode. Similarly, the "C2" part of the cavity controlled mode is a continuation of the "P1" part of the panel controlled mode.

The minimum decay time of the (0,0,1) cavity controlled mode (see in Figures 3.8 and 3.5) in the region ($0.054\ \text{Hz}^{-1} < n_p < 0.062\ \text{Hz}^{-1}$) is due mainly to the coupling of the (0,0,1) cavity mode and the (3,1) panel mode. In this region the transfer factor of these modes has a maximum (Figure 3.6). This coupling of the cavity mode and the panel mode strongly affects a *pair* of acoustical modes, one of which is the (0,0,1) cavity controlled mode and the other is the (3,1) panel controlled mode.

The resonance frequencies of the cavity controlled mode and the panel controlled mode in Figure 3.8(b) show some interesting changes in the minimum decay time region. On the left

of the minimum point, the resonance frequency of the (0,0,1) cavity controlled mode is lower than that of (0,0,1) cavity mode, but the resonance frequency of the (3,1) panel controlled mode is higher than that of the (3,1) panel mode. On the right side of this point, these inequalities are reversed. The resonance frequencies "jump" across the minimum decay time point. This "jump" can be partly explained by the phase change of the specific acoustical transfer impedance.

The coupling of a cavity and a panel mode is analogous to the coupling of two single degree of freedom oscillators. As is well known (Morse and Ingard 1968c), such coupling produces two new coupled modes in which the oscillators either move in phase at a resonance frequency lower, or in opposite phase at a resonance frequency higher than that of either oscillator taken individually. This indicates that the jump of the resonance frequency across the minimum decay time point is associated with a jump in the phase of the specific acoustical transfer impedance.

Figure 3.9(a1) shows the specific acoustical transfer impedance between location $(0, 0, 0)$ m in the cavity and location $(0.434, 0.575)$ m on the panel for the two acoustical modes as a function of the panel modal density. Figure 3.9(b1) shows the calculated specific acoustical impedance of the panel surface at (0.434,0.575) m for the same modes.

Figure 3.9(a2) and (b2) shows the phase of the transfer impedance and the impedance for each acoustical mode. Both the cavity controlled mode and the panel controlled mode have a impedance phase jump at the point of maximum sound absorption.

This phase jump indicates a change of the impedance state. (An impedance can be in a stiffness, resonance or mass controlled state.) However, unlike the coupling of two single degree of freedom oscillators, the transfer impedance is a function of location and so the phase of the specific acoustical impedance varies over the panel surface. At one position Z_{apN} could be mass controlled, and at another position it could be stiffness controlled. Therefore, whether the resulting resonance frequency of the cavity controlled acoustical mode will be higher or lower than that of the uncoupled cavity mode depends upon the integrated contribution of the distributed specific acoustic impedance from every point on the panel surface.

Table 3.2: Amplitudes of the components of (0,0,1) cavity controlled mode and the (3,1) panel controlled mode ($h = 6$mm)

cavity controlled mode				panel controlled mode			
sound field		panel vibration		sound field		panel vibration	
(l,m,n)	amplitude	(u,v)	amplitude	(l,m,n)	amplitude	(u,v)	amplitude
(0,0,0)	0.378	(1,1)	2.71×10^{-02}	(0,0,0)	5.64	(1,1)	3.46×10^{-02}
(0,1,0)	5.75×10^{-14}	(1,2)	1.24×10^{-17}	(0,1,0)	6.05×10^{-13}	(1,2)	2.40×10^{-17}
*(0,0,1)	238.	(2,1)	6.33×10^{-17}	*(0,0,1)	120.	(2,1)	1.71×10^{-16}
(1,0,0)	4.31×10^{-13}	(1,3)	1.57×10^{-02}	(1,0,0)	1.69×10^{-12}	(1,3)	7.93×10^{-03}
(0,1,1)	3.65×10^{-14}	(2,2)	1.04×10^{-17}	(0,1,1)	6.35×10^{-13}	(2,2)	5.65×10^{-17}
(1,1,0)	9.95×10^{-16}	(2,3)	3.18×10^{-15}	(1,1,0)	1.05×10^{-14}	(2,3)	3.64×10^{-15}
(1,0,1)	9.63×10^{-14}	*(3,1)	9.74×10^{-02}	(1,0,1)	1.07×10^{-13}	*(3,1)	0.355
(0,2,0)	0.437	(1,4)	2.59×10^{-16}	(0,2,0)	1.92	(1,4)	9.64×10^{-15}
(1,1,1)	1.16×10^{-15}	(3,2)	9.14×10^{-16}	(1,1,1)	6.60×10^{-15}	(3,2)	3.10×10^{-14}
(0,0,2)	0.252	(2,4)	6.11×10^{-18}	(0,0,2)	4.28	(2,4)	2.95×10^{-17}
(0,2,1)	0.586	(3,3)	2.15×10^{-03}	(0,2,1)	2.53	(3,3)	1.19×10^{-03}
(1,2,0)	6.68×10^{-14}	(1,5)	2.96×10^{-03}	(1,2,0)	8.43×10^{-14}	(1,5)	1.83×10^{-03}
(0,1,2)	7.42×10^{-13}	(4,1)	9.44×10^{-18}	(0,1,2)	1.14×10^{-13}	(4,1)	2.87×10^{-17}
(2,0,0)	1.42	(3,4)	1.89×10^{-19}	(2,0,0)	4.58	(3,4)	4.68×10^{-18}
(1,0,2)	2.84×10^{-14}	(2,5)	5.16×10^{-18}	(1,0,2)	3.29×10^{-14}	(2,5)	1.06×10^{-17}
(1,2,1)	1.04×10^{-13}	(4,2)	8.36×10^{-19}	(1,2,1)	1.27×10^{-13}	(4,2)	2.38×10^{-18}
(2,1,0)	1.30×10^{-14}	(4,3)	5.79×10^{-19}	(2,1,0)	6.65×10^{-14}	(4,3)	6.57×10^{-18}
(1,1,2)	4.33×10^{-16}	(1,6)	1.08×10^{-18}	(1,1,2)	6.35×10^{-16}	(1,6)	6.69×10^{-18}
(2,0,1)	2.32	(3,5)	3.31×10^{-04}	(2,0,1)	7.41	(3,5)	1.58×10^{-04}
(0,3,0)	4.22×10^{-15}	(2,6)	1.56×10^{-17}	(0,3,0)	9.37×10^{-14}	(2,6)	1.24×10^{-17}
(0,2,2)	0.294	(4,4)	1.66×10^{-17}	(0,2,2)	1.25	(4,4)	2.84×10^{-17}
(2,1,1)	2.24×10^{-14}	(5,1)	8.03×10^{-04}	(2,1,1)	1.13×10^{-13}	(5,1)	3.37×10^{-04}
(0,3,1)	8.35×10^{-15}	(5,2)	2.29×10^{-17}	(0,3,1)	1.60×10^{-13}	(5,2)	2.23×10^{-17}
(1,3,0)	7.14×10^{-16}	(1,7)	4.17×10^{-04}	(1,3,0)	2.10×10^{-15}	(1,7)	2.45×10^{-04}
(2,2,0)	0.456	(3,6)	1.64×10^{-17}	(2,2,0)	1.83	(3,6)	1.54×10^{-17}
(1,2,2)	6.19×10^{-14}	(5,3)	1.80×10^{-04}	(1,2,2)	7.87×10^{-14}	(5,3)	9.77×10^{-05}
(0,0,3)	9.45×10^{-02}	(4,5)	9.24×10^{-18}	(0,0,3)	1.57	(4,5)	3.32×10^{-17}
(1,3,1)	8.17×10^{-16}	(2,7)	2.92×10^{-17}	(1,3,1)	9.68×10^{-16}	(2,7)	1.10×10^{-17}
(2,0,2)	1.48	(5,4)	1.88×10^{-17}	(2,0,2)	4.70	(5,4)	2.56×10^{-17}
(2,2,1)	0.802	(4,6)	7.27×10^{-17}	(2,2,1)	3.22	(4,6)	8.00×10^{-17}
(0,1,3)	3.50×10^{-15}	(6,1)	3.57×10^{-17}	(0,1,3)	4.68×10^{-14}	(6,1)	7.32×10^{-17}
(2,1,2)	1.56×10^{-14}	(3,7)	8.46×10^{-05}	(2,1,2)	7.93×10^{-14}	(3,7)	3.93×10^{-05}
(1,0,3)	1.31×10^{-14}	(1,8)	7.24×10^{-18}	(1,0,3)	1.59×10^{-14}	(1,8)	3.31×10^{-17}
(0,3,2)	5.03×10^{-15}	(6,2)	2.62×10^{-17}	(0,3,2)	1.10×10^{-13}	(6,2)	1.42×10^{-16}
(1,1,3)	3.75×10^{-16}	(5,5)	6.18×10^{-05}	(1,1,3)	7.51×10^{-16}	(5,5)	3.11×10^{-05}
(3,0,0)	4.23×10^{-15}	(2,8)	5.42×10^{-17}	(3,0,0)	2.77×10^{-15}	(2,8)	6.50×10^{-17}
(0,2,3)	0.160	(6,3)	3.83×10^{-17}	(0,2,3)	0.674	(6,3)	2.87×10^{-17}
(0,4,0)	6.37×10^{-02}	(4,7)	5.55×10^{-17}	(0,4,0)	0.117	(4,7)	1.36×10^{-16}
(2,3,0)	2.76×10^{-15}	(6,4)	3.63×10^{-18}	(2,3,0)	2.62×10^{-14}	(6,4)	6.39×10^{-17}
(1,3,2)	9.26×10^{-16}	(3,8)	2.00×10^{-17}	(1,3,2)	1.18×10^{-15}	(3,8)	3.30×10^{-17}

* dominant modes

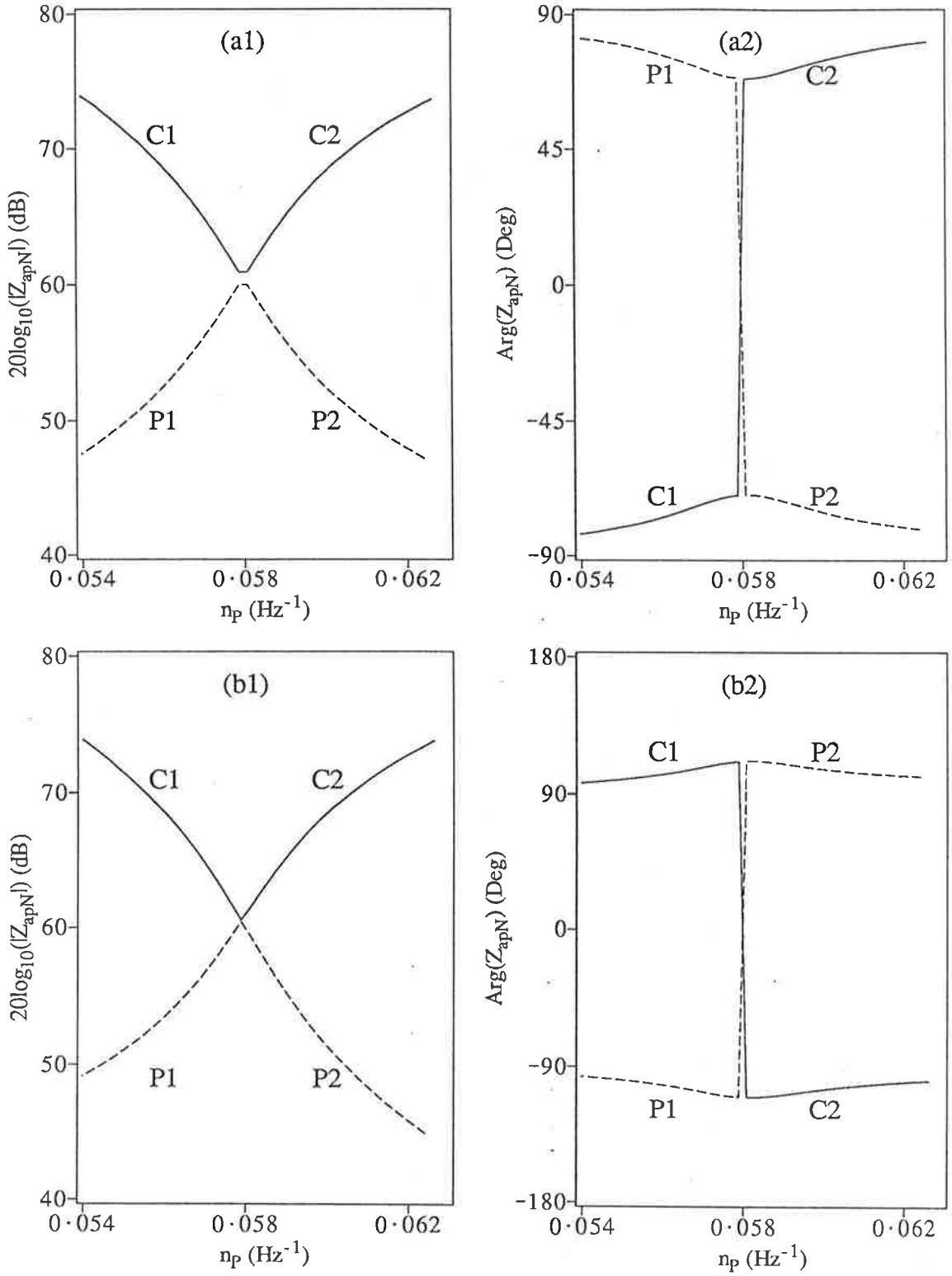

Figure 3.9: (a1) and (a2): acoustical specific transfer impedance of two acoustical modes (from (0.868,1.150,0.0) m to (0.434,0.575) m). (b1) and (b2): acoustical specific impedance at (0.434,0.575). (——) cavity controlled mode (0,0,1), (- - -) panel controlled mode (3,1). ($|Z_{apN}|$ and $\mathrm{Arg}(Z_{apN})$ are the amplitude and the phase angle of Z_{apN}).

It is clear from Figures 3.8 and 3.9 that the "P2" part of the panel controlled mode is a continuation of the "C1" part of the cavity controlled mode, and that the "C2" part of the cavity controlled mode is a continuation of the "P1" part of the panel controlled mode. The continuous change from curve "P1" to curve "C2" and from curve "C1" to curve "P2" indicates that "P1" and "C2" represent just one acoustical mode and that "C1" and "P2" represent a second acoustical mode. As the panel modal density increases and passes through the maximum sound absorption point, the first acoustical mode changes from cavity controlled to panel controlled. The second acoustical mode is initially panel controlled, but when it crosses the maximum sound absorption point it becomes cavity controlled.

If we only measure the sound pressure level in the cavity or if we only measure the panel acceleration, then we only observe one part of the coupled system. In a measurement of the cavity sound field it is the cavity controlled modes which are most easily observed. Naturally, when the panel vibration is measured, the panel controlled modes are easier to resolve. Experimentally, there is a jump in phase of the transfer impedance and resonance frequency of the observed mode as the panel modal density is varied across the maximum sound absorption point. However this jump is due to two simultaneous transitions. One transition is of a panel controlled mode into a cavity controlled mode, and the other is from a cavity controlled mode into a panel controlled mode.

3.5.3 Panel internal damping

The mechanical damping of the panel is represented in the calculation by the modal decay times of the uncoupled panel modes. The decay time of a cavity controlled mode can be directly related to the modal decay time of the uncoupled panel. Figures 3.10 and 3.11 show respectively the resonance frequencies and modal decay times of the first few cavity controlled modes as a function of the decay time of the panel modes (T_{pM}). In the calculation, the thickness of the aluminum panel is 6 mm and the decay time of the uncoupled cavity modes is 15 seconds. The decay time of every uncoupled panel mode is assumed to be equal. As the panel damping increases (T_{pM} decreases), the decay times of the cavity controlled modes decrease and approach a minimum. After this minimum, the decay times increase and tend to those of the uncoupled cavity modes. The resonance frequencies of the cavity controlled modes vary as the panel damping increases, but eventually they approach the uncoupled cavity resonance frequencies.

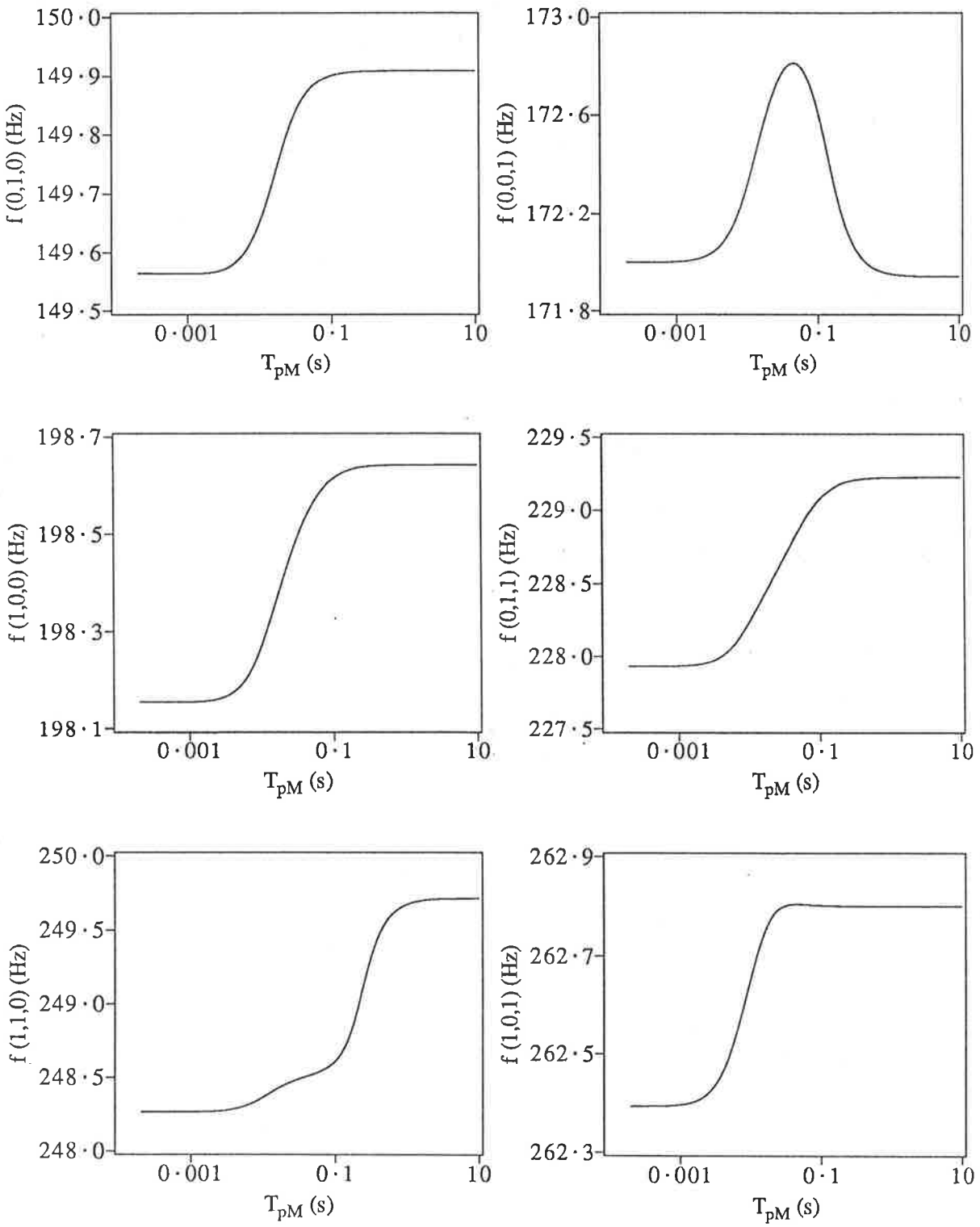

Figure 3.10: Resonance frequencies of the cavity controlled modes as a function of panel modal decay time; (h = 6 mm, T_{aN} = 15.0 s).

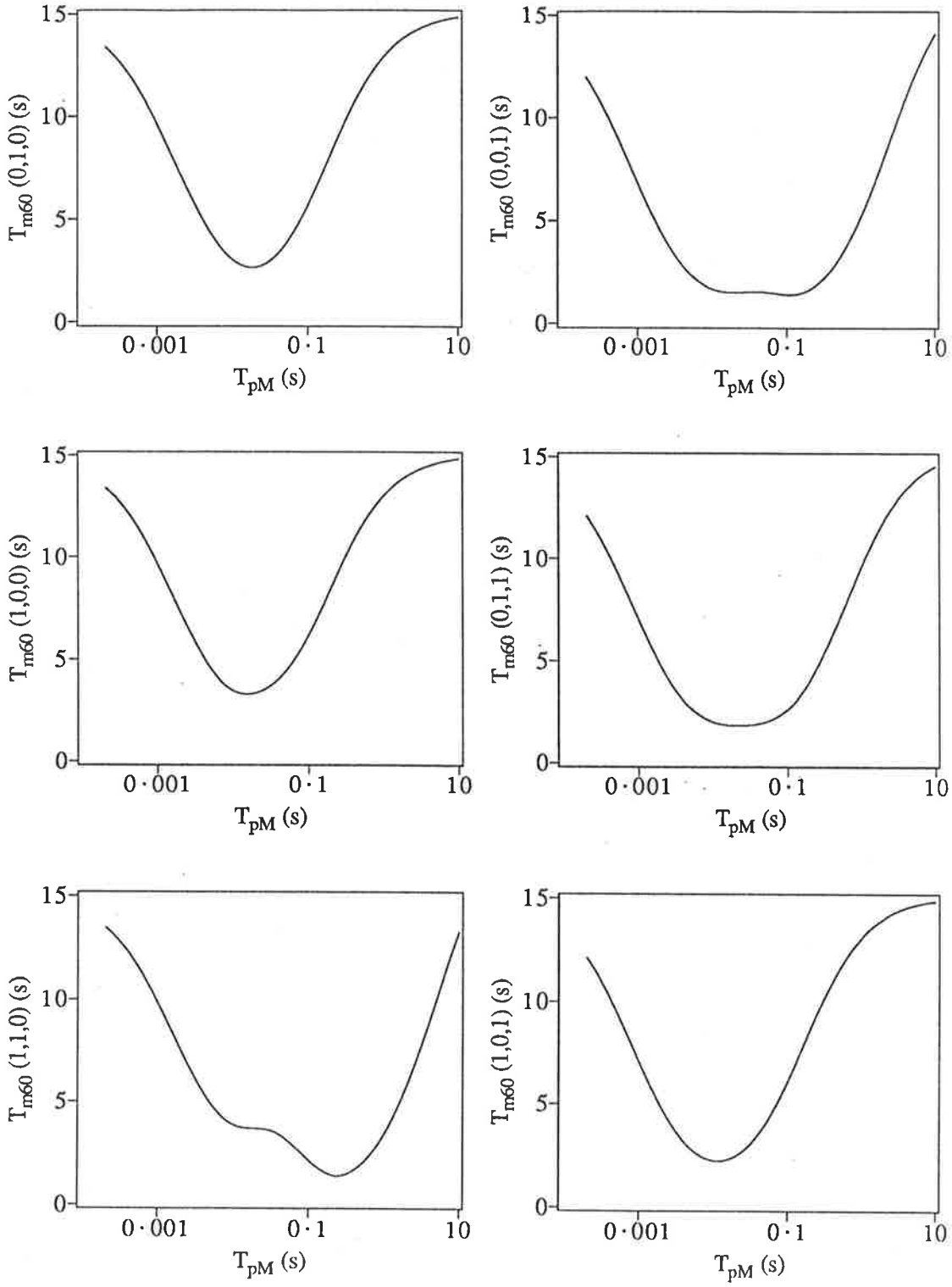

Figure 3.11: Decay times of the cavity controlled modes as a function of panel modal decay time; (h = 6 mm, T_{aN} = 15.0 s).

Panel damping is a measure of not only the ability of the panel to dissipate energy, but also its tendency to resist acquiring vibrational energy. Until the minimum decay time is reached, more and more energy is dissipated in the panel as its damping is increased, As the damping is increased further, it effectively restricts the motion of the panel and eventually the panel becomes rigid. Therefore no energy will be transferred from the sound field in the cavity into the panel and the modal characteristics of the cavity will not be affected.

The resonance frequencies and decay times of each acoustical mode (Figures 3.10 and 3.11) have different characteristics. For example, some curves in Figure 3.10 are monotonic and one of them has a maximum. According to Eq.(3.29), the first order approximation of the panel influence on the eigenvalue of the Nth cavity controlled mode is described by $U_{N,N}$ (Eq. (3.30)). The real part of $U_{N,N}$ modifies the resonance frequency of the mode and the imaginary part of $U_{N,N}$ affects its modal decay time. $U_{N,N}$ contains the contributions of all the panel modes. Among the nonzero terms in the summation of Eq.(3.30), those panel modes which have lower resonance frequencies than that of the cavity mode make a positive contribution (increase) to the resulting resonance frequency of the acoustical mode. On the other hand, the panel modes with higher resonance frequencies make a negative contribution (decrease) to the resonance frequency. The shift in resonance frequency is due to the combined effect of all the panel modes. Figure 3.12 shows the first few nonzero terms in $U_{N,N}$ which were used for the calculation of the eigenvalue of the (0,0,1) cavity controlled mode shown in Figure 3.10. For very small panel damping ($T_{pM} \approx 10$sec), the real part of the modification term $U_{N,N}$ for the (1,1) and (3,1) panel modes have comparable amplitudes but opposite signs. The net effect is to *slightly* reduce the resonance frequency. As panel damping increases ($T_{pM} \approx 0.1$sec) the influence of the (3,1) panel mode disappears, and only the effect of the (1,1) mode, which increases the resonance frequency, remains. As the panel damping increases further ($T_{pM} \approx 0.001$sec), the panel behaves as a rigid wall. Neither panel mode will affect the resonance frequency and the (0,0,1) acoustical mode degenerates into the (0,0,1) cavity mode. Figure 3.12 also shows the imaginary part of the first few terms of $U_{N,N}$ for (0,0,1) cavity controlled mode. The large peak values for the (1,1) and (3,1) modes are responsible for the two minima in the resulting modal decay time curve of the (0,0,1) mode (Figure 3.11).

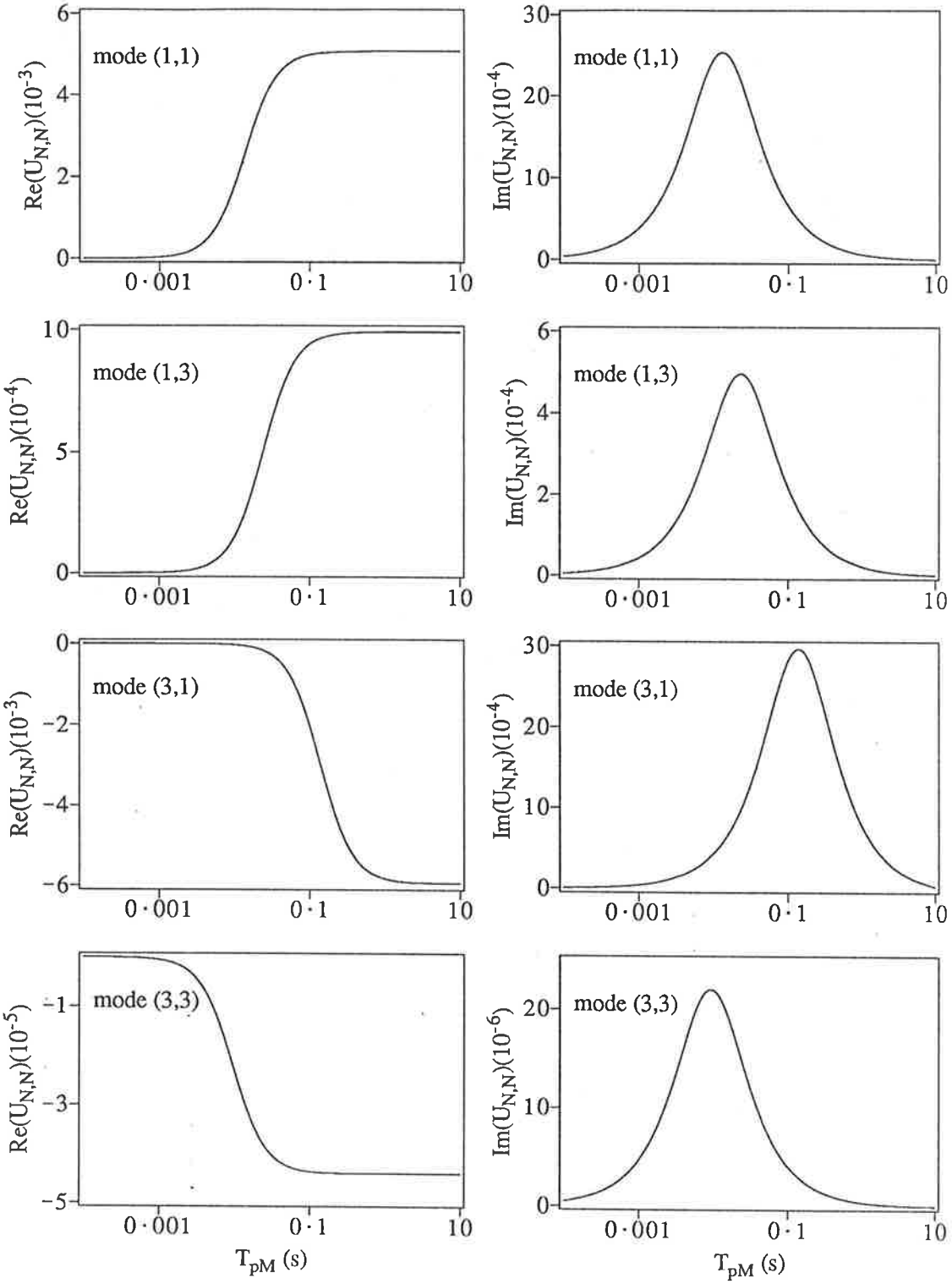

Figure 3.12: Real and imaginary parts ($\mathrm{Re}(U_{N,N})$, $\mathrm{Im}(U_{N,N})$) of the components in $U_{N,N}$ as a function of panel modal decay time T_{pM}, (N = (0,0,1))

3.5.4 Panel radiation

In previous studies of the structure-cavity coupling problem, external radiation from the panel was assumed to be negligible (Pretlove 1965a, Guy 1979a). Up to this point, the effect of panel radiation upon the characteristics of the acoustical modes has been neglected. In this section, this effect will be incorporated into the calculation of the eigenvalues (i.e resonance frequencies and modal decay times). Comparison with the results which exclude panel radiation effect, reveals the conditions determining the importance of external panel radiation.

The influence of panel radiation can be included into the calculation of the complex eigenvalues of the cavity controlled modes by adding an extra term Δ_N^{Pr} (given by Eq. (3.35)) to Eq. (3.29). The virtual mass terms $\sigma_{Im}(M,N)$ are neglected from Eq. (3.35) and the radiation efficiency $\sigma_{Re}(M,N)$ for Nth cavity controlled mode is estimated at the resonance frequency of the Nth cavity mode.

The 60 dB decay times of the first three cavity controlled modes are shown in Figure 3.13 as a functions of panel modal density. In part (a), the decay times of the cavity modes and the panel modes are 15 seconds and 5 seconds respectively. The curves obtained by considering the panel radiation modification term are shown as solid lines. Comparison of the dashed curves (neglect the panel radiation) with the solid curves shows that the panel radiation contribution to the modal decay times increases as the panel modal density increases (or as the panel thickness decreases).

According to the mass law for sound transmission loss (Vér *et al.* 1971), the sound transmission loss through a panel decreases as the panel thickness decreases. This means that more energy is transmitted through the panel to external space. This increased energy loss to the external space results in increased sound absorption by the panel, and so decreased modal decay times.

The effect of the panel radiation upon the modal decay time is different for different cavity controlled modes. For example, decay time of the (0,0,1) cavity controlled mode is more strongly affected by the panel radiation than other modes shown in Figure 3.13(a). The panel vibration part of (0,0,1) cavity controlled mode is dominated by volume displacement panel modes ("odd-odd" modes), such as (1,1) and (3,1). These volume displacement panel modes have higher radiation efficiencies (Fahy 1985).

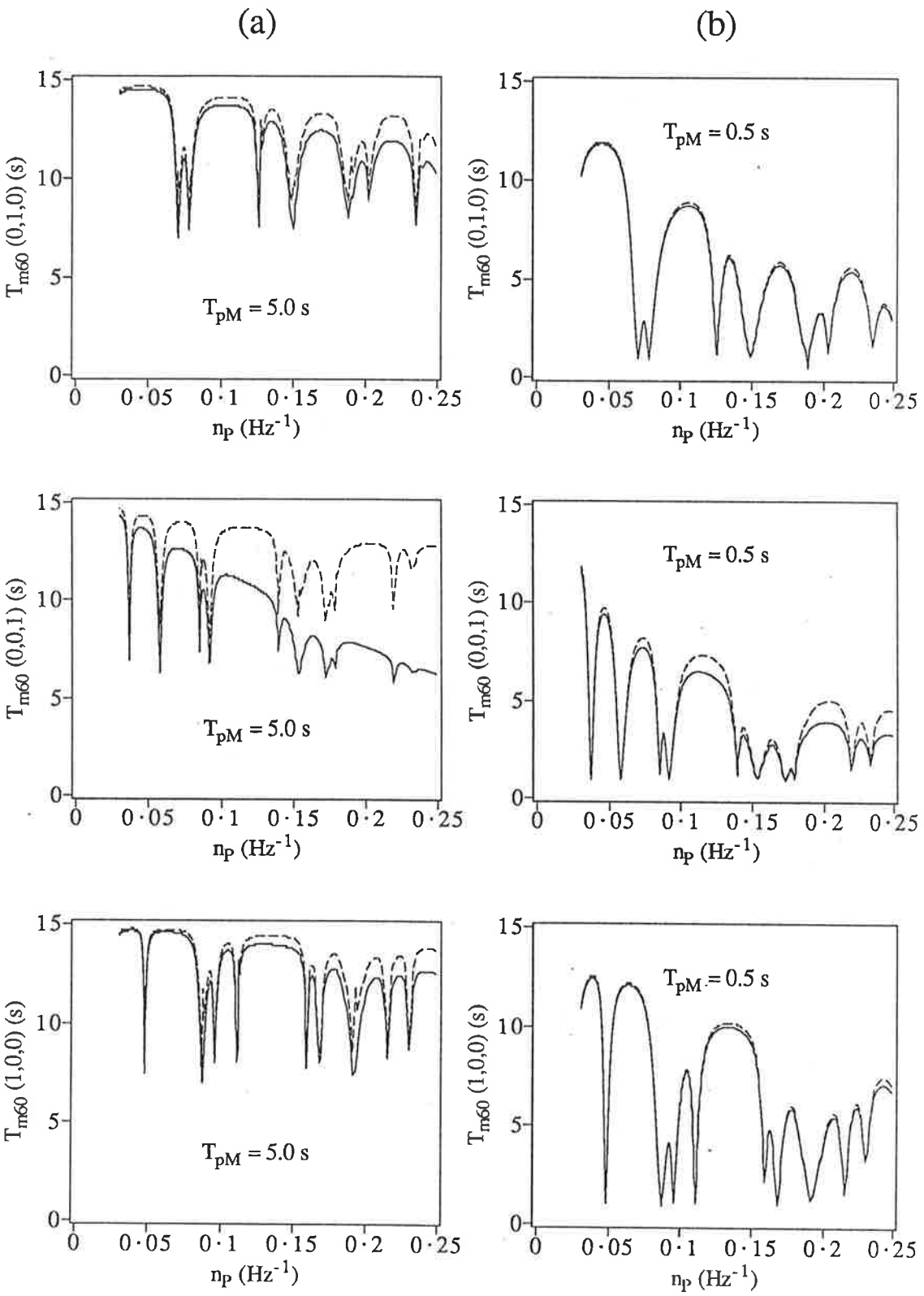

Figure 3.13: Effect of panel radiation on the decay times of cavity controlled modes, (——) with radiation effect; (- - -) without radiation effect (T_{aN} = 15.0 sec).

Figure 3.13(b) shows the modal decay times of the same modes as in Figure 3.13(a) except that the input decay times of the panel modes have been changed to 0.5 seconds. In this case, the panel damping increases and the contribution of the sound radiation of the panel is less important.

In the previous calculations, the panel decay times were fixed at 5.0 seconds and 0.5 seconds in (a) and (b) respectively. Figure 3.14 shows the influence of panel radiation on the decay time of the (0,0,1) cavity controlled mode as a function of reciprocal panel decay time. Both this result and that given in Figure 3.13 (b) show that the panel radiation only has minor effect on the decay times when the panel decay time is 0.5 seconds.

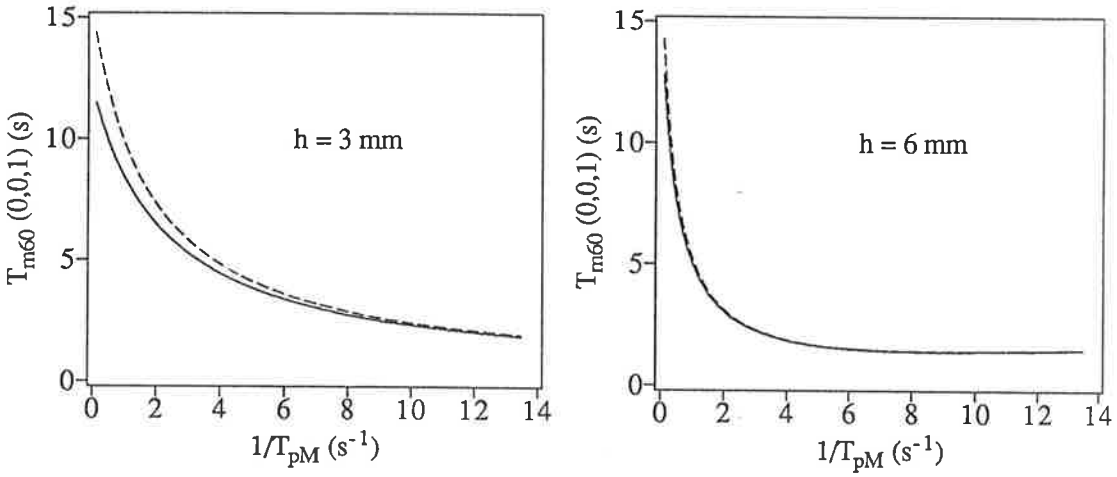

Figure 3.14: The decay time of (0,0,1) cavity controlled mode as a function of reciprocal panel modal decay time; with (——) and without (- - -) radiation effect (T_{aN} = 15.0 s).

3.6 Discussion and conclusions

This chapter describes the sound field in a cavity in terms of the coupling in a panel-cavity system. The traditional description of a sound field in an enclosure isolates the sound field from the motion of the enclosing structure and from the external sound field, and the influence of the boundary is modelled as a locally reactive acoustical impedance.

In order to correctly describe the sound field in an enclosure with modally reactive boundaries, it is necessary to consider the internal sound field, the vibration of the boundaries

and the external sound field as a single coupled system. In this system, the sound field in the enclosure cannot be modelled in isolation. The acoustical behavior of the whole system is described by acoustical modes, each of which has a sound field part and a boundary vibration part.

A modal coupling analysis has been used to investigate the free vibration of a coupled panel-cavity system. Numerical tests of this method show that the approximate solution converges rapidly and that the coupling of the panels with the cavity is weak. This approach allows calculation of the characteristics of the acoustical modes from the properties of the uncoupled cavity modes and panel modes (which are themselves based on fundamental parameters of the cavity and the panel). The geometry of the cavity and the boundaries used in this analysis is very simple, but the method of modal coupling does not in fact constrain the analysis to simple geometries. The low frequency modal behavior of a complicated enclosure can be estimated in a similar way. Numerical methods are available for finding the mode shapes of such uncoupled enclosures and boundary structures.

Modal decay times characterize the transient behavior of a system. If a sound source drives a sound field at a resonance frequency of an acoustical mode, (provided that the source is not located at a node of the mode,) the sound field will decay at the decay rate of that mode. If the sound field is driven at an off-resonance frequency, or by a band of noise, the decay response will contain contributions from more than one mode. The decay behavior of an enclosure can be obtained by analysis similar to that of Hunt *et al.* (1939). Hunt's result depends only upon the cavity modes, but the results presented here are influenced by both the cavity modes and the panel vibrations. The participation of the sound field part of panel controlled modes is not predicted by the classical model, but it can be important. The sound field component of a cavity controlled mode and a panel controlled mode can combine to form beating decays and double decay rates.

The modal decay times of the system are related to the coupling coefficients, the distribution of resonance frequencies, the panel modal density, the panel damping and the panel radiation loss to external space. In conclusion,

1. The matching or mismatching of the uncoupled mode shapes on the interacting surface of the sound field and boundary determines the possible energy transfer between these two modes. The coupling coefficients Eq. (3.18) are a measure of this matching.

2. If the mode shapes of two uncoupled modes are well matched ($B_{M,N} \neq 0$), the difference between their resonance frequencies determines the rate of energy transfer. By adjusting (or tuning) this difference, different modal decay times can be obtained. The smaller this difference is, the smaller is the modal decay time (provided that the decay rates of the uncoupled cavity modes are smaller than those of the uncoupled panel modes). The strength of interaction between two modes can be expressed as a transfer factor $F_{M,N}$. On average, the modal decays time of low frequency cavity controlled modes decrease as panel modal density increases.

3. The resonance frequency of a cavity controlled mode, can be different from that of its corresponding cavity mode. A panel mode with a particular resonance frequency will tend to "push away" (i.e. change the frequency of) the cavity modes with which it interacts.

4. As the panel modal damping is increased, the decay time of each cavity controlled acoustical mode first decreases to a minimum value, and then increase, eventually reaching the "rigid wall" value.

5. If the panel is thin and its damping is low, radiation into the external space is an important cause of sound energy loss in the cavity. Otherwise, the effect of radiation upon modal decay times is negligible. Radiation by the boundary structure into the external space can be large if the internal cavity mode is well coupled with a panel mode.

Chapter 4

Effect of fluid-structural coupling — experiments

4.1 Introduction

The classical model of the sound field in a reverberation room is based upon modal analysis and the locally reactive boundary assumption. In Chapter 2, it has been shown that this model cannot be used to predict the modal decay times when the boundaries of the room are not locally reactive. The latter work has demonstrated that the concrete walls of a typical reverberation room are extensively rather than locally reactive, and that the coupling of the room modes and wall structural modes affects the modal decay times in the room.

Chapter 3 is concerned with the formulation of a theoretical model of the modal coupling within a panel-cavity system. In parallel with this work, an experimental investigation is carried out to provide a practical view which can direct the theoretical work and to verify the predictions of the mathematical analysis.

A panel-cavity system, with five rigid walls and a flexible top panel, was used for the experiment. A similar experimental arrangement has been used by several workers. Dowell and Voss (1963) concentrated on the measurement of the influence of a backing cavity on the natural frequencies of a top panel. Fahy (1969) examined the sound radiation resistance of a vibrating panel by measuring the average sound pressure level in the cavity and acceleration

level on the panel. The sound transmission loss of a cavity backed panel was evaluated by Bhattacharya (1970).

In this Chapter, information about the properties of the uncoupled cavity and the panels used in the experiments to be described is provided. Then the general behavior of the panel-cavity system is investigated experimentally and the disturbances of the coupling to the uncoupled sound field and panel vibration are demonstrated.

The measured resonance frequencies and decay rates of the cavity controlled modes in the coupled system are compared with the predictions of the theoretical analysis discussed in Chapter 3. The comparison shows that the theoretical method can be used to predict the acoustical decay times of those rooms where the classical sound absorption model does not apply. The dependence of the decay times of the cavity controlled modes upon the characteristics of the test panel, such as the resonance frequencies, mechanical damping and radiation efficiency of the panel are also reviewed.

4.2 Description of the panel-cavity coupling system

A rectangular concrete box open at the top was formed by bolting five 0.2 m thick concrete slabs together (see Figure 4.1(a) and (b)). On its top, either a concrete lid of identical thickness as the other five walls can be put in place for the measurement of background sound absorption of the cavity, or various test panels may be mounted for experimental investigation. The coordinates and the internal dimensions of the cavity are the same as described in Chapter 3 (see Figure 3.1). The inside surfaces of the cavity are smooth and have been left unpainted. All the joins between the slabs are sealed with plasti-bond to prevent air leaks.

The sound field in the cavity can be driven at an inside corner (taken as the origin of coordinates) with an externally placed high power loudspeaker through a high impedance tube (Hunt 1939b) made by packing a steel tube (inside diameter 24 mm, and length 230 mm) with thin copper wires. This sound generation system, as shown in Figure 4.2, has the property of low sound absorption and uniform output. Almost in all cases, a microphone is placed at the opposite corner ($X = 0.868$ m, $Y = 1.150$ m, $Z = 0.000$ m) to measure the sound pressure in the cavity.

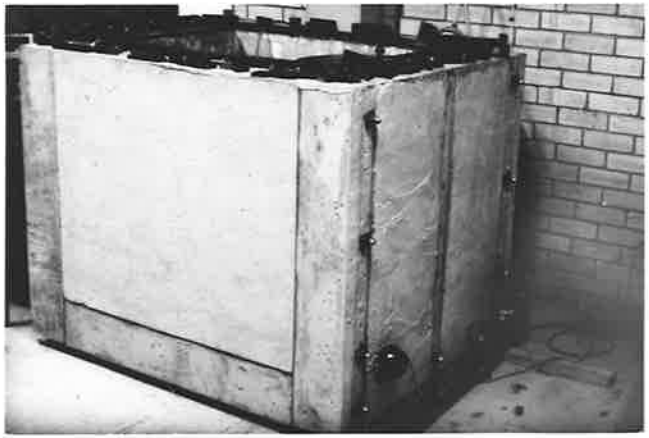

(a)

(b)

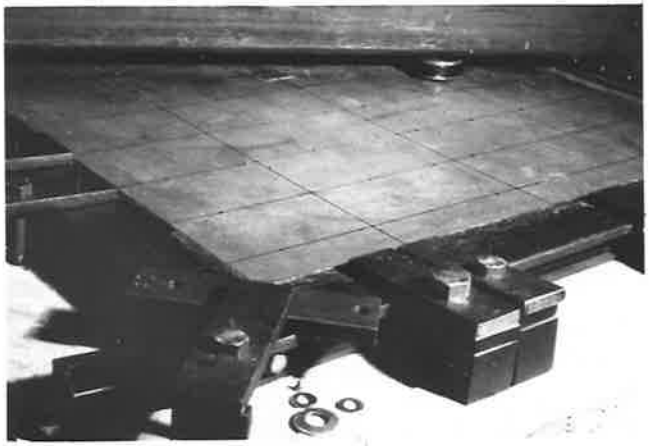

(c)

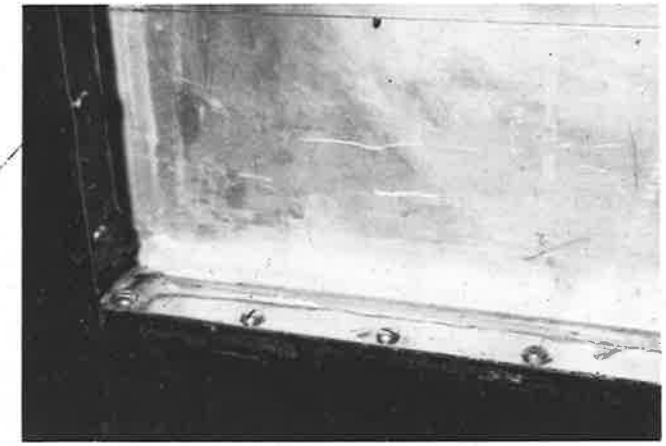

(d)

Figure 4.1: (a) concrete box; (b) concrete lid; (c) panel clamping arrangement; (d) simply supported panel.

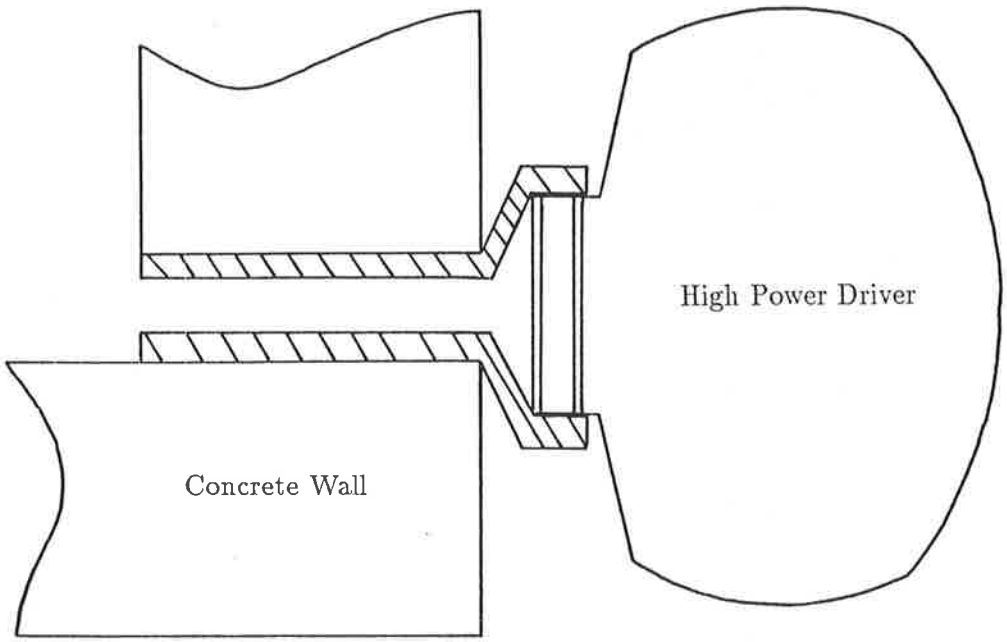

Figure 4.2: The high input impedance tube sound driving system.

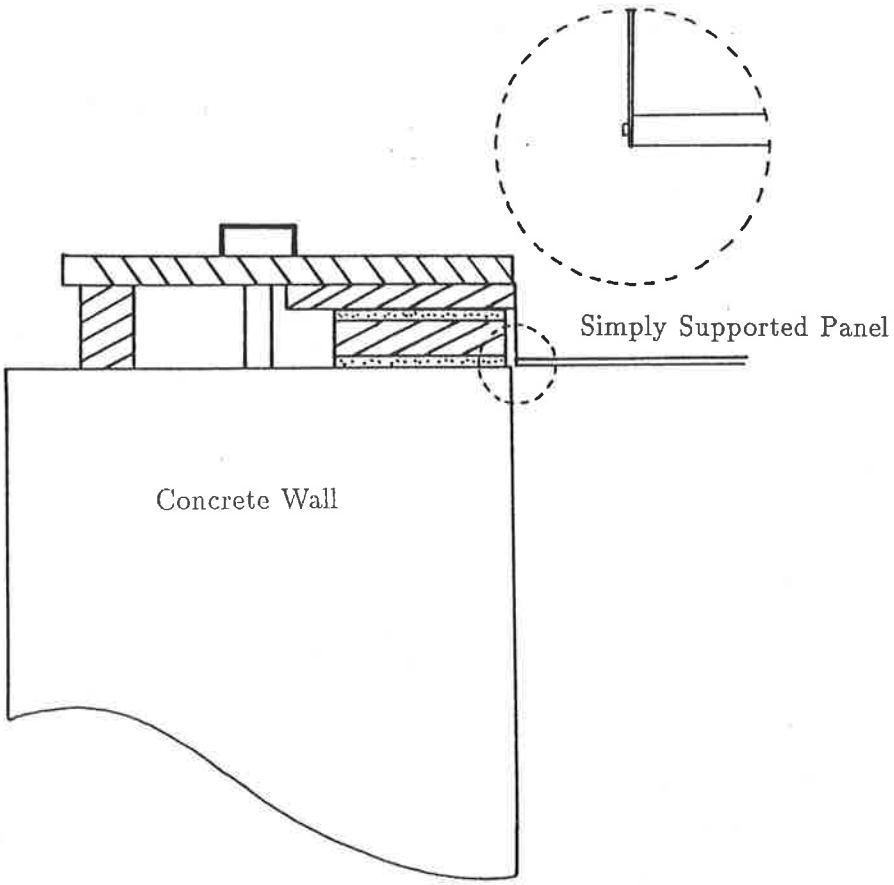

Figure 4.3: The panel and panel frame arrangement on the box.

The arrangement of the panel frame on the concrete box, as well as the magnetic driving system for the panel vibration measurements are shown in Figure 4.3, Figure 4.1(c) and (d). The magnet is attached to a steel beam, which is clamped above the concrete box, and can drive the panel without touching the panel. The position of the magnet over the surface of the test panel is adjustable so that individual panel modes can be generated by driving the mode at an antinode.

A test panel is made of a 6 mm aluminum plate. A simply supported boundary condition (Figure 4.3) was adopted for this panel, which is made by using a steel skirt pinned around the edges of the panel (Snowdon 1974).

4.3 Uncoupled concrete cavity

A cavity mode is described by its resonance frequency, modal decay time and mode shape. With the concrete lid in place, the resonance frequencies and modal decay times of the cavity can be measured. The power spectral density (PSD) of the cavity sound field response to white noise generated through the loudspeaker is shown in Figure 4.4. Since every mode in the rectangular cavity has an antinode at the corner, all the resonance frequencies of the cavity modes can readily be identified from the peaks in the PSD.

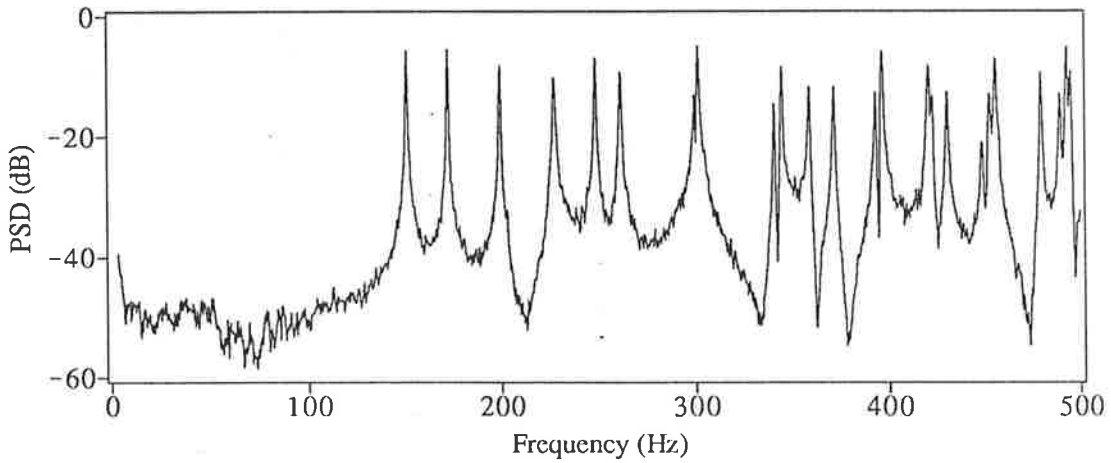

Figure 4.4: PSD of the sound field in the uncoupled concrete cavity.

The decay time of each cavity mode was measured by the decay method. The output from the loudspeaker was suddenly interrupted and the decay rate was determined from the recorded sound pressure level decay curve using a sound level recorder. For those modes, which are strongly disturbed by the nearby modes, the microphone was placed at a position where

their amplitudes are large and the nearby modes have minimum pressure amplitudes. This reduced modal beating in the decay curves.

By comparing the measured resonance frequencies with those calculated (Eq.(3.41)), the modal indices can be allocated to the measured resonance frequencies. Therefore the modal shape for each resonance can be determined by Eq.(3.8). The resonance frequencies and the decay times of the first twenty cavity modes are listed in Table 4.1. In this table the theoretical values are also included. The modal decay times are related to the sound absorption of the concrete walls at the resonance frequencies.

Table 4.1: Resonance frequencies and modal decay times of the concrete cavity

$(T = 18°C)$

Mode (l, m, n)	$f_{l,m,n}$ (Hz) Theoretical	$f_{l,m,n}$ (Hz) Experimental	Modal Decay Time (Sec)
0, 1, 0	149.57	149.59	10.5
0, 0, 1	172.00	171.48	10.2
1, 0, 0	198.15	198.16	9.5
0, 1, 1	227.9	227.6	7.0
1, 1, 0	248.3	248.1	7.0
1, 0, 1	262.4	261.9	5.7
0, 2, 0	299.1	299.1	8.5
1, 1, 1	302.0	301.7	4.8
0, 0, 2	344.0	342.5	7.2
0, 2, 1	345.1	344.8	5.7
1, 2, 0	358.8	358.6	5.5
0, 1, 2	375.1	373.8	6.3
2, 0, 0	396.3	395.6	5.6
1, 0, 2	397.0	396.3	5.5
1, 2, 1	397.9	398.1	3.23
2, 1, 0	423.6	422.8	4.2
1, 1, 2	424.2	424.3	2.75
2, 0, 1	432.0	431.8	4.0
0, 3, 0	448.7	448.8	5.6
0, 2, 2	455.9	454.6	5.6

The 1/3 octave frequency band reverberation times of the concrete cavity were measured for comparison with those of a particle board box which has the same interior dimension. The comparison in Figure 4.5 shows that the concrete cavity provides low sound absorption, so that the influence of panel-cavity modal coupling would become prominent. Increased sound absorption due to variation in panel-cavity coupling is well within the range of the sound level recorder used in these experiments.

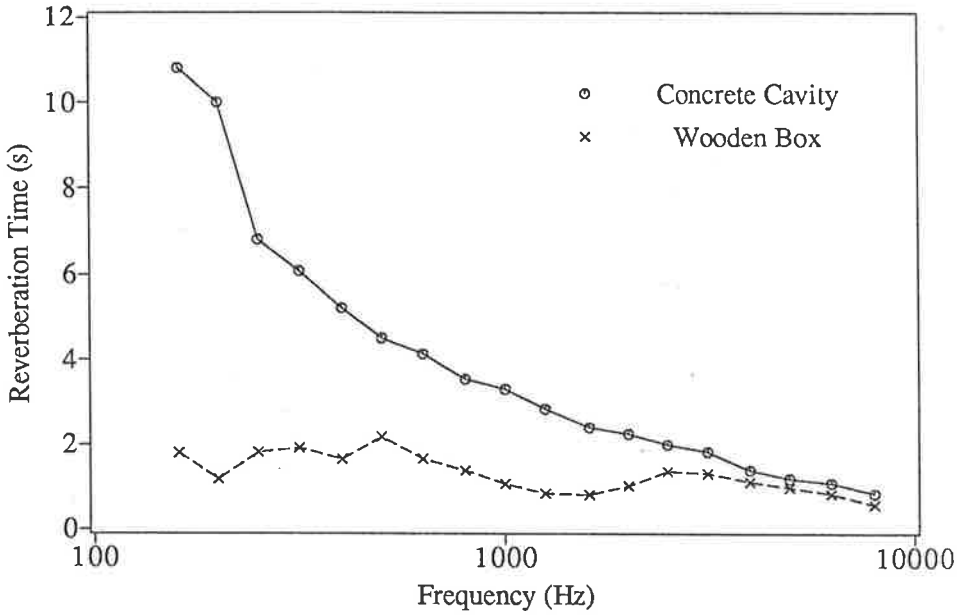

Figure 4.5: reverberation times (1/3 octave band measurement) of the concrete cavity and a wooden box with the identical internal dimensions.

4.4 Test panels

The mechanical damping of a test panel is not only depended upon the internal damping of the panel but also upon the mounting condition on the cavity. Therefore the panel should be tested under the same mounting condition as in the measurement of the coupled panel-cavity system but without the sound reflection from the bottom of the cavity. To satisfy this requirement, the cavity was filled with sound absorptive material which absorbed the sound radiated from the vibrating panel.

The PSD of the panel acceleration due to the driving of a magnet fed with a white noise signal at ($X = 0.20$ m, $Y = 0.67$ m) was obtained from the output of an accelerometer at ($X = 0.46$ m, $Y = 0.36$ m). Figure 4.6 shows the measured power spectral density of a 6 mm aluminum panel. The first 20 resonance frequencies of the panel modes are listed in Table 4.2, with theoretical prediction (Eq.(3.35)) for comparison.

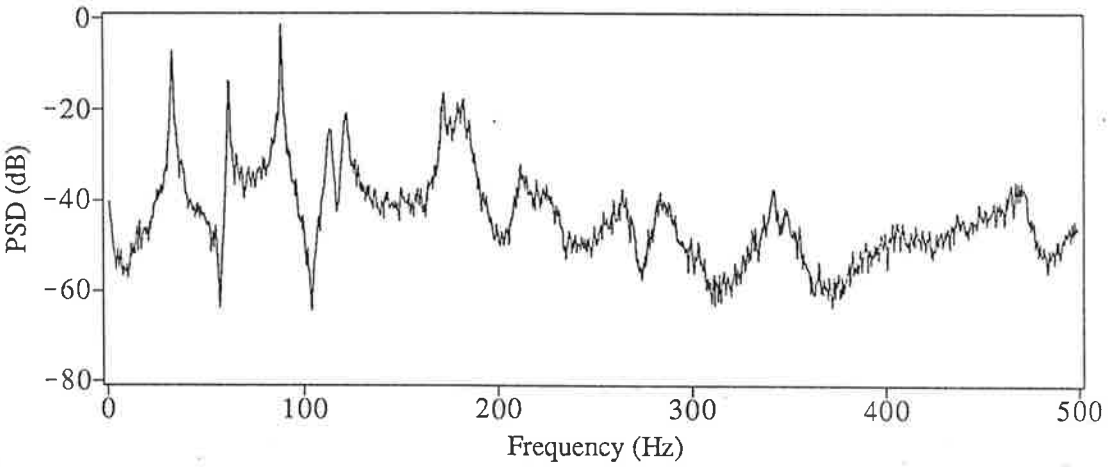

Figure 4.6: PSD of the panel acceleration (uncoupled panel $h = 6$ mm).

Table 4.2: Resonance frequencies and modal decay times of an aluminum panel ($h = 6$ mm, without cavity influence)

Mode (u, v)	$f_{u,v}$ (Hz) Theoretical	$f_{u,v}$ (Hz) Experimental	Modal Decay Time (Sec)
1 1	29.911	34.00	9.3
1 2	62.477	63.13	19.8
2 1	87.076	89.19	11.9
1 3	116.756	115.91	5.1
2 2	119.643	122.84	3.5
2 3	173.921	173.86	11.4
3 1	182.351	184.50	4.3
1 4	192.745	190.90	5.4
3 2	214.918	216.0	4.4
2 4	249.910	251.3	4.7
3 3	269.196	268.4	5.0
1 5	290.445	285.9	1.6
4 1	315.737	315.6	1.6
3 4	345.185	343.8	2.6
2 5	347.610	347.9	1.5
4 2	348.303	348.3	0.42
4 3	402.581	401.9	0.62
1 6	409.857	408.9	0.42
3 5	442.886	437.9	1.3
2 6	467.022	460.9	0.38

The shapes of the panel modes are represented by the index (u, v). The integers u and v indicate the number of antinodes in X and Y directions. The decay times of the panel modes have also been listed in Table 4.2. The measured panel damping is due to mechanical damping and to the panel radiation to each side of the panel.

4.5 Experimental results and interpretation

4.5.1 Measurement of the panel-cavity system

Replacing the concrete lid by a test panel, the coupling behavior of the panel-cavity system can be examined. The power spectral density of the sound field in the cavity was measured for the 6 mm aluminum panel. A comparison of the PSD of the coupled system(Figure 4.7 (a)) with that of the concrete cavity (Figure 4.4) shows the presence of extra resonant peaks in the coupled system. The frequencies of the extra peaks can be traced back to the resonance frequencies of the test panel. When some damping material or weight, such as a few sand bags, was placed on the surface of the panel, the extra peaks disappeared or shifted in frequency.

Due to the fluid-structural coupling, the sound pressure on the inside surface of the panel forces the panel to vibrate. On the other hand, the vibrating panel radiates sound back into the cavity, so that the original sound field is perturbed. Near the resonance frequencies of the panel, the panel will have large response and so large sound radiation into the cavity is the result. All the extra peaks are caused by radiation of vibrating panel modes. They may be observed in the cases when the panel mode is well coupled with a cavity mode or in the frequency ranges where the sound pressure level is very low so that the panel radiation is not submerged. Once the vibration of the panel is stopped by the sand bags, the radiation ceases and the extra peaks disappear. The PSD of the panel acceleration was also measured for the same case (Figure 4.7 (b)). It shows a strong response at frequencies corresponding to the extra peaks in the sound field PSD.

The PSD of the sound field in the cavity can also be obtained by using a magnet to drive the test panel. In this case, almost every cavity controlled mode and every panel controlled mode can be identified in the PSD, as shown in Figure 4.7(c).

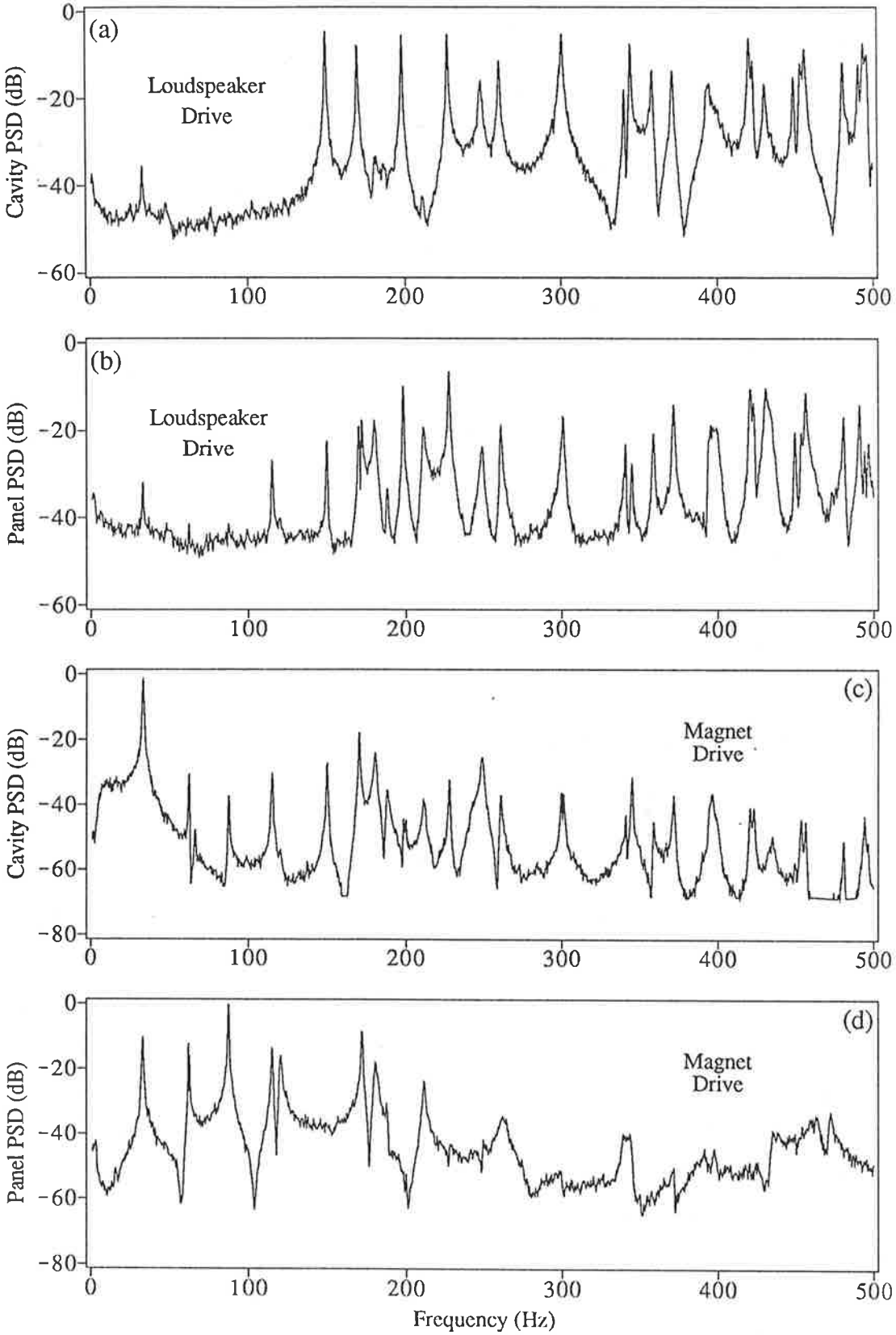

Figure 4.7: Power spectral densities of a panel-cavity system. (a) sound field response, loudspeaker drive; (b) panel response, loudspeaker drive; (c) sound field response, magnet drive; (d) panel response, magnet drive. ($h = 6$ mm).

When the sound field in the cavity is directly generated by a loudspeaker, the radiated sound field due to induced panel vibration is weaker than the direct sound field. Therefore the modal radiation is usually submerged in the direct field. However, the vibration level of the panel becomes higher when it is directly driven by a magnet. The vibrating panel then behaves like a loudspeaker with its own resonance characteristics. Therefore both the panel modal radiation and cavity modal response can be recorded in the cavity.

Different levels of the sound field response can be obtained for different locations of the driving magnet. The panel modal response is dependent upon the position of the driving force thus the panel controlled mode may be altered by alteration of the panel response. The sound field of the cavity controlled modes is dependent upon the selection of the modal coupling of the panel modes and the cavity modes. If the panel mode, which is responsible for the cavity mode, is not well generated with the selected location of the magnetic driver then the response of the cavity controlled mode will be suppressed.

4.5.2 Comparison of measured and predicted results

The modal coupling analysis from Chapter 3 was used to predict the modal parameters of the coupled system. In these analyses, the resonance frequencies and modal decay times of the coupled system are calculated from the fundamental properties of the uncoupled panel and cavity modes. The first 20 cavity modes and 20 panel modes (listed in Tables 4.1 and 4.2) were used in the calculation. The orthogonal expansion method was used for theoretical predictions. The resonance frequencies and the modal decay times of the coupled system were also measured experimentally. The first thirteen cavity controlled modes of the panel-cavity system were calculated and measured for the 6 mm aluminum panel and are all listed in Table 4.3 for comparison. The agreement between the measurements and the theoretical predictions indicates that the coupling theory can be used to evaluate the reverberation time in enclosures where the boundaries are modally reactive.

Table 4.3: Comparison of the measured and predicted resonance frequencies and modal decay times of the panel-cavity system (h = 6 mm)

mode(l,m,n)	Measurement		Prediction	
	$f_{l,m,n}$ (Hz)	T_{m60} (s)	$f_{l,m,n}$ (Hz)	T_{m60} (s)
0,1,0	149.82	10.1	149.91	10.02
0,0,1	170.23	7.9	172.23	7.90
1,0,0	198.34	9.2	198.66	9.2
0,1,1	227.9	5.5	229.32	6.07
1,1,0	248.9	1.5	249.79	1.83
1,0,1	260.9	3.2	262.81	5.43
0,2,0	297.7	4.9	299.68	4.73
1,1,1	299.3	3.8	302.45	4.49
0,0,2	339.2	7.4	344.61	6.84
0,2,1	342.6	5.0	345.72	5.11
1,2,0	356.6	4.3	359.25	4.60
0,1,2	369.7	4.0	375.51	5.92
2,0,0	393.9	5.0	396.53	5.52

4.5.3 Sound wave properties & panel characteristics

The resonance frequencies and decay times of the acoustical modes in a coupled system are the focus of this investigation. Due to sound field coupling with the test panel, the sound wave boundary conditions are different from the rigid wall condition. The phase of the panel velocity with respect to the phase of the incident sound pressure in the cavity will affect the superposition of the traveling waves in the cavity. Therefore the resonance, which occurs when the reflected waves coincide with the incident waves, will be perturbed and so will the resonance frequency. The energy flow between the test panel and sound field in the presence of the coupling will directly affect the decay of the sound field. The magnitude of this energy flow is determined by the coupling condition between individual panel and cavity modes.

Theoretical consideration of the panel-cavity coupled system suggests that some interesting phenomena associated with the sound wave behavior may be observed in the cavity when some characteristic of the panel (such as modal density of the panel) is varied. For example, the decay times of the acoustic modes experience relative minima and the resonance frequency of each mode exhibits an interesting jump on crossing the panel modal density region of maximum sound absorption.

Experimentally, it was found that each resonance frequency of the test panel incrementally shifted in the direction of lower frequencies when sand was incrementally and uniformly spread on the panel surface. The dependence of the first few normalized resonance frequencies $\frac{f_{u,v}(s)}{f_{u,v}(0)}$ (where $f_{u,v}(s)$ and $f_{u,v}(0)$ are resonance frequencies of (u,v) panel mode with and without sand influence respectively) of the 6 mm aluminum panel as a function of the amount of added sand is shown in Figure 4.8.

The effect of sand on the structure has been studied by Kuhl and Kaiser (1952) and the loss factors of sand filled structures were investigated by Sun *et al.* (1986a) using Statistical Energy Analysis. When a thin layer of sand covers a panel, the effective mass and the damping of the panel are changed and the speed of the wave propagation is lowered. Reference to Figure 4.8 shows that increasing the amount of sand causes the panel resonance frequencies to concentrate towards the low frequency end of the scale. This means that the panel modal density is increased. In confirmation of this observation, the measured modal density of the panel is shown in Figure 4.9 as a function of the amount of added sand. The measured panel damping due to added sand is plotted in Figure 4.10. After an initial quick decrease of the decay times, the panel dampings do not change substantially with the further addition of sand although the panel modal density changes substantially. This result suggests that the main effect of adding sand on the sound behavior in the cavity is due to the variation of the panel modal density.

The modal decay times of the first three cavity controlled acoustical modes are plotted in Figure 4.11 as a function of panel modal density. Although the range of the panel modal density variation is not very large in this experiment, the observed minimum modal decay times confirm the predictions of Chapter 3.

The measured resonance frequencies of the same modes are plotted in Figure 4.12 as a function of the panel modal density. As the panel modal density increases the resonance frequency of each mode has a jump from low frequency to high frequency. On the modal density scale, the resonance frequency jumps of a mode coincide with its decay time minima.

The results shown as solid lines in Figures 4.11 and 4.12 were calculated by the successive iteration method. In this case, the resonance frequency and decay time of each panel mode was estimated from the experimental results shown in Figures 4.9 and Figure 4.10. The calculation started with the experimentally obtained values of panel modal density. The resonance frequency of each panel mode was calculated from these panel modal densities according to Eqs. (3.43) and (3.42). The value assigned to the decay time of each panel mode is obtained by selecting the reverberation time of the 1/3 octave frequency band in which the panel mode is located. The 1/3 octave reverberation times are read from Figures 4.10 and 4.9. In the other words, those panel modes with resonance frequencies in the same 1/3 octave frequency band are assigned the same decay times. The variation in panel mass due to the added sand was also taken into account in the calculation.

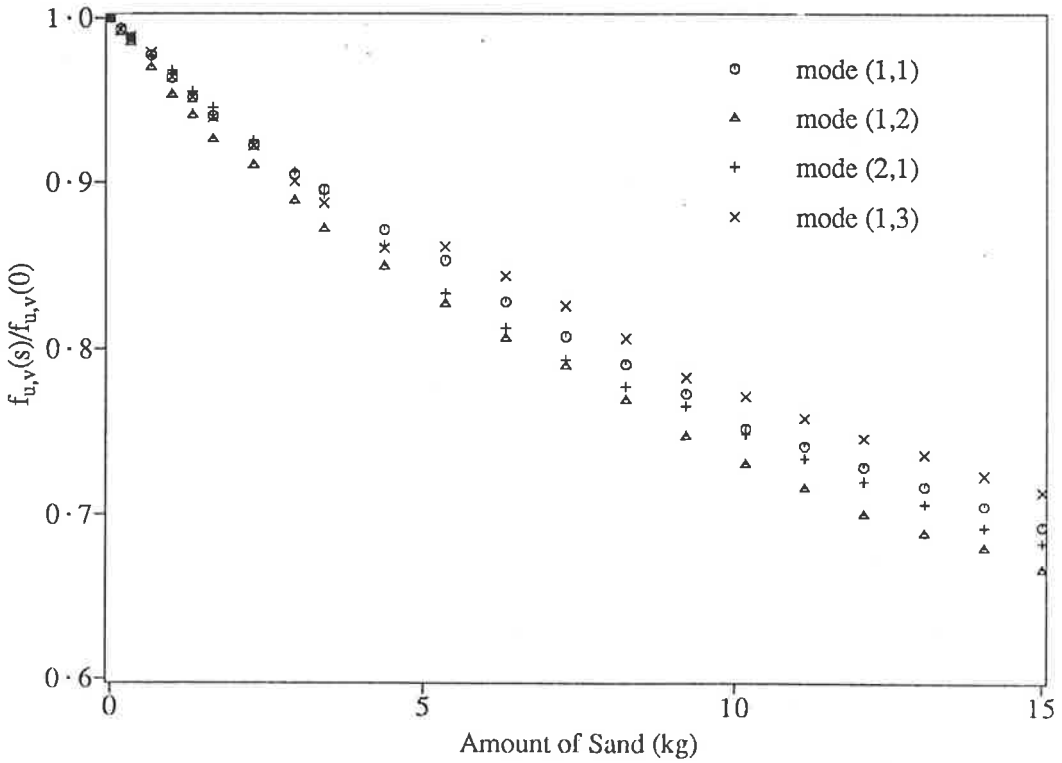

Figure 4.8: Normalized panel resonance frequencies as a function of amount of added sand, $f_{u,v}(s)$ and $f_{u,v}(0)$ are the resonance frequencies of the (u, v) panel mode with and without added sand respectively.

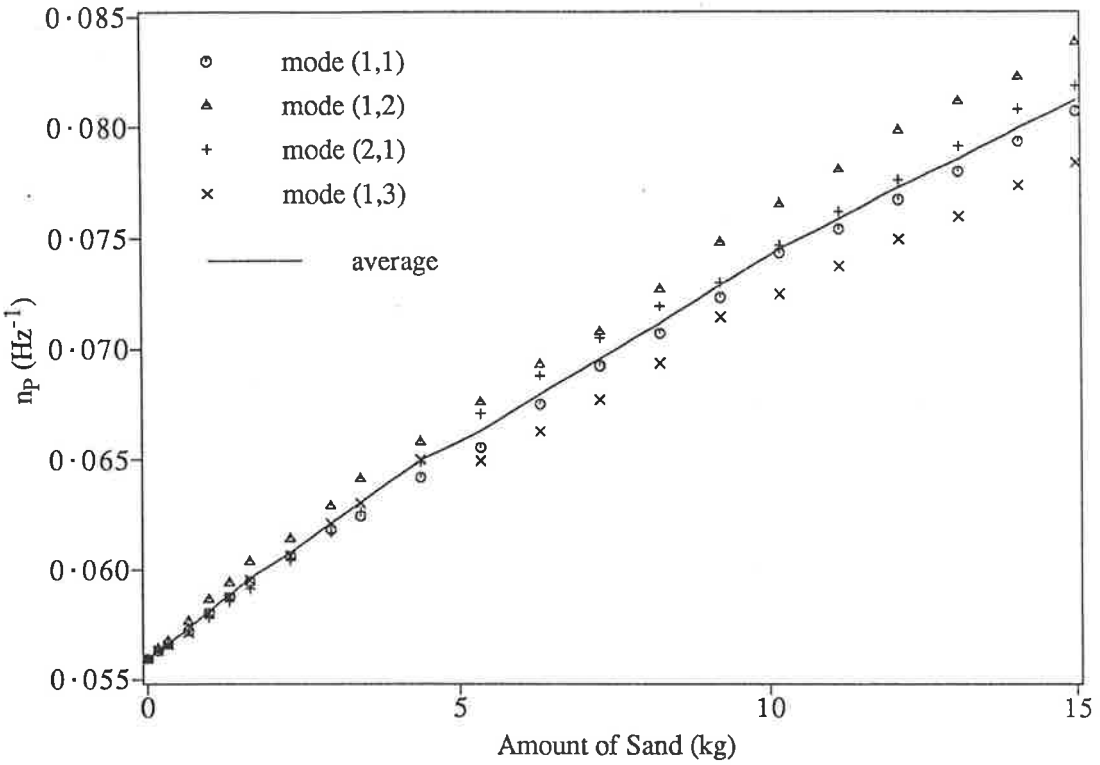

Figure 4.9: Panel modal density as a function of amount of added sand.

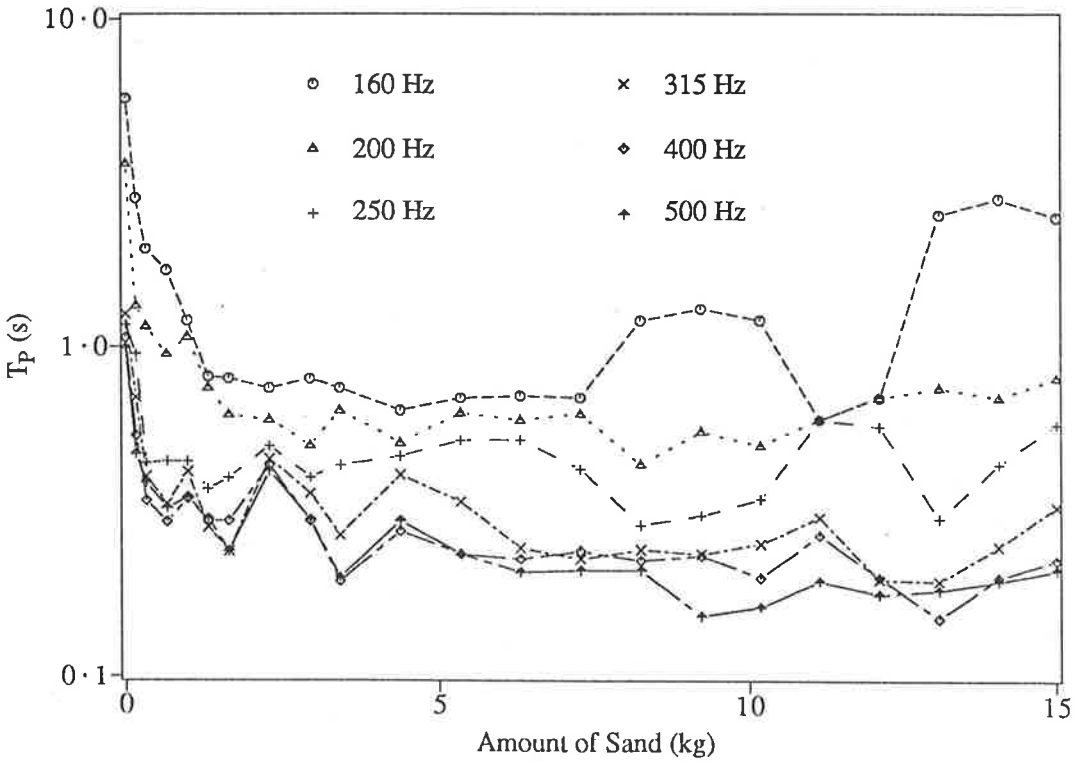

Figure 4.10: Reverberation time (1/3 octave band measurement) of the panel as a function of amount of added sand.

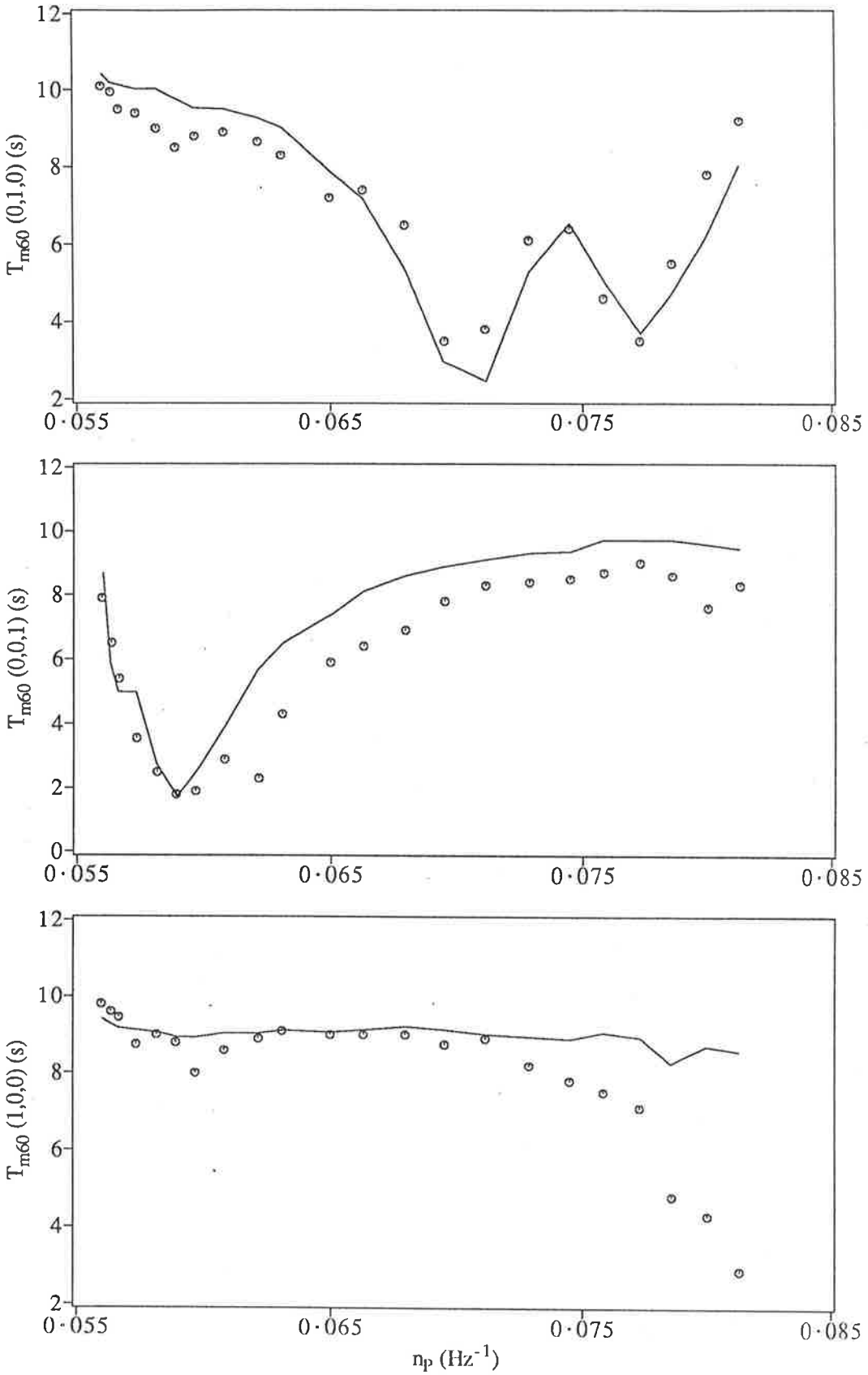

Figure 4.11: Decay times of the first few cavity controlled modes as a function of panel modal density. (——) calculated results; (o o o) measured results.

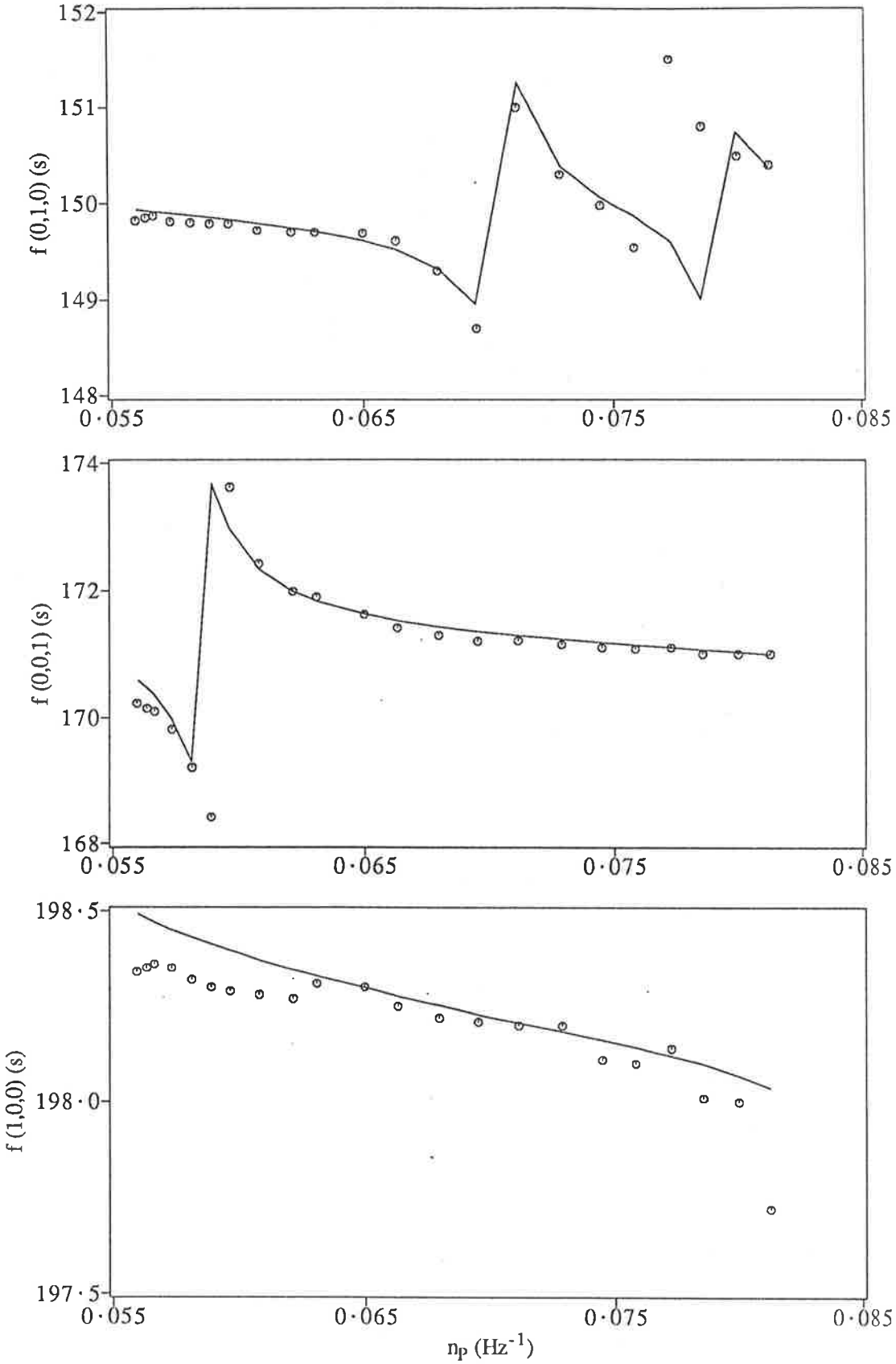

Figure 4.12: Resonance frequencies of the first few cavity controlled modes as a function of panel modal density. (——) calculated results; (o o o) measured results.

The cavity controlled mode (0,0,1) and the panel controlled mode (3,1) have been examined closely. The relationship between the sound field part and the panel vibration part of each mode has been investigated in the region of their resonance frequencies.

Figure 4.13 shows the power spectral densities of the sound field and the panel acceleration near the resonance frequencies of (0,0,1) mode and (3,1) mode for a number of closely spaced panel modal densities. The PSD of the sound field is due to loudspeaker driving of the cavity, while the PSD of the panel vibration is due to magnetic driving of the panel. In the latter case, the accelerometer was placed at the center of the panel and at a node of a nearby panel mode (which does not couple with (0,0,1) cavity mode) to avoid its appearance in the spectrum. The range of panel modal density shown in Figure 4.13 covers the maximum sound absorption region of the (0,0,1) cavity controlled mode (see Figure 4.11).

As the panel modal density is increased by incrementally increasing the sand, the power spectral densities of the sound field and the panel vibration show some interesting changes. Referring to Figure 4.13, at the beginning ($n_P = 0.0560$ Hz^{-1}), one low frequency peak in the PSD of the cavity sound field is clearly identified, and a high frequency peak is also visible but with much lower amplitude. However, for the corresponding panel vibration spectrum, the high frequency peak has higher amplitude, while the low frequency peak has lower amplitude. In this case, the cavity controlled mode (0,0,1) and the panel controlled mode (3,1) can easily be distinguished by the respective relative amplitudes of response.

As the modal density is increased (moving up the page), the higher frequency peak in the sound field PSD becomes larger while the lower frequency peak moves slightly toward lower frequencies and becomes smaller. Eventually only the high frequency peak remains and the low frequency peak disappears. The PSD of the panel vibration shows almost the opposite behavior. The lower frequency peak becomes bigger and its bandwidth becomes wider, while the higher frequency peak becomes smaller and narrower.

The low frequency peaks in the cavity sound field and panel vibration spectra at each particular panel modal density are resonance peaks for one coupled acoustical mode as measured in different parts of the coupled system. The peak of larger amplitude in the cavity sound field spectra shows that this peak of the acoustical mode is a cavity controlled mode. Similarly the peak of larger amplitude in the panel spectra shows that it is a panel controlled mode. All of these changes in the peaks of Figure 4.13 demonstrate that the cavity controlled

mode and the panel controlled mode interchange their positions in the frequency domain as the panel modal density is increased in the region of maximum sound absorption.

In this maximum sound absorption region, the specific acoustical transfer impedance between the microphone location (0.868 m,1.150 m,0.000 m) and the accelerometer location (0.434 m,0.575 m) was measured at the peak frequencies in Figure 4.13. Figure 4.14(a1) and (a2) shows the amplitude and phase of this impedance for (0,0,1) cavity controlled mode and (3,1) panel controlled mode as a function of panel modal density. The corresponding resonance frequencies and decay times of the modes are plotted in Figure 4.14 (b) and (c). The results shown Figures 4.14(a1), (a2), (b) and (c) may be compared with the theoretical results of Chapter 3 shown in Figure 3.9(a1), (a2) and Figure 3.8(b) and (c). The general trends in the experimental results are the same as those produced by the theoretical calculations.

When the panel modal density is far from the maximum sound absorption position, the cavity controlled mode and panel controlled mode are easily distinguished because they have very different amplitudes of specific transfer impedance. The impedance amplitudes of the two modes tends to be equal at the maximum sound absorption point. Although the phase shifts in the instrumentation are unknown, the jump in the phase of each mode is still observed when the modal density is crossing the maximum sound absorption point. The resonance frequencies and the modal decay times plotted in the Figure 4.14 also qualitatively confirmed the theoretical results shown in Figure 3.8(b) and (c).

Quantitative differences between the experimental results and the theoretical modelling are observed and there are many reasons for these differences. For the theoretical calculation, panel damping was assumed to be the same for every panel mode, but in the experiment, each panel mode has a different decay time. The modal decay times of the panel also vary as sand is added to change the panel density. Each panel modal frequency decreases at a different rate (Figure 4.8) as sand is added. In the theoretical prediction, the characteristics are taken from the normal modes of free vibration, but in the experiment, the characteristics of these modes can be measured only if the vibration is forced continuously at the resonance frequency. The near field effect of the driving source in the cavity is not expected to be entirely negligible.

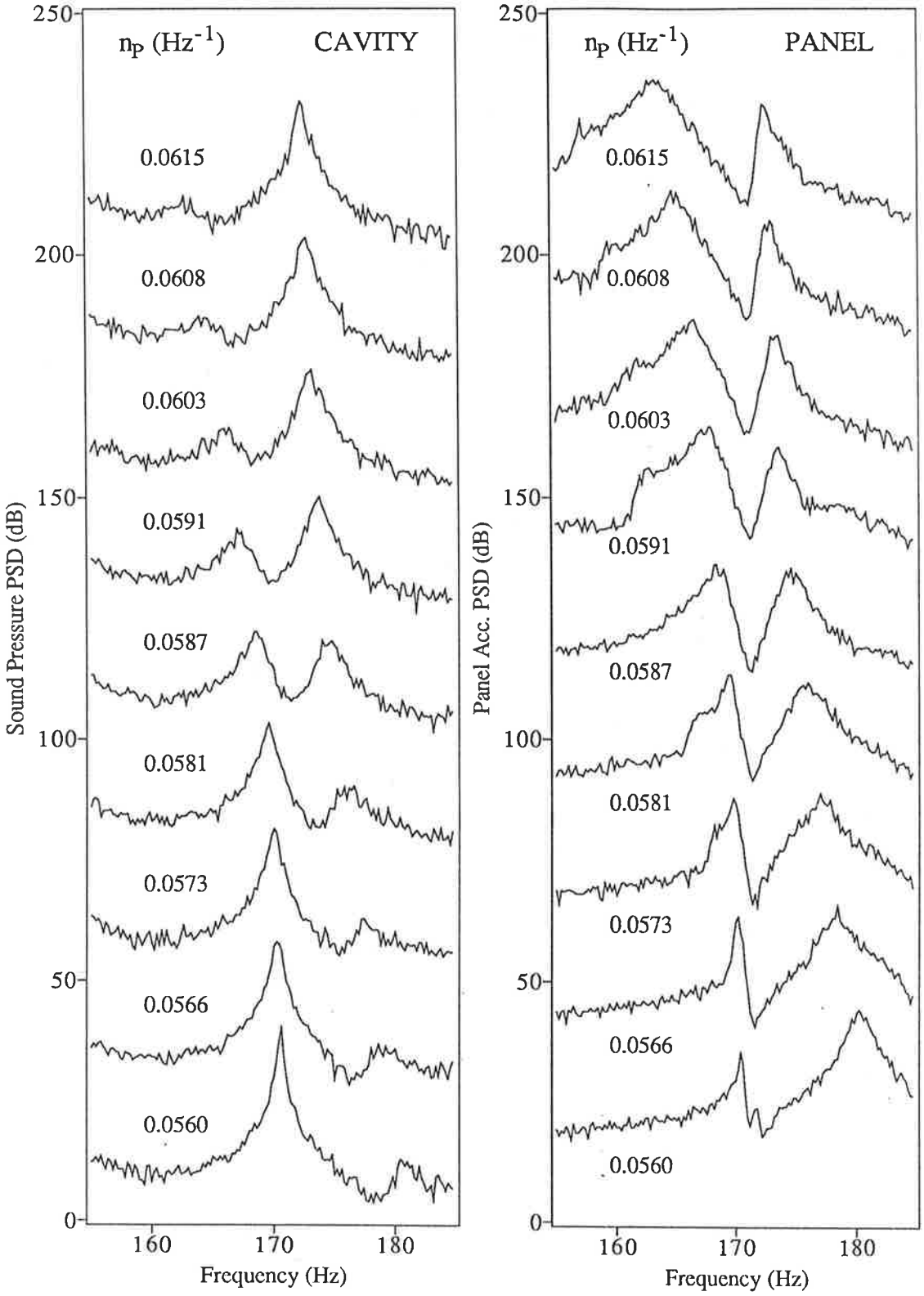

Figure 4.13: Power spectral density of the cavity sound pressure and the panel acceleration for each increment of panel modal density. (loudspeaker (0.0,0.0,0.0) m, microphone at (0.868,1.15,0.0) m; magnet driver at (0.30,0.80) m, accelerometer at (0.434,0.575) m.) Each curve is offset from the one underneath it by 25 (dB).

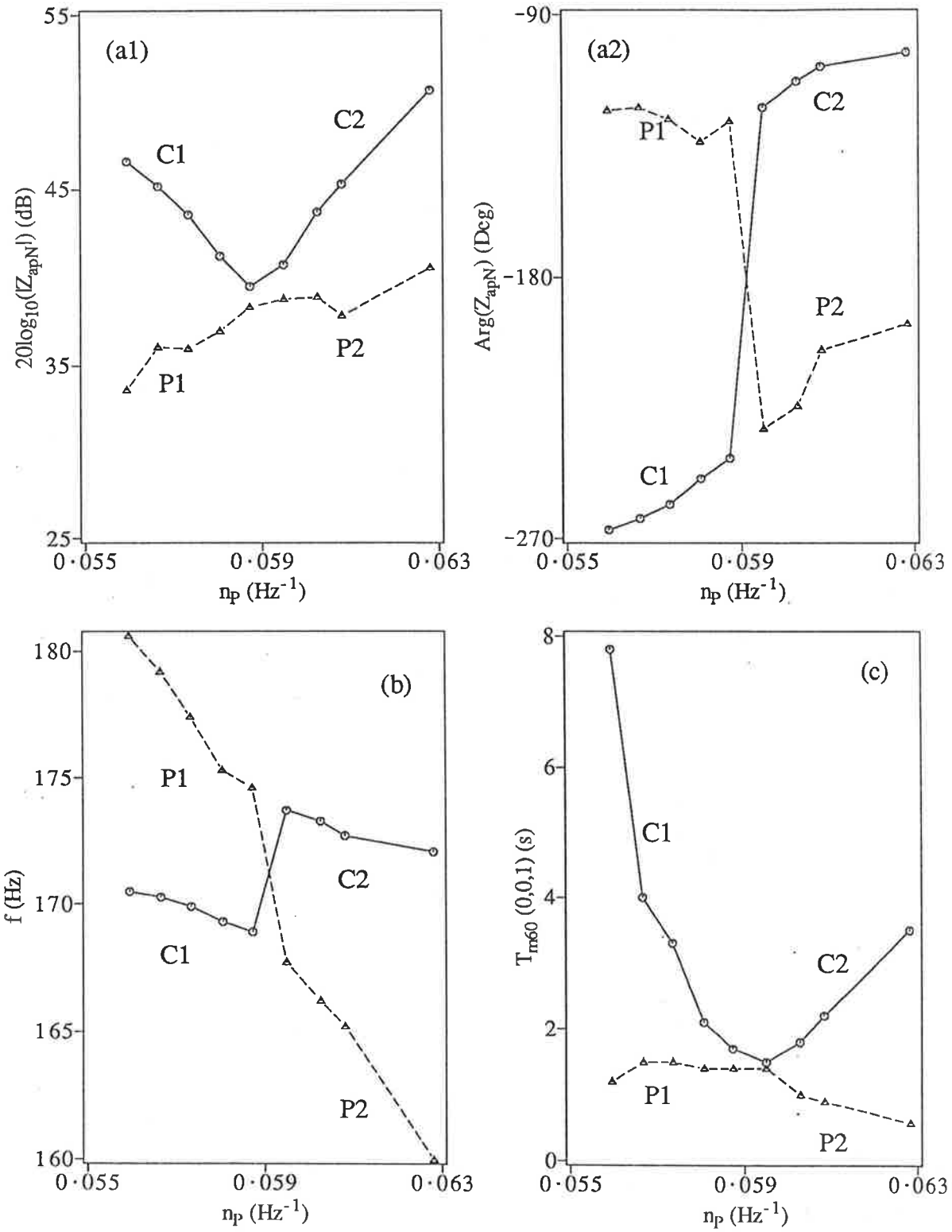

Figure 4.14: (a1) and (a2): specific acoustical transfer impedance of two acoustical modes (from (0.868,1.150,0.0) m to (0.434,0.575) m); (b1): resonance frequencies; (b2): 60 dB modal decay times. (——) (0,0,1) cavity controlled mode, (- - -) (3,1) panel controlled mode. The amplitude and phase scales of the transfer impedance are displaced because neither the accelerometer nor the microphone used in this measurement were calibrated.

4.5.4 Influence of panel damping on modal decay time

In the low frequency range, the sound energy in the cavity is mainly dissipated at the boundaries. The sound energy incident on the test panel is partly radiated back into the cavity, partly dissipated by the mechanical damping of the panel and partly radiated into the outside space. That is, the damping of the panel directly influences the reverberation time in the cavity.

In order to illustrate this fact, the damping of a 6 mm aluminum panel was changed by placing a layer of sand (weighting 1.6 kg) on it. The average reverberation times of the panel (with and without sand) are plotted in Figure 4.15 and the corresponding cavity acoustic field reverberation times are plotted in Figure 4.16. These results show that the damping of a panel which is coupled to the cavity affects the reverberation time of the cavity. The panel with the larger damping factor (the one with a layer of sand) produces a smaller cavity reverberation time.

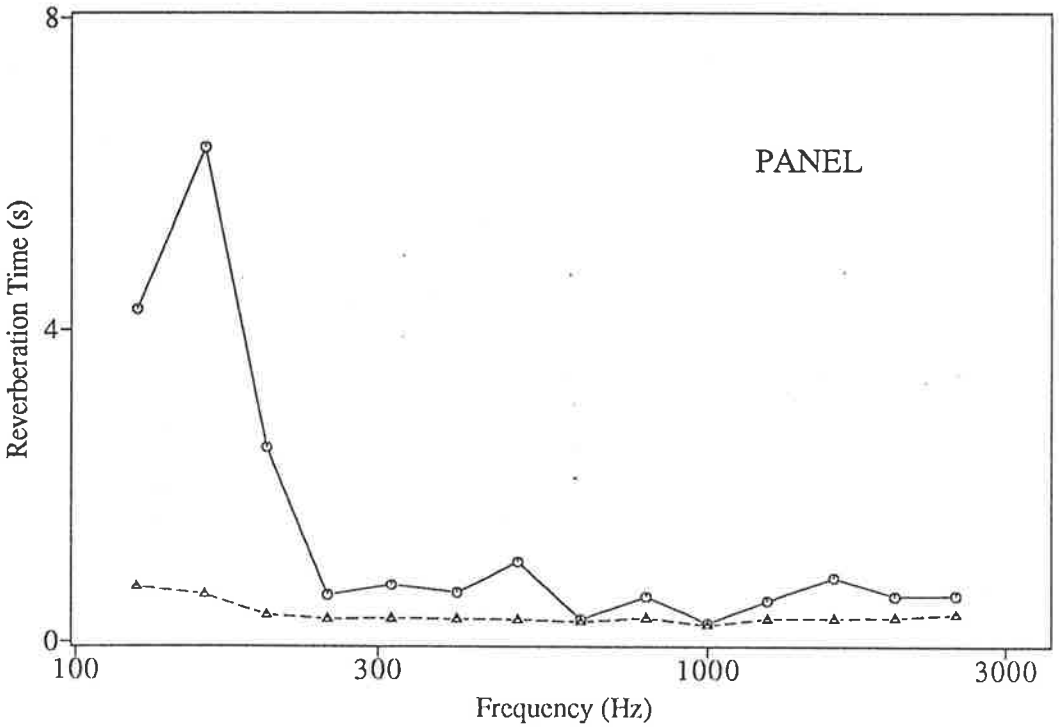

Figure 4.15: The reverberation times of the test panels. (——) 6 mm aluminum panel; (- - -) 6 mm aluminum panel covered by sand (1.6 kg).

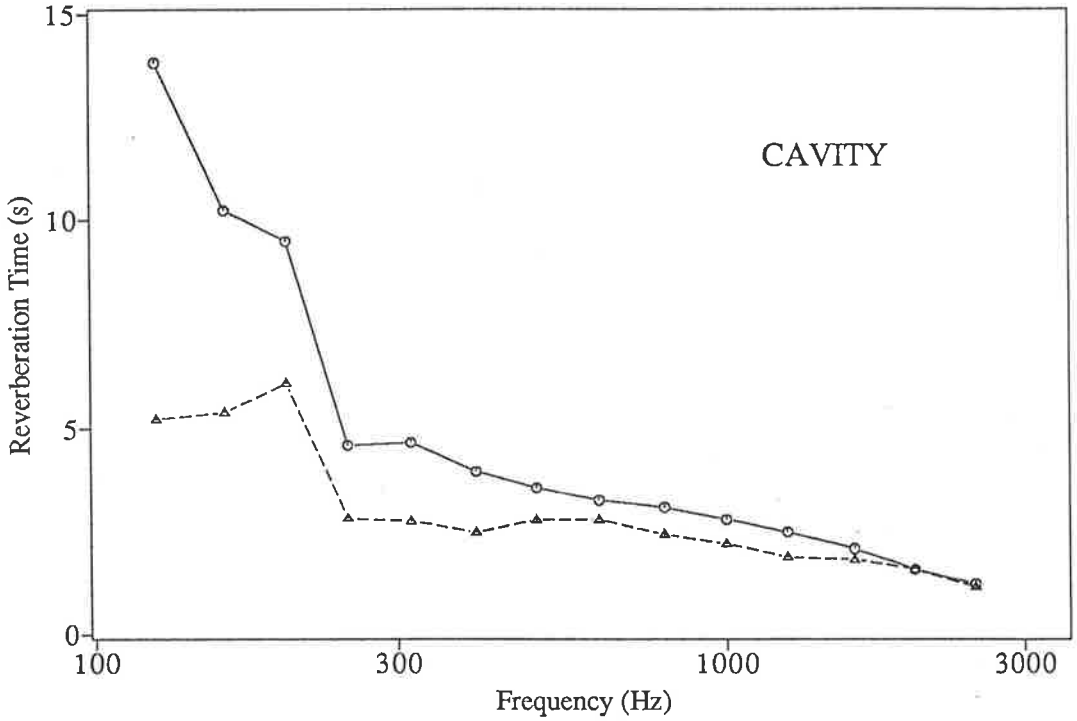

Figure 4.16: The reverberation times of the sound field in the cavity. (——) 6 mm aluminum panel; (- - -) 6 mm aluminum panel covered by sand (1.6 kg).

4.5.5 Influence of panel radiation

The radiation of a flexible panel is most important in the consideration of sound transmission through the panel. However, when consideration is turned to the estimation of reverberation time in the cavity, the radiation loss of the panel will only be one part of the total energy dissipation in the vibrating panel. The following experiment shows that when the panel is well damped, the contribution of the sound radiation loss of the panel to the total absorption is smaller than that of the mechanical damping of the panel.

To estimate the contribution of the panel radiation loss to the total sound absorption of the panel, the energy dissipations of both the mechanical damping and the radiation loss are measured separately. In steady state the modal damping constant k_m is related to the total sound energy in the cavity E_A and the power loss P_A into the boundaries by the following equation (Morse 1948b)

$$k_m = \frac{1}{2}\frac{P_A}{E_A}. \tag{4.1}$$

The 60 dB modal decay time T_{m60} and modal damping constant are related as follows:

$$T_{m60} = \frac{6.91}{k_m}. \tag{4.2}$$

The measurement was conducted in a rectangular particle-board box, which was made of six 20 mm thick flexible particle boards with the same internal dimensions as those of the concrete box. The internal surfaces of the box were painted in order to eliminate surface porosity. The first few resonance frequencies of the acoustic modes are well separated and the modal shapes can be described approximately by cosine functions. Therefore the sound energy (E_A) in the box can be determined from the sound pressure in a corner and the modal index. There are two terms which contribute to P_A in Eq.(4.1), the panel mechanical damping term P_{dA}, and radiation loss term P_{rA}. P_{dA} can be estimated from the average panel vibrational energy E_P and average panel damping constant k_p at each resonance frequency from

$$P_{dA} = 2k_p E_P = \frac{13.8}{T_p} E_P. \tag{4.3}$$

P_{rA} can be obtained by measuring the average sound intensity $\bar{I}_i$ over each external surface of the box,

$$P_{rA} = \sum_i \bar{I}_i S_i, \tag{4.4}$$

where S_i is the area of the ith surface.

The average reverberation time (T_p) of the box boundaries are measured at each resonance frequency and listed in Table 4.4. A sound intensity meter was used to measure the average energy flow rate on each side of the box. By means of Eqs.(4.3) and (4.4), contributions of the mechanical damping and the radiation loss of the particle-board to the total absorbed power can be evaluated. Substituting both these results (P_{dA} and P_{rA}) and the measured sound energy in the cavity (E_A) separately into Eqs.(4.1) and (4.2), the estimated modal decay times (T_{m60}) due to the panel damping and the radiation loss are obtained. The results are shown in Table 4.5, with measured modal decay times for comparison.

These results indicate that the radiation loss makes little contribution to the modal decay time in the cavity when the boundary structure has large damping. However, the radiation effect may become important when the mechanical damping is small and the tested modes are panel controlled. In this case the panel radiation may have comparable effect to that of the panel damping on the modal decay in the cavity. For example, in Table 4.5, mode(0,0,1;2) is a panel controlled mode. In this case, the estimated radiation contribution is obviously large as the corresponding value of estimated modal decay time T_{m60} is small.

Table 4.4: Average reverberation times of the boundaries of a particle board box

($T = 16°C$)

mode	(0,1,0)	(0,0,1;1)	(0,0,1;2)	(1,0,0)	(0,1,1)	(1,1,0)
f (Hz)	154.9	171.7	184.0	201.8	230.9	250.5
T_p (s)	0.69	0.69	0.69	0.49	0.22	0.22

mode(0,0,1;1)—— cavity controlled mode

mode(0,0,1;2)—— panel controlled mode

Table 4.5: A comparison of the panel damping and radiation loss contributions to decay times of the acoustical modes in a particle board box

acoustical	panel damping		panel radiation		measured	
mode	T_{m60} (s)	T_{m60}^{-1} (s^{-1})	T_{m60} (s)	T_{m60}^{-1} (s^{-1})	T_{m60} (s)	T_{m60}^{-1} (s^{-1})
(0,1,0)	1.85	0.54	22.4	0.045	2.5	0.40
(0,0,1;1)	0.71	1.41	24.0	0.042	1.27	0.79
(0,0,1;2)	0.87	1.15	2.77	0.36	0.77	1.30
(1,0,0)	1.0	1.0	6.61	0.15	0.86	1.16
(0,1,1)	2.90	0.35	27.4	0.038	1.6	0.36
(1,1,0)	2.83	0.35	24.8	0.040	2.3	0.44

Another experiment was carried out to measure the average sound intensity radiated from the vibrating panel of the concrete cavity-panel system at the peak frequencies of Figure 4.13. Each acoustical mode was generated at its resonance frequency by the loudspeaker and the sound pressure level was monitored at the opposite corner on the floor by a microphone. A sound intensity meter was used to measure the sound power radiated from the panel. The sound intensity was measured at the node points of an 5 × 7 uniform grid on the panel surface. The total radiation power for each mode and at each measured panel modal density value was then obtained by summation of the measured intensities over the grid. Figure 4.17 shows that for the same reference sound pressure level in the cavity, the total radiation power varies with the panel modal density (which is varied by adding sand to the panel surface). The sound radiation becomes large when the acoustical modes reach the maximum sound absorption region, and becomes even larger when the acoustical modes become panel controlled (because in these two cases, the panel vibration level is high).

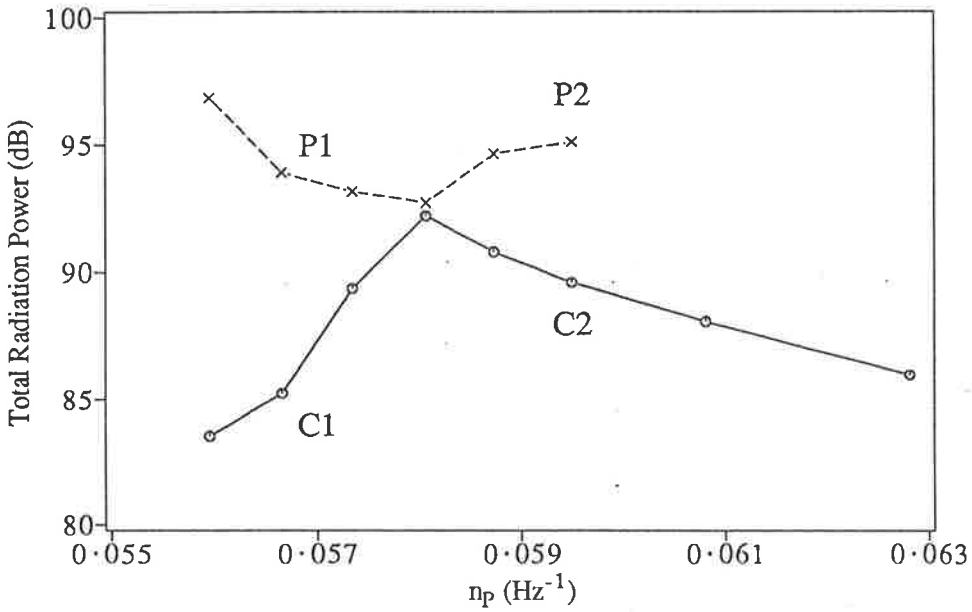

Figure 4.17: Total radiation power from the panel to the external space with constant sound pressure level in the cavity. (——) (0,0,1) cavity controlled mode; (- - -) (3,1) panel controlled mode. (Loudspeaker excitation at the resonance frequencies of the acoustical modes)

4.6 Discussion and conclusions

The first part of this experimental work was to determine the properties of the uncoupled cavity and panels. From knowledge of these properties, the theoretical results in Chapter 3 were used to predict the resonance frequencies and the modal decay times of the coupled system. The second part of the experimental work was to directly measure the behavior of the coupled panel-cavity system, and to compare these results with the predictions. The comparison in table 4.3 and Figures 4.11 and 4.12 shows that the modal coupling theory, upon which the predictions are based, can be used to estimate the sound decay when the boundaries of the enclosure are modally reactive.

The dependence of the resonance frequencies and modal decay times of the system upon the modal density of the panel, panel damping and radiation loss were investigated experimentally. The results confirm the theoretical predictions.

Instead of using many panels of different thicknesses, a layer of sand has been used to change the modal density of a test panel. This simple method enabled us to observe the dependance of the modal decay times of the acoustical modes on panel modal density. Particularly, the existence of minimum modal decay time regions and of frequency jumps of cavity controlled modes has been demonstrated. Measurement of the specific acoustical transfer impedance revealed a possible reason for these jumps. The large impedance phase changes of the examined acoustical modes in the minimum modal decay time region indicated that a change in the state of panel behavior takes place in this region.

However, sand increases the panel damping of the higher order panel modes. It is difficult to identify the modal decay times for higher order panel modes. In this case, the 1/3 octave panel decay times were used as panel modal decay times. This approximation often underestimates the panel modal damping. This may explain the discrepancies between the predicted and the measured results shown in Figures 4.11 and 4.12.

The effect of the panel damping on the decay of the acoustical modes in the enclosure is substantial. If the panel is thick and heavily damped, the contribution of the panel radiation to the sound absorption of the cavity controlled modes is negligible. However, the radiation contribution to the sound transmission into the external space can be important for the panel

controlled modes.

The measurement of the panel modal decay times includes the effect of both mechanical damping and radiation loss. In this experiment, these measured decay times have been used as panel modal decay times for the prediction of acoustical modes. In effect, the radiation loss has been incorporated into the model as extra mechanical damping. There is no theoretical proof that this is a valid approximation, but the close agreement between experiment and the prediction indicates that it does not produce significant error.

Although the experiments have been confined to a simple panel-cavity system, the general relationships between the sound field and the modal characteristics of its extensively reactive boundary have been demonstrated. Other boundary conditions of the test panel, or a more complicated shape of the enclosure might give different quantitative relationships between the modal decay times and the boundary characteristics, but the basic phenomena, such as the maximum sound absorption and the sudden change of resonance frequency in the maximum sound absorption regions should still remain.

Acoustic coupling with more complicated structures (for example, a cylindrical shell) can be studied in a similar way. In nearly all practical situations, cavities have more than one flexible wall (Dickinson and Warburton 1967), and there is structural coupling between adjacent walls. In such cases there are more and different parameters which can be chosen to control the acoustical behavior.

The decay rates of the acoustical modes investigated here were evaluated mode by mode. However, when a sound field is generated at an off-resonance frequency, several modes may participate in the decay. In this case the behavior of the decay will be the combined result of all the participating modes. Interference may occur between the contributing modes, and the decay curve may not be linear. Beating may be observed and the behavior of the decay will then depend upon the relative amplitude and phase of each mode at the measuring point. Early work on this aspect of the problem has been done for locally reactive boundary enclosures (Hunt *et al.* 1939). However once the boundary coupling effect is introduced, the decay behavior of a number of modes can not be divided into seven groups of modes, in which each group will have the same decay time. Panel characteristics, especially the participation of the structure dominated modes, must then be considered.

Chapter 5

Effect of fluid-structural coupling on acoustical decays — SEA approach

5.1 Introduction

The classical sound absorption theory (Morse 1939), which is based on the locally reactive boundary assumption, can produce an incorrect prediction for the low frequency modal decay times in a reverberation room. Experimental evidence (Pan and Bies 1988) showing that the walls of the room are modally reactive rather than locally reactive, explains this failure. Results of theoretical and experimental investigations (Chapters 3 and 4) into the effect of fluid-structural coupling upon the sound absorption in a panel-cavity system show that the decay times of the low frequency resonant modes can be predicted by modal coupling analysis.

Modal coupling analysis is an effective approach for estimating the decay behavior of low frequency coupled modes. In the low frequency range, the modal parameters of the uncoupled room and panel can easily be determined, because the resonance frequencies of the room modes are well separated from one another, and so are the structural mode frequencies. However above the low frequency range, the resonance frequencies of the room are close together and many room modes can be generated at the same time. The modal decay times of the structural modes also decrease so that the resonance peaks broaden and overlap.

Consequently the determination of the modal parameters of the room and of the panel becomes difficult. At these higher frequencies, modal coupling analysis is impractical but a description of the average behavior of the coupled system by the Statistical Energy Analysis (SEA) is possible and practical.

Traditionally, the reverberation times of high frequency sound fields in a reverberation room has been related to the sound absorption coefficient of the boundaries. If the boundaries are locally reactive, their sound absorption coefficient α is related to the normal acoustical impedance of the boundary material. When the boundaries, such as panel sound absorbers, are modally reactive, the relationship between the sound absorption coefficient of the boundaries and the boundary properties becomes more complicated. The sound absorption behavior of such boundaries is usually determined experimentally using Sabine absorption theory (Sabine and Ramer 1948, Parkin and Purkis 1951 and Knudsen *et al.* 1967). The measured sound absorption coefficient α_{Sab} is called the Sabine absorption coefficient. However the physical interpretation of α_{Sab} is unclear, and there has been no way of calculating it from the structural properties of the boundaries.

In this Chapter, the effect of the coupling of a sound field in a reverberation room with panel absorbers upon the decay behavior of each is investigated by the SEA method. In this analysis the sound field in the room and the panel vibration response have been characterized in terms of the average modal parameters (such as modal densities, loss factors and coupling loss factors). A quasi-transient solution of the average energies in the room and the panels is used to evaluate the reverberation times of the sound field in the room and also to compute the decay curves of a test panel and the room. An accompanying experiment has also been conducted to verify the result of the analysis.

The calculated and experimental results for the sound decay in the room agree in the high frequency range. This agreement shows that the average decay behavior of the room and panels can be analysed in terms of average modal parameters. The amalgamation of average modal parameters (of the test panels and the reverberation room) can be related to α_{Sab} of the panels. This result provides a possible interpretation for the α_{Sab} of a modally reactive surface and suggests a way to estimate this quantity by the SEA method. The dependence of the Sabine absorption coefficients of the panels upon the the characteristics of the room in which they are measured is also demonstrated both experimentally and analytically.

The purposes of the following sections are to,

1. formulate a mathematical description for the proposed experiment,
2. measure the values of the parameters required for the prediction of reverberation times in the room and of decay curves of a test panel,
3. compare the actual reverberation times of the room (with the panels) with the corresponding theoretical predictions,
4. explain the physical meaning of the Sabine absorption coefficient of the panels in terms of SEA.

5.2 Description of the room and the panels

The reverberation room used for the experiment to be discussed has been described in Chapter 2 (see Figures 2.2 and 2.3). Six identical panels were placed on the floor of the reverberation room as shown in Figure 5.1 (a) for the experiment. Each test panel of 1.2 m by 1.5 m surface dimensions is made of 10 mm thick particle board screwed at the edges to timber frames 90 mm high and 20 mm thick. A cavity (90 mm in depth) is formed between the panel and the floor surface on which the panels are mounted.

5.3 Quasi-transient solution of panel-room coupled system

According to the format of SEA,the behavior of a panel-room coupled system can be described in terms of the average energies distributed between the panel and the room, the energies dissipated within and flowing between each of them and the input powers to the room and the panels. The steady state distributions and the dynamic flow of the average energies can be determined in terms of average modal parameters of the system. Figure 5.2 shows the energy flow relationship of the two subsystems.

η_A and η_P are the loss factors of the room and the panel respectively. η_{AP} is the coupling loss factor from the room to the panel while η_{PA} is the coupling loss factor from the panel to the room.

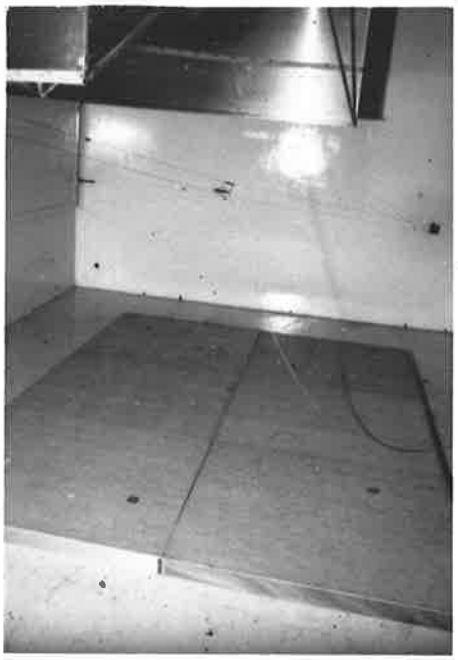

(a)

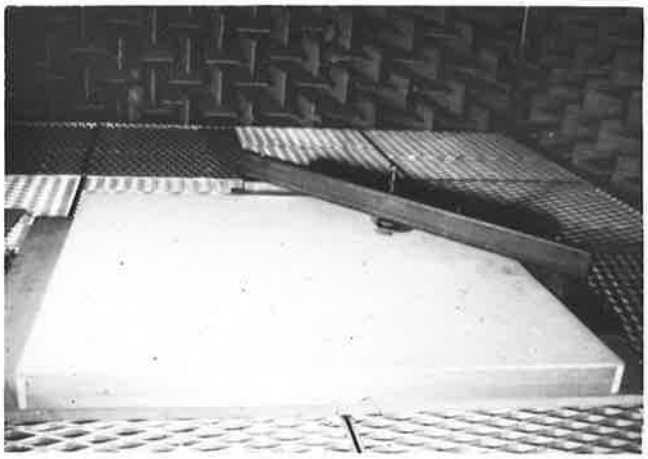

(b)

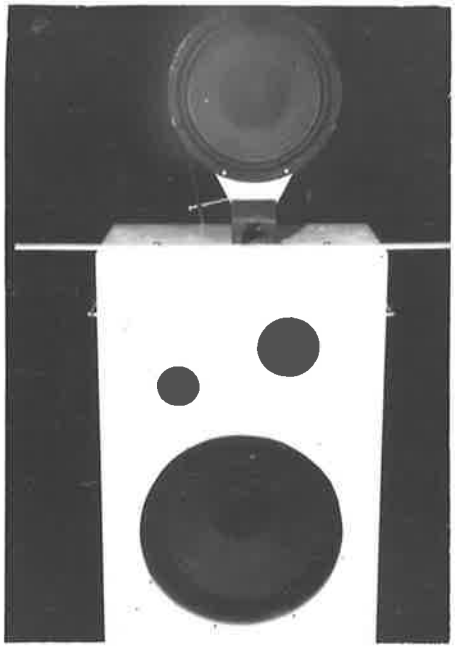

(c)

Figure 5.1: (a) inside of the reverberation room and test panels; (b) a test panel in an anechoic room; (c) two loudspeakers used im the experiment.

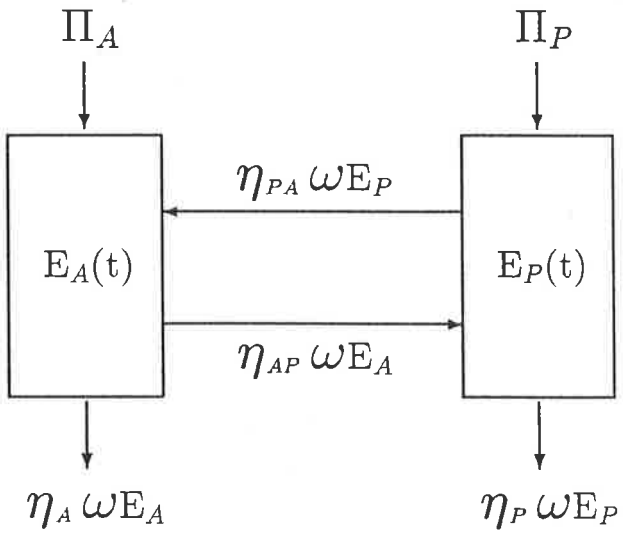

Figure 5.2: Power flows between the room and the panel.

The cavity behind the panel could be taken as yet another subsystem, but in this analysis, the panel and its backed cavity are considered as a single subsystem. Therefore the panel internal energy loss includes both the energy loss in the panel and into the back cavity.

Many workers have applied the SEA approach to the fluid-structural coupling problem and obtained a steady state solution for the acoustical response and radiation properties of coupled systems (Lyon and Maidanik 1962, Maidanik 1962 and Smith 1962) and for the study of partition transmission loss between rooms (Lyon 1963 and Crocker *et al.* 1969). In order to determine the SEA parameters for complex structural systems from experiments, Maidanik (1977) considered both the steady state and the quasi-transient conditions (transient state for the gross parameters, e.g. the average energies). He also argued that the reverberation time can be interpreted within the format of SEA. Sun *et al.* (1986b) have applied a quasi-transient solution of a coupled system to coupled structures and obtained good agreement with experiment.

Based upon this previous work, the dynamic relationship of the band energies in the room $E_A(t)$ and in the panel $E_P(t)$ can be expressed as follows:

$$\begin{bmatrix} \frac{\partial}{\partial t} & 0 \\ 0 & \frac{\partial}{\partial t} \end{bmatrix} \begin{bmatrix} E_A \\ E_P \end{bmatrix} + \begin{bmatrix} (\eta_A + \eta_{PA})\omega & -\eta_{AP}\omega \\ -\eta_{PA}\omega & (\eta_P + \eta_{AP})\omega \end{bmatrix} \begin{bmatrix} E_A \\ E_P \end{bmatrix} = \begin{bmatrix} \Pi_A \\ \Pi_P \end{bmatrix}, \qquad (5.1)$$

where Π_A and Π_P are the input powers to the room and the panel. ω is the central angular frequency of the examined angular frequency band $\Delta\omega$.

When the coupled system is in steady state and then the input power is suddenly cut off, the time dependent energies in the room and in the panel can be obtained by applying the Laplace transform to Eq. (5.1).

$$E_A(t) = E_A(0)[\frac{s_1 + d_1}{s_1 - s_2}\exp(s_1 t) - \frac{s_2 + d_1}{s_1 - s_2}\exp(s_2 t)] \,, \tag{5.2}$$

$$E_P(t) = E_P(0)[\frac{s_1 + d_2}{s_1 - s_2}\exp(s_1 t) - \frac{s_2 + d_2}{s_1 - s_2}\exp(s_2 t)] \,, \tag{5.3}$$

where $E_A(0)$ and $E_P(0)$ are the initial energies in the room and in the panel respectively and

$$s_1 = -\frac{1}{2}\omega[(\eta_A + \eta_P + \eta_{AP} + \eta_{PA}) - ((\eta_A + \eta_{AP} - \eta_{PA} - \eta_P)^2 + 4\eta_{AP}\eta_{PA})^{\frac{1}{2}}] \,, \tag{5.4}$$

$$s_2 = -\frac{1}{2}\omega[(\eta_A + \eta_P + \eta_{AP} + \eta_{PA}) + ((\eta_A + \eta_{AP} - \eta_{PA} - \eta_P)^2 + 4\eta_{AP}\eta_{PA})^{\frac{1}{2}}] \,, \tag{5.5}$$

$$d_1 = \omega(\eta_P + \eta_{PA} + \eta_{PA}\frac{E_P(0)}{E_A(0)}) \,, \tag{5.6}$$

$$d_2 = \omega(\eta_A + \eta_{AP} + \eta_{AP}\frac{E_A(0)}{E_P(0)}) \,. \tag{5.7}$$

5.4 Description of the experiment

5.4.1 Determination of the modal densities

The modal density of the reverberation room can be calculated using the following formula (Morse 1948c):

$$n_A = \frac{4\pi f^2 V}{C_0^3} + \frac{\pi f A}{2C_0^2} + \frac{L}{8C_0} \,, \tag{5.8}$$

where V, A and L are the total volume, surface area and edge length of the reverberation room and C_0 is the speed of sound in the air. Experimentally, the modal density can also be determined by counting the resonance peaks in the room spectral response in the low frequency region (e.g. below 200 Hz in the reverberation room mentioned above). Figure 5.3 shows the power spectral density of the room sound field.

The modal density of a test panel can be determined either by counting the resonance peaks of the panel spectrum or by measuring the longitudinal sound speed in the panel and calculating the modal density. Figure 5.4 shows the measured power spectral density of the panel acceleration. The average modal density of the panel determined by counting the peaks in Figure 5.4 is 0.130 Hz^{-1}. The panel longitudinal sound speed C_L is 2540 m/sec, which was

obtained by measure the resonance frequencies of a simply supported rectangular panel. The modal density of the panel is related to C_L, the surface area A_P and the panel thickness h by

$$n_P = \frac{\sqrt{3}A_P}{C_L h} \ . \tag{5.9}$$

The calculated modal density is 0.124 Hz^{-1}. The power spectral density of the panel includes any contribution of the backed cavity and the participation of cavity modes is also possible. This may account for the greater measured modal density by peak counting method.

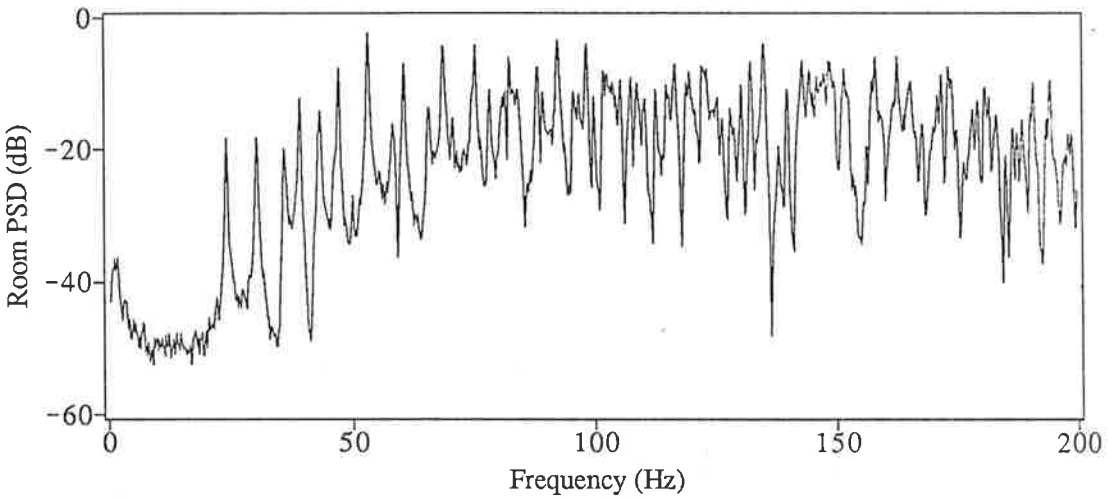

Figure 5.3: PSD of the sound field in a reverberation room.

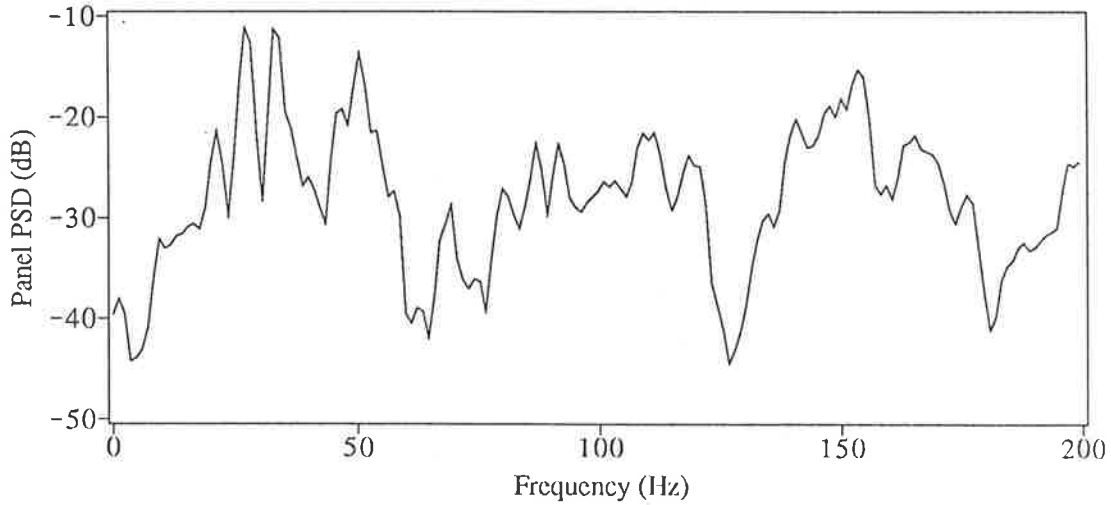

Figure 5.4: PSD of the particle board panel acceleration.

5.4.2 Determination of the loss factors

The loss factor of a subsystem is defined as follows

$$\eta = \frac{P}{\omega E} , \tag{5.10}$$

where E is the total energy stored in the subsystem and P is the energy dissipated per radian cycle in the subsystem. The loss factors of the room (without panels) can be determined by measuring its reverberation times. The relationship between the reverberation time T_{60} and the loss factor of the room is

$$\eta_A = \frac{13.8}{\omega T_{60}} . \tag{5.11}$$

One third octave band reverberation times (Figure 5.5) of the sound field in the reverberation room in the absence of the test panels were measured by using two different loudspeakers. Detailed descriptions of these two loudspeakers(Figure 5.1 (c)) can be found in Munro's thesis (1982). The results of these tests show that the loudspeaker box absorbs a significant proportion of the energy in the low frequency range. The measured sound absorption of the room includes the effect of losses to the loudspeakers.

The total panel loss factor (internal loss and radiation loss) was obtained by measuring the reverberation time of the panel (Heckl 1962). To avoid the influence of the reverberation room upon the panel decay, the panel was tested in an anechoic room. Thick panels were put underneath the test panel so that the same air cavity behind the panel was maintained. Decay times were recorded after a driving magnet was switched off. Since the decay times above 800 Hz are very short, a recorder was used to record the decay at high speed and play back for the measurement at low speed. Measured panel reverberation times are shown in Figure 5.6.

The internal loss factor can be obtained by subtracting the coupling loss factor η_{PA} from the measured total loss factor of the panel $(\eta_P + \eta_{PA})$. In this experiment the internal loss factor is determined by the measured ratio of the panel vibration energy to room sound energy and the modal densities. When the sound field is driven by a loudspeaker, this ratio is related to the internal loss factor η_P and the total loss factor of the panel (Vér *et al.* 1971) by:

$$\frac{E_P}{E_A} = \frac{n_P}{n_A} \frac{\eta_{PA}}{\eta_P + \eta_{PA}} . \tag{5.12}$$

Once the energy ratio, the modal densities and the total loss factors of the panel $\eta_P + \eta_{PA}$ are known, the η_{PA} can be calculated from Eq. (5.12) and then the loss factor η_P for a test panel can be obtained (Figure 5.7).

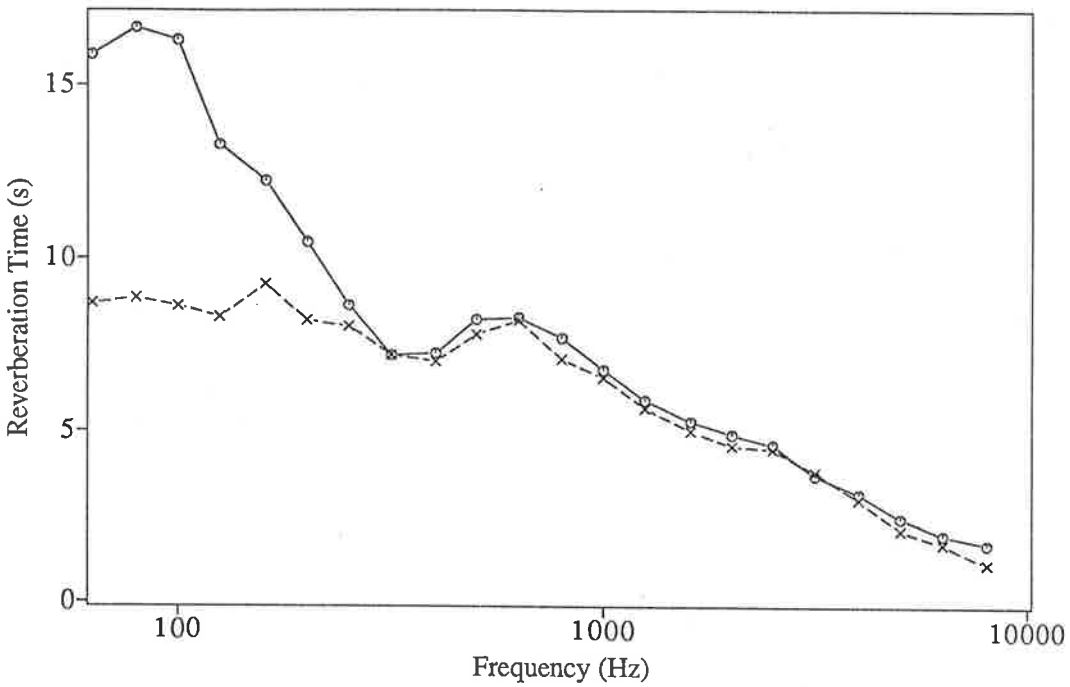

Figure 5.5: Reverberation times of the empty reverberation room; (o o o) small loudspeaker; (× × ×) large loudspeaker.

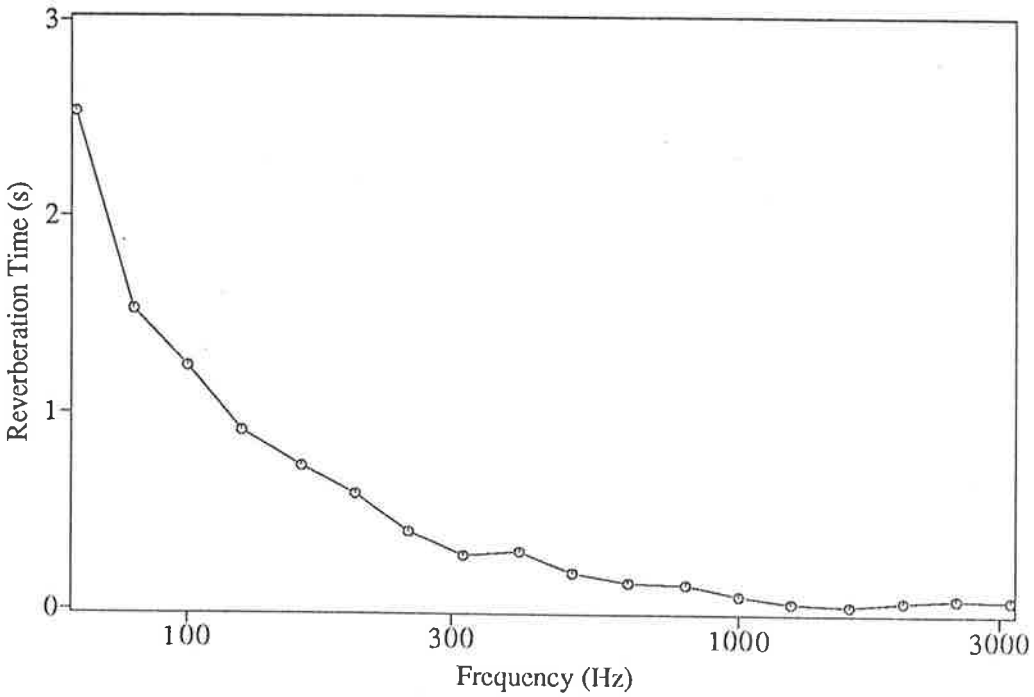

Figure 5.6: Reverberation times of the panel vibration (measured in an anechoic room).

5.4.3 Determination of the coupling loss factors

The coupling loss factor from the panel to the room η_{PA} is related to the sound radiation efficiency σ_{Rad} of the panel (Vér *et al.* 1971) by (for one side radiation)

$$\eta_{PA} = \frac{\rho_0 C_0 \sigma_{Rad}}{\rho} \ . \tag{5.13}$$

Theoretical expressions for the radiation efficiency of a simply supported panel have been obtained by Maidanik (1962). Expressions for the radiation efficiency for panels with different edge conditions, such as clamped edge, are also available (Fahy 1969).

Experimentally the coupling loss factor η_{PA} can be determined by the measurement of the ratio of the panel vibration energy to the sound field energy in the room or by measuring the radiated sound power from the vibrating panel and the average velocity of the panel. Figure 5.7 (a) shows the η_{PA} of the particle board obtained from the energy ratio measurement.

The coupling loss factor from the room to the panel η_{AP} (see Figure 5.7 (c)) is usually calculated using the following relation:

$$\frac{\eta_{PA}}{\eta_{AP}} = \frac{n_A}{n_P} \ . \tag{5.14}$$

The assumption implicit in the use of Eq. (5.14) is that of equal energy distribution among the modes and the same coupling loss factors between the modes (Lyon 1975).

5.4.4 Average energy measurements

Energies contained in the room and in the panel are related to the time and spatial averaged squared sound pressure $< \bar{p}^2 >$ and acceleration $< \bar{a}^2 >$ respectively by

$$E_A = \frac{V}{\rho_o C_o^2} < \bar{p}^2 > \ , \tag{5.15}$$

$$E_P = \frac{\rho A_p h}{\omega^2} < \bar{a}^2 > \ . \tag{5.16}$$

The density of the particle board ρ is 691 kg/m^3.

Two set of the measurements have been conducted. In the first the room only is driven by a loudspeaker and in the second the panel only is driven by a magnetic driver. In both of the measurements, only one panel is placed in the reverberation room.

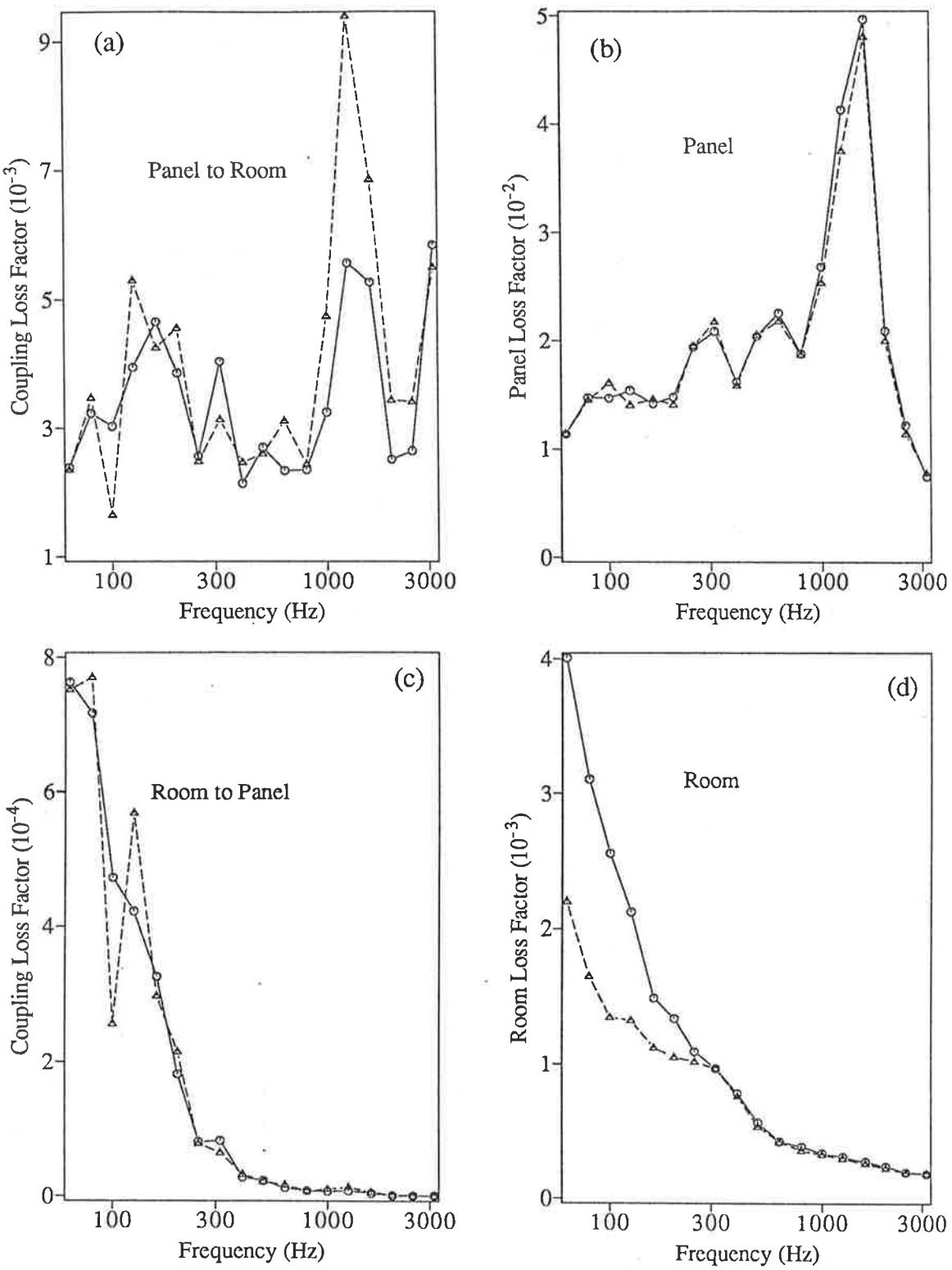

Figure 5.7: Measured loss and coupling loss factors of the coupled system. (a) coupling loss factor from panel to room η_{PA}; (b) panel loss factor η_P; (c) coupling loss factor from room to panel η_{AP}; (d) room loss factor η_A; (——) large loudspeaker, (- - -) small loudspeaker.

The sound pressure in the reverberation room is measured in one third octave bands using a traversing microphone. A rotating diffuser is used to increase the accuracy of the measurement. The acceleration level of the panel was measured using an accelerometer placed sequentially at twelve points chosen at random on the panel for the spatial average. Figure 5.8 (a) shows the panel-room energy ratio as a function of frequency from the results of the first measurement and Figure 5.8 (b) shows the room-panel energy ratio when the panel is driven by a magnetic driver.

5.5 Results and discussion

The reverberation times of the sound field in the room with six test panels on its floor were obtained by driving the sound field with one third octave bands of noise through a loudspeaker and measuring decay rates after the loudspeaker was switched off. The reverberation times can be determined by the decay rates and linear decays were observed in the logarithmic scale of the recorded sound pressure. Decay curves of one panel in the room were also measured after the driving magnet was switched off.

Based on the average parameters obtained in the last section, we can calculate the decay times of the reverberation room and the panel using Eqs. (5.2) and (5.3). Since the six panels are identical, when the coupling of the six panels with the sound field is considered, the measured panel energy and the coupling loss factor η_{AP} for one panel will be increased by a factor of six when used in Eq. (5.2).

Figure 5.9 shows the calculated and the measured results using large and small loudspeakers. These results agree in the 200 Hz and higher frequency bands. The width of the 200 Hz band is 46Hz and there are 5 panel modes and 102 room modes in this frequency band, thus there are a sufficient number of modes excited in the room and in the panel to enable satisfaction of the requirements of SEA (Swift and Bies 1978) to give satisfactory results in this and higher frequency bands. In the lower frequency range, the main reason for the discrepancies in Figure 5.9 is that the sound field in the room is not uniform which is reflected in variation in the measured reverberation time and the average energy in the sound field.

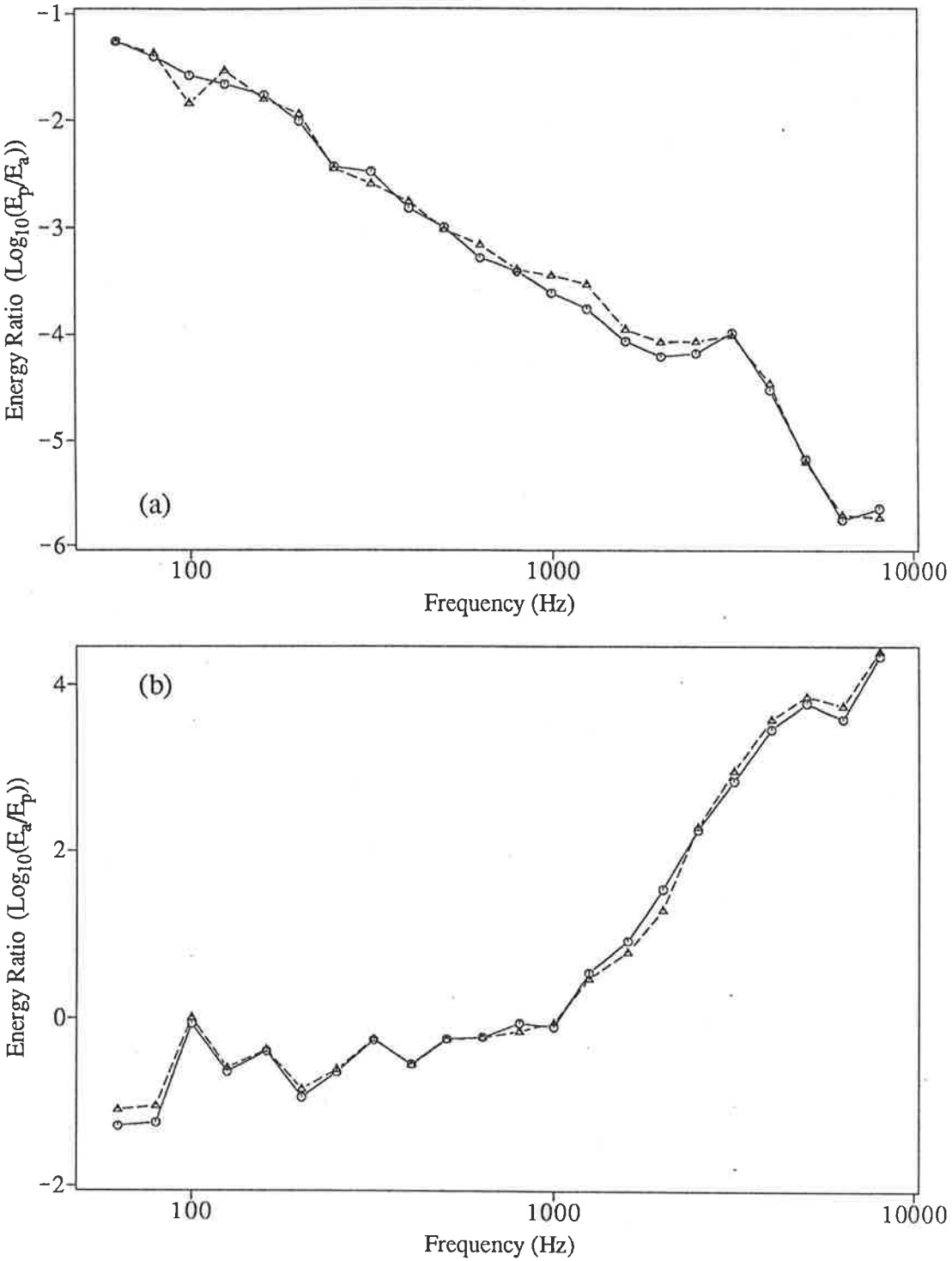

Figure 5.8: Measured energy ratios. (a) ratio of the panel vibration energy to the sound field energy, room driven by a loudspeaker; (b) ratio of the sound field energy to the panel vibration energy, panel driven by magnetic shaker. (——) large loudspeaker, (- - -) small loudspeaker.

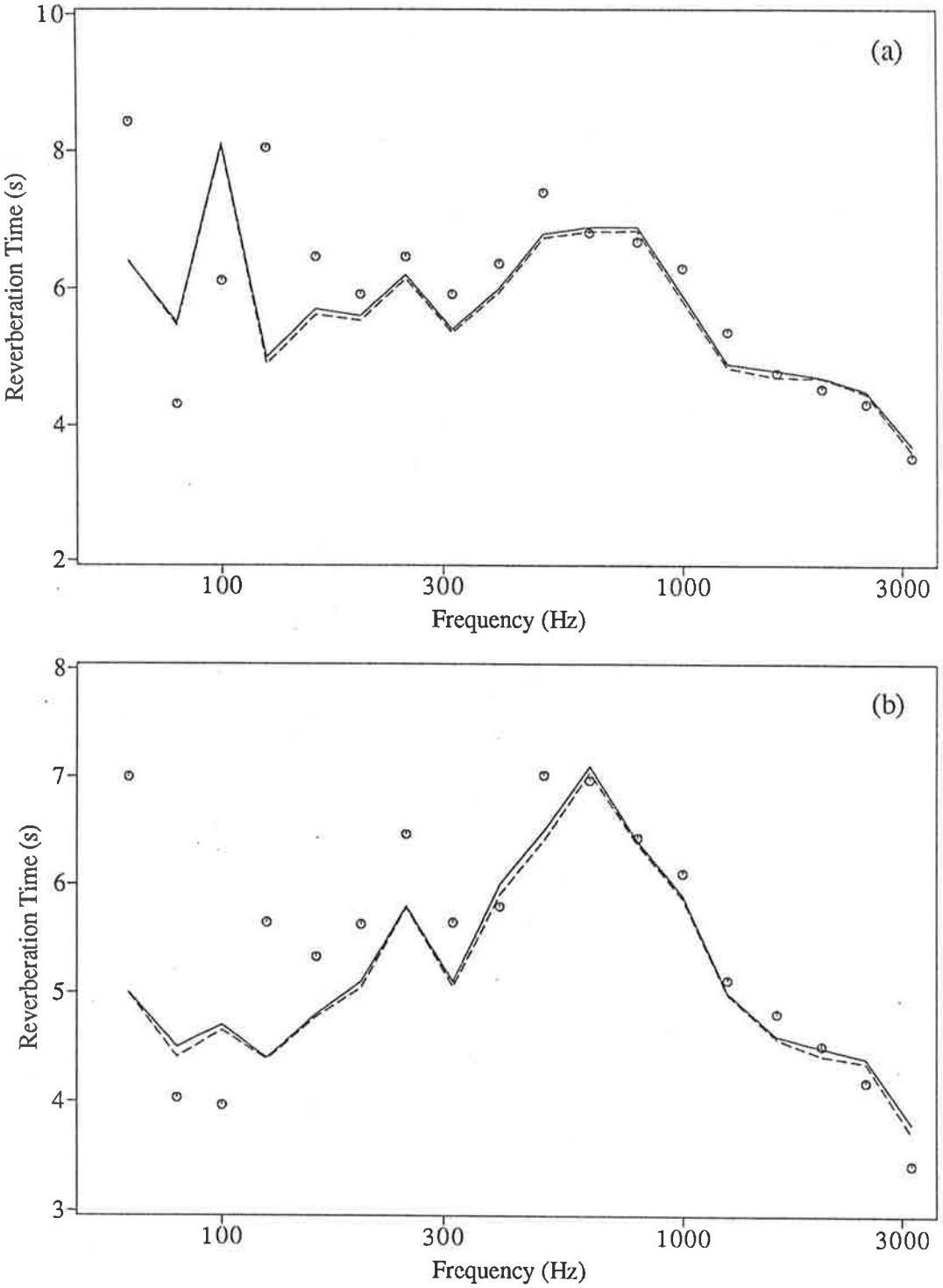

Figure 5.9: Reverberation times of the sound field in a reverberation room with six panel sound absorbers, (o o o) measured, (——) calculated from Eq. (5.2), (- - -) calculated from Eq.(5.17). (a) small loudspeaker; (b) large loudspeaker.

Figure 5.10 shows the decay curves of a test panel in the reverberation room and the decay curves for the sound field. Double decay rates are observed in the panel decay curves. The initial decay is close to that due to the panel loss factor and the second decay is close to that due to the room loss factor. The sound field shows linear decay behavior. The calculated panel and room decay curves are also shown in the figure. To interpret the decay behavior of the room and the panel, the expressions for their decay (Eqs. (5.2) and (5.3)) are evaluated. Both Eq. (5.2) and Eq. (5.3) are composed of two exponential terms. The first one has the smaller decay rate which is close to the uncoupled room decay rate and the second one has the larger decay rate which is close to the uncoupled panel decay rate. Their contributions to the decay behavior of the coupled system is dependent upon their relative amplitudes and the value of the decay constants.

In the case of the coupling of the reverberation room and test panels, two characteristics of the system must be taken into consideration: (1) the loss factor of the room is smaller than that of the panels; (2) at high frequencies, the modal density of the room is much larger than that of the panel (for example, at 200 Hz, the modal density ratio of the panel to the room is about 0.05 and this ratio becomes much smaller at higher frequencies).

5.5.1 The room decay

Referring to Eq. (5.2) of the sound energy decay, some estimations of the amplitude ratio and the exponential ratio of the first to the second term of this equation are made in Appendix B. The corresponding results calculated from the measured data are shown in Figure 5.11 (a) and (b). These results demonstrate that the amplitude of the first term is much larger than that of the second term because of the mentioned two characteristics. As the decay continues the exponential ratio also increases exponentially.

Because of this property of the Eq. (5.2), we can use the first term to approximate the decay behavior of the sound field in the room. Therefore the approximated reverberation time of the room can be written as:

$$T_{60} \cong \frac{27.6}{\omega|(\eta_A + \eta_P + \eta_{AP} + \eta_{PA}) - ((\eta_A + \eta_{AP} - \eta_{PA} - \eta_P)^2 + 4\eta_{AP}\eta_{PA})^{\frac{1}{2}}|} . \qquad (5.17)$$

The reverberation times calculated using the above formula are also plotted in Figure 5.9. They are in agreement with the results calculated using Eq. (5.2).

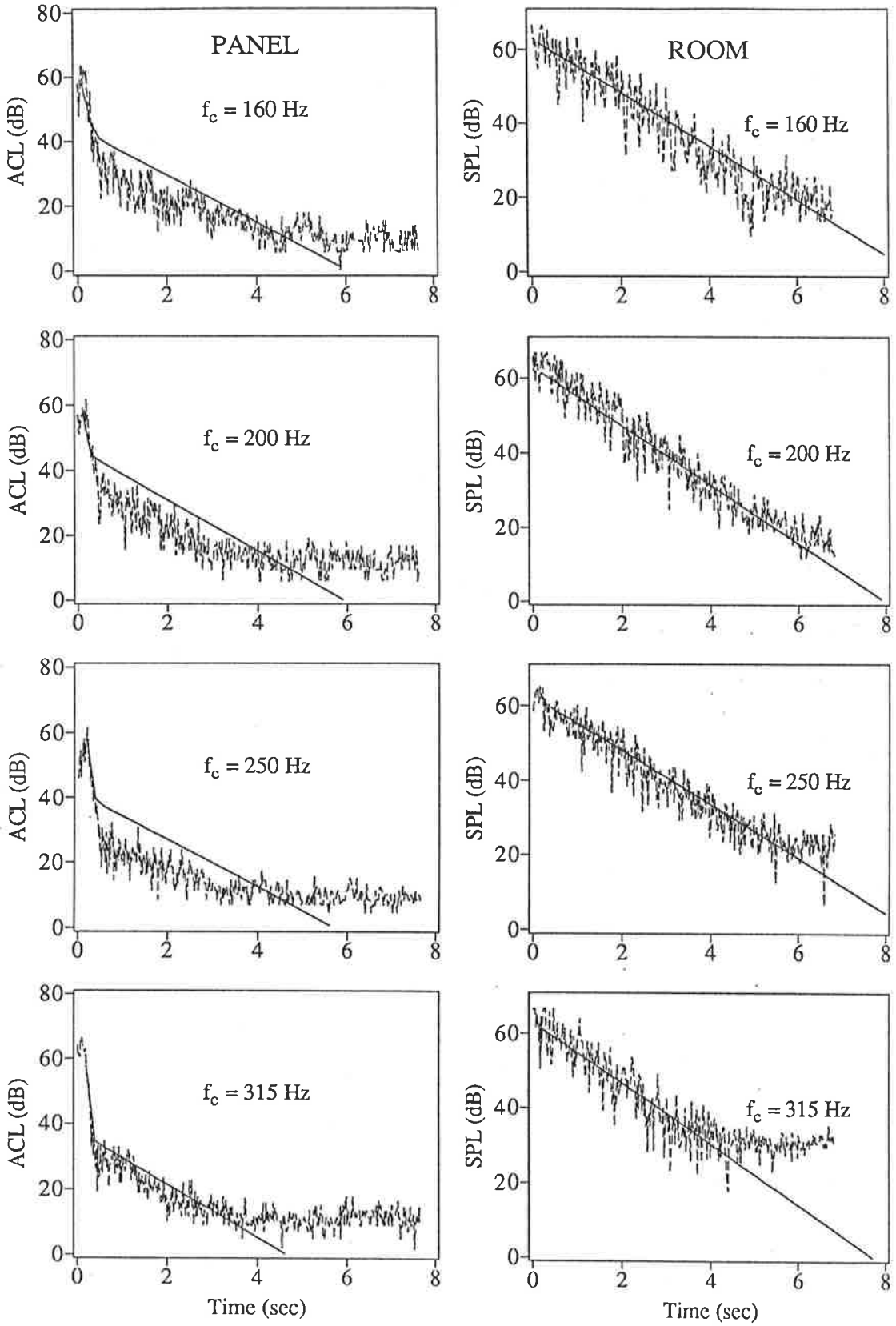

Figure 5.10: Decay curves of one panel acceleration level and of the sound pressure level in the reverberation room. (——) calculated results; (- - -) measured results. (f_c: 1/3 octave band central frequency).

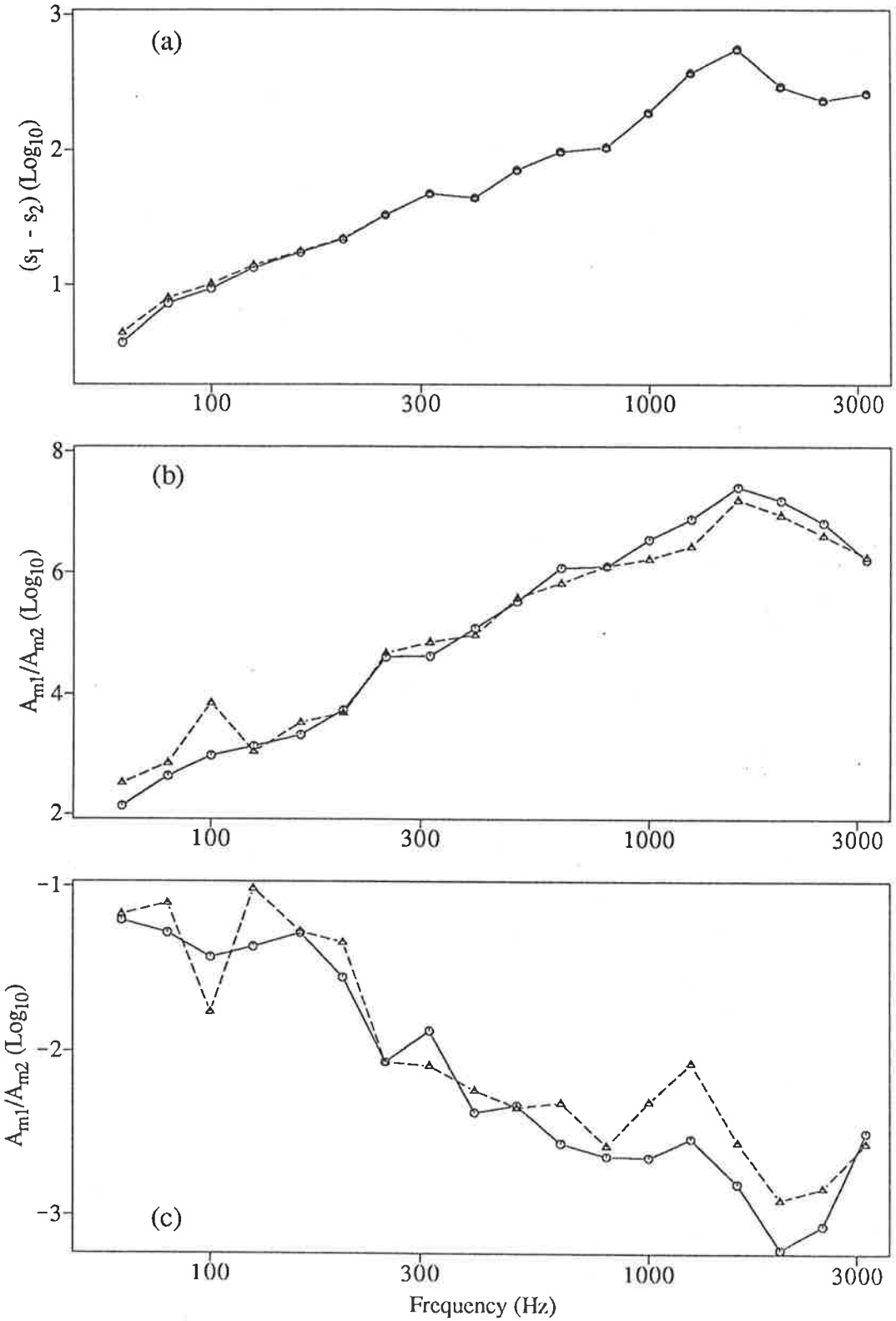

Figure 5.11:Comparison of the two terms in Eq. (5.2) and in Eq. (5.3). (——) large loudspeaker, (- - -) small loudspeaker. (a) The difference of the indices of the two exponential terms; (b) amplitude ratio (A_{m1}/A_{m2}) of Eq. (5.2); (c) amplitude ratio (A_{m1}/A_{m2}) of Eq. (5.3).

In a reverberation room measurement, the Sabine absorption coefficient of the panels can be estimated from the following relation (AS 1971):

$$\alpha_{Sab} = \frac{55.3V}{SC_o}(\frac{1}{T'_{60}} - \frac{1}{T_{60}}) , \tag{5.18}$$

where T'_{60} and T_{60} are the reverberation times after and before the test panels are put in the reverberation room; S is the total surface area of the panels. Substituting Eq. (5.17) in Eq. (5.18), we obtain the following

$$\begin{aligned} \alpha_{Sab} &= \frac{55.3V}{27.6SC_o}\omega(|(\eta_A + \eta_P + \eta_{AP} + \eta_{PA}) \\ &\quad -((\eta_A + \eta_{AP} - \eta_{PA} - \eta_P)^2 + 4\eta_{AP}\eta_{PA})^{\frac{1}{2}}| - 2\eta_A) . \end{aligned} \tag{5.19}$$

The modally reactive panels form a boundary of the sound field in the room. In the high frequency range, the wavelengths in the modally reactive panels grow shorter and the acoustical modes in the room increase in number without bound. The various standing waves generated by the acoustical modes interact at the boundary with each other so that the vibration of the panel surface tends to uniformity. In this frequency range, the interaction between the sound field and the boundaries is described more suitably by the average behavior of the sound field and the boundaries, rather than by the details of each mode. Therefore when Sabine's formula is used, the Sabine absorption coefficient of a modally reactive boundary is only the effective representation of the average fluid-structural coupling effect on the sound decay of the room.

Equation (5.19) indicates that the Sabine absorption coefficient α_{Sab} of test panels is dependent upon the room in which they are measured. Different reverberation times and sizes of the empty room, used to determine the loss factor η_A and the coupling factor η_{AP}, will give rise to different values of Sabine absorption coefficient α_{Sab} for the same panels. For example, the room loss factors are varied when two different driving loudspeakers are used(Figure 5.5). Figure 5.12 (a) shows the experimental resulting Sabine absorption area $\frac{55.3V}{C_0}(\frac{1}{T'_{60}} - \frac{1}{T_{60}})$ of the panels in these two different situations. About thirty percent difference in a few frequency bands is observed. The calculated values of Sabine absorption area by the SEA method, also gives a comparable result(Figure 5.12 (b)).

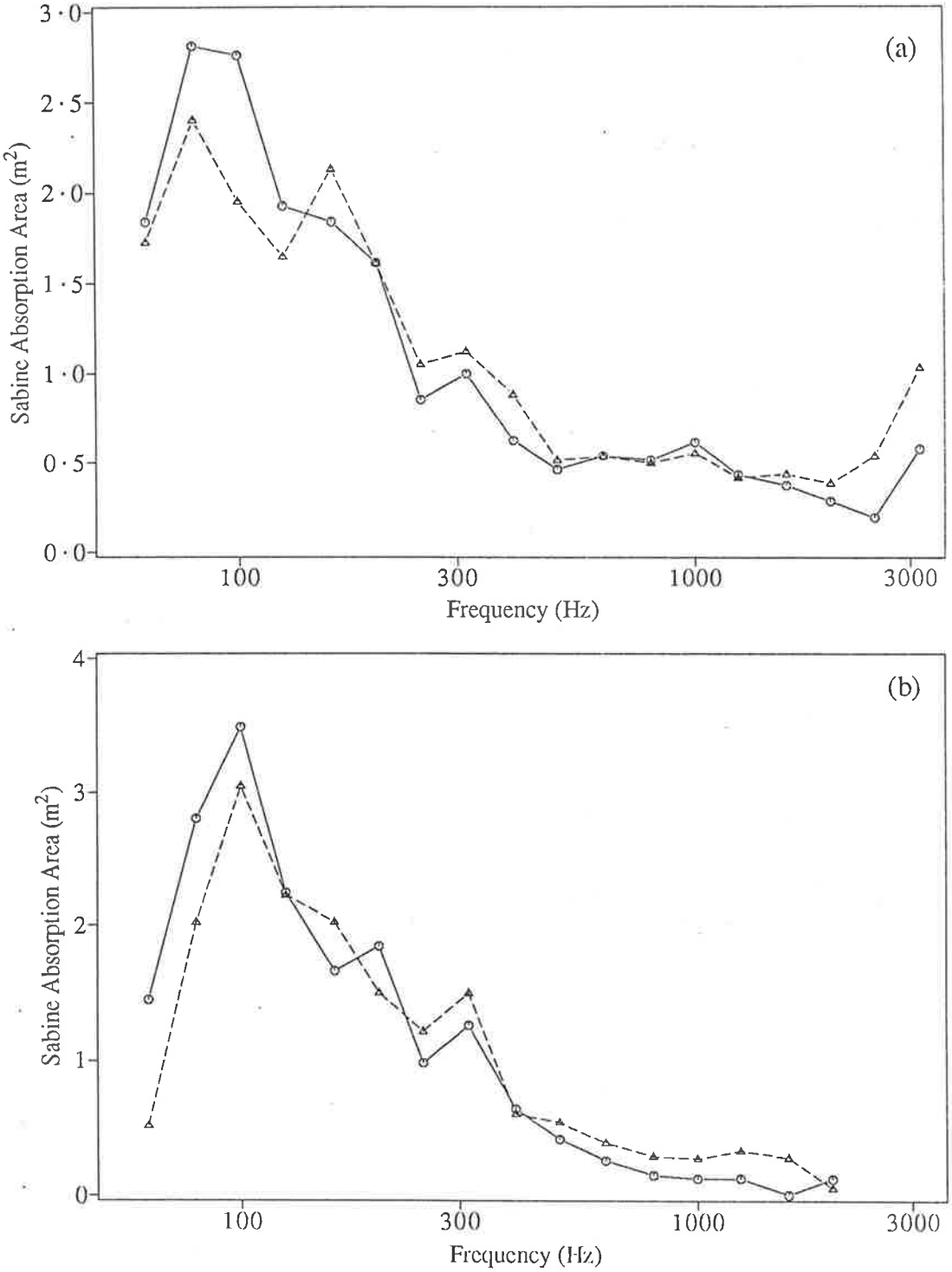

Figure 5.12: (a) Measured Sabine absorption area using a large and a small loudspeaker. (b) Calculated Sabine absorption area of the panels for the cases of a large and a small loudspeakers (see Munro 1982 for description of speakers) (——) large loudspeaker; (- - -) small loudspeaker.

Some efforts have been made to estimate the average normal acoustical impedance of a panel sound absorber (Ford *et al.* 1969 and Kiesewetter 1986), in order to predict its sound absorption coefficient. However, a simple relationship between acoustical impedance and sound absorption coefficient only exists if the surface is locally reactive (Morse 1948a). Sound waves impinging on a panel surface in an enclosure have angles of incidence ranging from 0 to 90 degrees and the modal excitation of the wall depends on the angle of incidence. Therefore, any calculation of the normal acoustical impedance which is used to predict the sound absorption coefficient of the panel, must include consideration of the wave angle of incidence. How the sound absorption coefficient of a modally reactive surface depends on the normal acoustical impedance is unknown, and so is still a topic for further research.

Models other than the acoustical impedance model can be used to describe the interaction between a sound field and its modally reactive boundaries. This may be justified by experimental evidence which shows that a modally reactive surface tends toward locally reactive behavior as frequency or damping is increased. For example, the mutual cancelling of superimposed modes tends to produce a field of uniform amplitude vibration at high frequencies. Determining under what circumstances a locally reactive model can be used as a simple approximation for a modally reactive boundary will be part of a future investigation.

5.5.2 The panel decay

A similar estimation and calculation is also made for the panel decay behavior by analysing Eq.(5.3) (see Appendix B). The calculated results of the exponential term ratio for the panel decay situation is the same as that in the case of the sound field decay. They are all shown in Figure 5.11(a), This indicates that the first term will dominant as time goes by. However the amplitude ratio of the first term to the second term Figure 5.11(c) is much less than 1, which indicates that the second term will dominate the initial stage of the decay. The observed double slope in the panel decay curves is thus explained.

If the panel and the room are physically separated, the panel and the room will each decay at their own rates which are expressed by their individual loss factors. The fluid-structural coupling is relatively weak, that is to say the energy transferred from one subsystem to the other is smaller than the total energy in the subsystems. Therefore when a panel and a room are coupled together, their decay rates will not be greatly changed.

If we drive the sound field and measure the sound decay in the room and if the reverberation time of the uncoupled room is longer than that of the panel, the energy in the room will always flow into the panel during all of the decay period. Linear decay is expected in this case and this is what is observed in the measurement. On the other hand, if the uncoupled room reverberation time is shorter than that of the panel, then after the energy in the room becomes smaller than the energy in the panel, the energy in the panel will flow back into the room. During this time, the energy in the room decays at the decay rate of the panel. In this case two slopes in the decay curve are expected. The same phenomenon can be observed when the panel is driven by a magnet and the panel decay is measured by an accelerometer. In the experiment, the panel damping is much higher than that of the room damping, which is why double decay slopes were obtained in the panel decay curves (Figure 5.10).

5.6 Conclusions

The effect of the fluid-structural coupling on the decay behavior of a coupled sound field and vibrating boundary structures at high frequencies has been investigated by the SEA method. A quasi-transient solution for the energies in two subsystems has been used to calculate the 60dB decay times in a reverberation room containing modally responsive panels, and to calculate the decay curves of panel vibration in a room.

The following conclusions are obtained from this study,

1. In the middle and high frequency ranges, modally reactive boundaries (such as panel absorbers and panel diffusers) can be described by average modal parameters (such as loss and coupling loss factors and modal density). The acoustical behavior of the sound field and the panel can be described in the SEA format.

2. The sound absorption property of a panel absorber was previously defined in terms of sound absorption coefficients. These sound absorption coefficients could only be obtained empirically and are considered to be properties of the panel only. However, by considering the coupling between the two multi-mode systems, the decay behavior of the sound field can be determined without using the sound absorption coefficient. This analysis also provides an interpretation of the sound absorption coefficient in terms the modal

parameters of the panel *and* the modal parameters of the room.

These conclusions suggest that

- The modal parameters of the panel and the room should be used to predict the acoustical behavior.
- The Sabine absorption coefficient of a panel absorber is not a property of only the panel. It also depends upon the properties of the room in which the panel is measured.

Chapter 6

The effect of a semi-circular diffuser on the sound field

6.1 Introduction

Standard measurements in a reverberation room are based upon the assumption that the diffuse sound field condition is satisfied. However, in some situations, such as for low narrow range frequency band measurements, this condition is very often not satisfied. In order to overcome this difficulty, rotating sound diffusers are generally used to increase the diffusion of the sound field and consequently to increase the accuracy of the measurements. Moreover stationary diffusers are also very often used in theaters for acoustical design purposes (Knudsen and Harris 1978) and in reverberation rooms to improve the measurement of sound absorption coefficients (Benedetto *et al.* 1981).

Due to these applications of diffusers, the nature of the sound field and the boundaries in an enclosure under the influence of diffusers has long been a topic of interest in the investigation of room acoustics. The effect of a rotating diffuser on the diffusion of the sound field has been reviewed by Schultz (1971). He summarized some qualitative criteria for adequate performance of a rotating diffuser. The phenomenon of side-band production by a rotating diffuser in a pure tone sound field introduced into a reverberation room is reported and discussed by Lubman (1971), Tichy *et al.* (1975), Hansen *et al.* (1980) and Lyamshev (1983). The variation of the radiation impedance of a vibrating plate caused by a rotating diffuser has

been investigated by Bies and Hansen (1979,1980). They found that the radiation impedance varied dramatically as the diffuser was rotated, but that the average measured value of the radiation impedance approached the free-field measured value when the diffuser was rotated faster than 20 rpm.

Thomas Munro studied the influence of a diffuser on acoustical modes at low frequencies in a reverberation room (Munro 1982). His experimental results showed that both the resonance frequencies and the decay times of the investigated modes were altered with the orientation of the diffuser. Further experimental work (Pan and Bies 1988) showed that the diffuser changes the modal distribution of the air borne (fluid) sound field over the surface of the floor in a reverberation room. Different orientations of the diffuser result in different couplings between the room modes and the structural modes of the floor, and variable modal decay times result from the variable modal coupling. In this situation, the coupling between the air born cavity modes and the boundary (in fact the diffuser is an important part of the boundary) must be taken into consideration. Especially, when the boundaries are extensively reactive, the coupling between each individual cavity mode and the boundary structural modes will be varied as the orientation of the diffuser is varied. Effectively energy transfer from cavity modes to the boundaries will be altered. The decay behavior of the sound field can be determined through consideration of such energy transfer. In order to gain a physical insight and a quantitative relationship, an numerical approach is required to the effect of the diffuser upon a sound field in an enclosure.

The energy exchange between a sound field and a modally responsive boundary may be described in terms of the uncoupled cavity modes and the uncoupled structural modes in the boundary. Thus to study the effect of the diffuser on the sound field decay time as a function of the diffuser orientation, or in the case when the rotation of the diffuser is included, the characteristics of the cavity modes need to be investigated first. Here cavity modes are defined as the air born acoustical modes in the presence of a diffuser but without coupling between the air born modes and the diffuser and boundaries.

This Chapter reviews some preliminary theoretical and experimental investigations into acoustical modal behavior under the influence of a semi-circular diffuser in a cavity. As a start of a numerical approach to find a qualitative relationship between the characteristics of a sound field and the behavior of a diffuser, a finite element approach is used to calculate

the resonance frequencies and the modal distributions of the sound field. An accompanying experimental investigation is also reviewed, which shows good agreement with the numerical results.

6.2 Two dimensional sound field

The mathematical model used in the analysis is of a two-dimensional rectangular cavity containing a semi-circular diffuser. The centers of the diffuser and the cavity are the same. The diffuser is 1 mm thick. Other dimensions of the cavity and the diffuser, are shown in Figure 6.1.

A constant sound pressure source of 0.001m radius is located at one corner of the cavity taken as the origin of the coordinates. All the boundaries of the sound field (including the surface of the diffuser) are assumed to be rigid, which provides a Neumann boundary condition (normal gradient of the sound pressure at the boundaries is zero).

A two dimensional finite element package called "TWODEPEP" (1985) is used for calculating the resonance frequencies and the modal distributions of the two dimensional sound field. The result of these calculations can be extended to describe the characteristics of a sound field in a three dimensional cavity. The three dimensional cavity with semi-cylindrical diffuser is illustrated in Figure 6.2. The height of the diffuser is the same as that of the cavity. The horizontal section of this system is exactly the same as that of Figure 6.1. In this cavity only those modes, which have non-zero wave propagation number in the horizontal (X-Y) plane, will be affected by the diffuser.

The wave equation for the free vibration sound field in the cavity in Figure 6.2 can be separated into two: a two dimensional wave equation in the horizontal (X-Y) plane and another one dimensional wave equation in the vertical (Z) direction. Therefore the distribution of the sound field and resonance frequencies in the three dimensional cavity is a combination of the results from the two-dimensional calculation and from the solution of the sound wave equation in the Z direction (with rigid boundary conditions at $Z = 0$ and $Z = L_z$). The resonance frequencies $f_{l,m}$ from the two-dimensional cavity model and the resonance frequencies $f_{l,m,n}$ of the three dimensional cavity are related as follows,

$$f_{l,m,n} = \frac{C_0}{2}\left[(\frac{2f_{l,m}}{C_0})^2 + (\frac{n}{L_z})^2\right]^{1/2} . \qquad (6.1)$$

C_0, n and L_z are the speed of sound in air, the modal index indicating the number of nodes in Z direction and the height of the cavity. Eq. (6.1) shows that if a mode in the cavity has a zero wave numbers in the (X-Y) plane, its resonance frequency will not be affected by the diffuser.

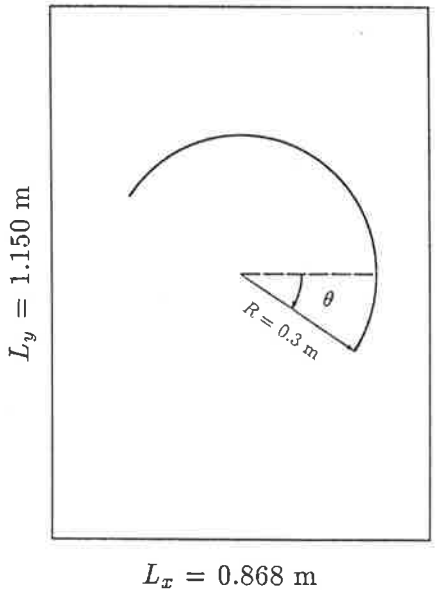

Figure 6.1: Two dimensional sound field, boundaries and a semicircular diffuser.

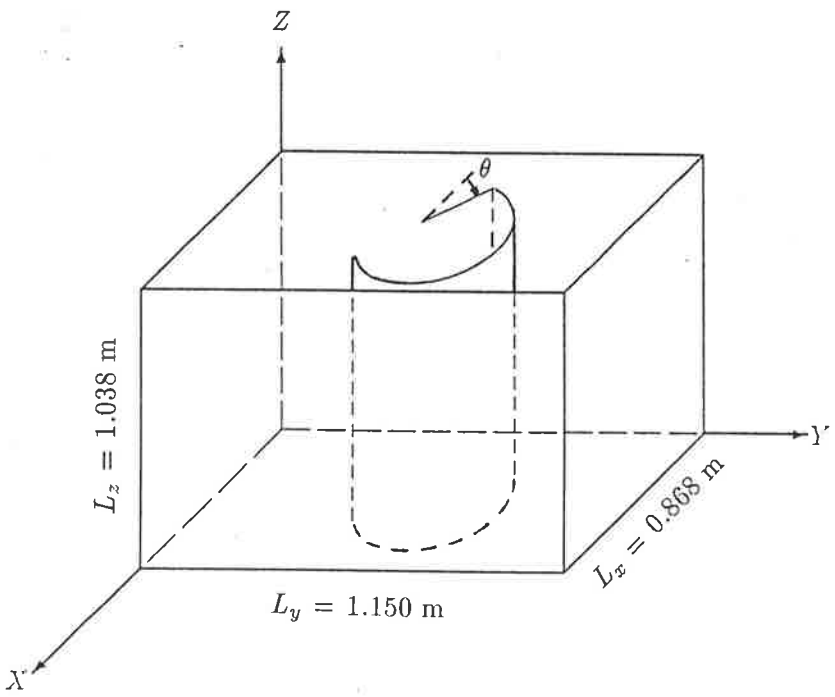

Figure 6.2: Three dimensional cavity with a semi-cylindrical diffuser.

6.3 Experimental arrangement

To verify the numerical result from Eq. (6.1), a semi-cylindrical diffuser made of 1 mm thick steel plate was placed in a concrete rectangular cavity (which has been described in Chapter 4). The horizontal cross section of the cavity and the diffuser dimensions are identical to those of the numerical calculation. The height of the cavity is 1.038 m. A handle was mounted on the central shaft of the diffuser, so that the diffuser could be turned from outside. The sound waves propagating in the Z direction were unaltered by this arrangement, so that the measured resonance frequencies could be compared with the calculated values (see Figure 6.3).

In the experiment, a white noise signal was introduced into the cavity by a horn loudspeaker through a high impedance tube (see Chapter 4). A microphone was placed in the corner opposite from the origin and on the floor. The acoustical response was obtained by passing the output of the microphone through a spectrum analyser. The resonance frequencies of the cavity were then determined by identifying the peaks in the spectrum.

6.4 Numerical calculations

To calculate the resonance frequency and modal distribution of each cavity mode for a particular position of the diffuser, a two dimensional homogeneous wave equation is solved numerically.

$$\frac{\partial^2 P}{\partial x^2} + \frac{\partial^2 P}{\partial y^2} + \frac{\omega^2}{C_0^2} P = 0 \, . \tag{6.2}$$

In this calculation, the boundary condition on both the surfaces of the cavity and the diffuser is

$$\left. \frac{\partial P}{\partial n} \right|_{\Gamma} = 0 \, . \tag{6.3}$$

n indicates the normal direction to the boundaries and Γ represents over all boundaries.

TWODEPEP has the capacity to refine the triangular mesh. Two hundred grid points were chosen for the calculation. Figure 6.4 shows the input triangular mesh for the finite element method (FEM) calculation when the orientation of the diffuser is 0^o.

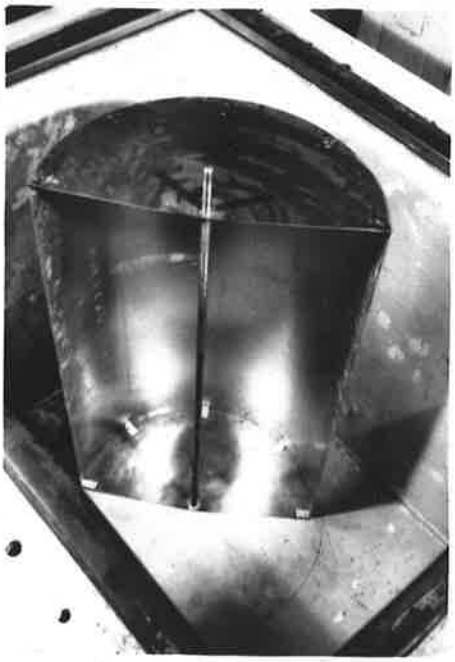

Figure 6.3: Concrete cavity and a semi-cylindrical diffuser.

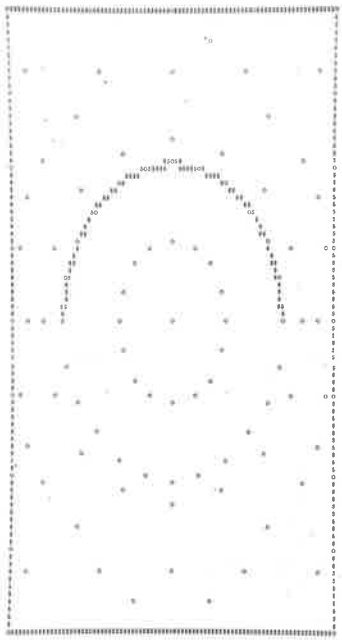

Figure 6.4: Vertices (O) and boundary ($) in the final triangulation points for the FEM calculation ($\theta = 0°$).

The acoustical response at (L_x,L_y) to a unit constant sound pressure source at the origin is computed by increasing the driving frequency f ($f = \frac{\omega}{2\pi}$) by incremental steps. Twenty four positions of the diffuser (15° increments) are examined. The resonance frequencies are then determined by the peaks in response. Because of the symmetrical property of the cavity and the diffuser, the calculation of the resonance frequencies can be reduced to one quarter of the total positions. The sound pressure distributions at each resonance frequencies and for each orientation of the diffuser can also be obtained. When the cavity is driven by a sound source at resonance, the distribution of the sound field will be dominated by that resonance mode, though the source may slightly disturb the nearby sound field.

6.5 Numerical and experimental results

Figures 6.5 (c),(a) and (b) show respectively the calculated response of the sound field when the diffuser is at 0 degree (see Figure 6.1), and the measured power spectral densities of the sound field in the cavity with and without the influence of the diffuser. Comparing Figure 6.5 (c) with Figure 6.5 (b) shows that the latter has more resonance peaks than the former. The extra peaks are due to the contributions of the modes in the Z direction or the combination of the plane modes and the vertical modes. For those modes which have zero index in the Z direction, the shift of the peaks from the PSD in the cavity without a diffuser can be directly compared with the calculated peaks (Figure 6.5 (c)).

The number of the resonance peaks of the sound field for each position of the diffuser remains the same as that without a diffuser in the cavity. This result indicates that the fixed diffuser does not increase the mode number of the sound field, it only alters the resonance distribution and mode shapes. The contribution of the diffuser to the diffusion of a sound field comes from its periodically altering the resonance frequencies and spacial distributions of the cavity modes. This alteration leads to a more uniform sound field during steady state measurement and to more participation of different decays corresponding to each diffuser position during a decay measurement.

As the diffuser orientation is incrementally varied, the resonance peaks both in the calculated sound field response and in the measured PSD incrementally change. Therefore the resonance frequencies of each mode can be obtained for each incremental orientation of the diffuser. The calculated and measured relationships between the resonance frequencies of several cavity modes and the diffuser orientations are shown in Figure 6.6.

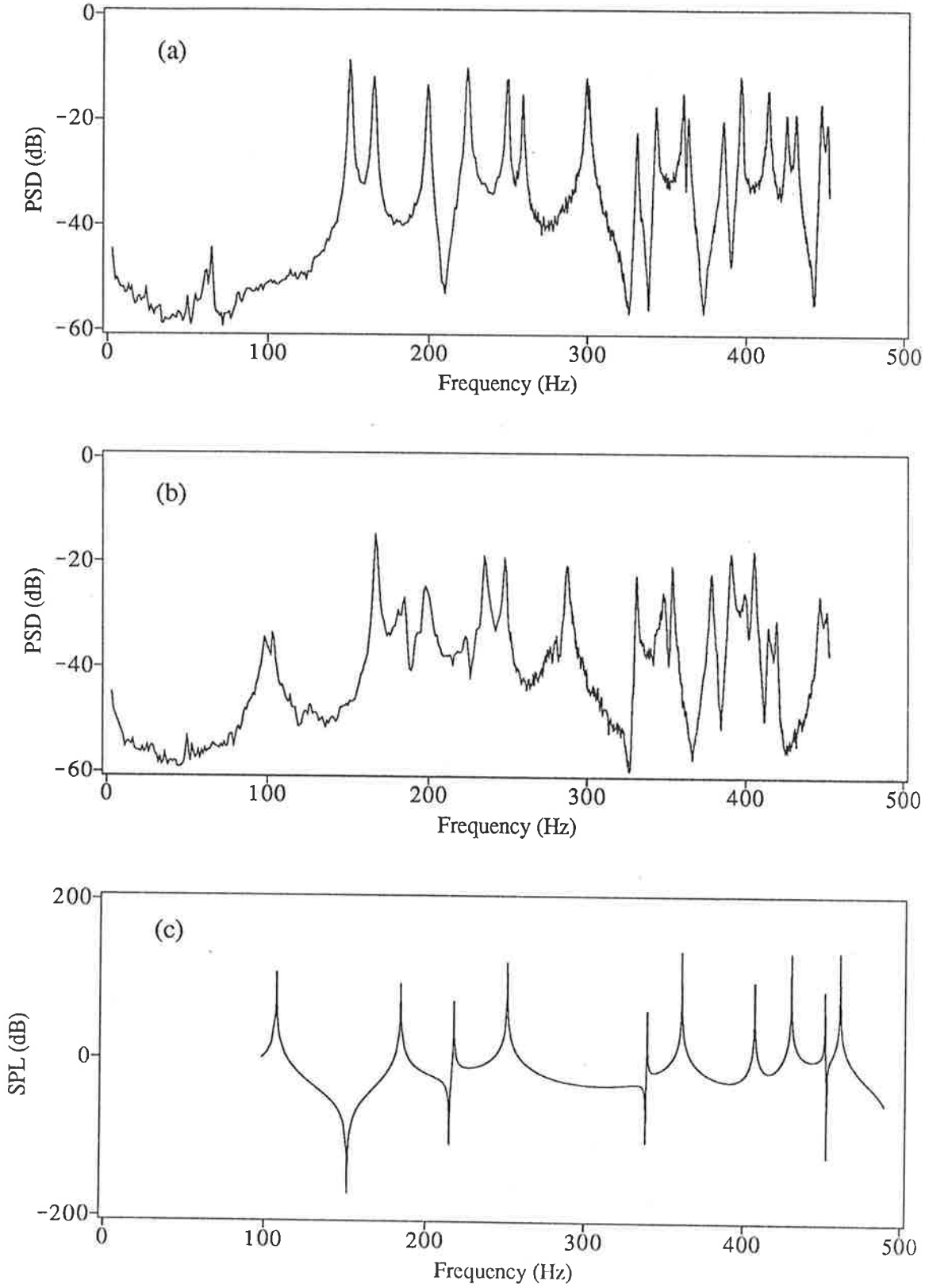

Figure 6.5: Measured PSD of the sound field in the cavity: (a) without diffuser, (b) with diffuser, $\theta = 0^o$; (c) calculated sound pressure level in the cavity with diffuser, $\theta = 0^o$. Sound field is measured and calculated at (0.868,1.150,0.000) m .

As shown in Figure 6.6, the resonance frequencies of the $(0,0,1)$ and $(0,0,2)$ modes are not affected by the diffuser, because $(0,0,n)$ modes are standing waves reflecting from floor to ceiling and parallel to the sidewall of the diffuser. However, the resonance frequencies of all other modes are affected by the diffuser. Therefore these other modes will be masked from time to time by the frequency-invariant $(0,0,n)$ modes as the diffuser orientation is varied and this is the reason that some experimental points are missing.

A standing wave, or sound mode, in a rectangular cavity (two dimensional) without the diffuser can be divided into four traveling waves and can be described respectively by the wavenumber vectors $\pm(\frac{\pi l}{L_x}\vec{i} + \frac{\pi m}{L_y}\vec{j})$, and $\pm(-\frac{\pi l}{L_x}\vec{i} + \frac{\pi m}{L_y}\vec{j})$, where $\vec{i}$ and $\vec{j}$ are unit vectors in X and Y directions respectively. Once the diffuser is put in the cavity, these traveling waves will be scattered. Morse and Feshbach (1953) calculated the distortion of standing waves in a rectangular cavity by a strip using a Green's function method. Although their result is only for a small strip far away from the walls, a physical similarity still exists in the influence of the strip and the diffuser upon the resonance frequencies. If a strip is parallel to the X-Z surface, as its width is increased, the resonance frequencies of the Y axis modes will gradually become lower than the corresponding undisturbed modes.

Similarly in Figure 6.6, the resonance frequencies for the modes (0,1,0), (0,1,1) and (0,1,2), are affected by the diffuser in the same way. In the (X-Y) plane, each standing wave can be considered as two waves traveling along the Y direction. As seen by reference to Figure 6.1 when the diffuser is at 0^o or at 180^o, a maximum section in the passage of the traveling waves is blocked. In this case the wave fronts take the longest time to reach the opposite walls, in other words, the passage of the traveling wave becomes the longest among all diffuser positions. This results in the minimum resonance frequencies. However, when the diffuser is turned to 90^o or 270^o, a minimum section of the passage is blocked by the diffuser. The diffuser has the smallest effect on the reflection time of the traveling waves. In the latter case the corresponding resonance frequencies are closest to the unperturbed frequencies. The same explanation can be given for the observed effect of the diffuser upon the (1,0,0), (1,0,1) and (1,0,2) modes. Large variation in the amplitude of each resonant mode was observed. This suggests a large change in the sound field distribution of each mode for different diffuser positions. Calculated sound field distributions of a few cavity modes are shown in Figure 6.7.

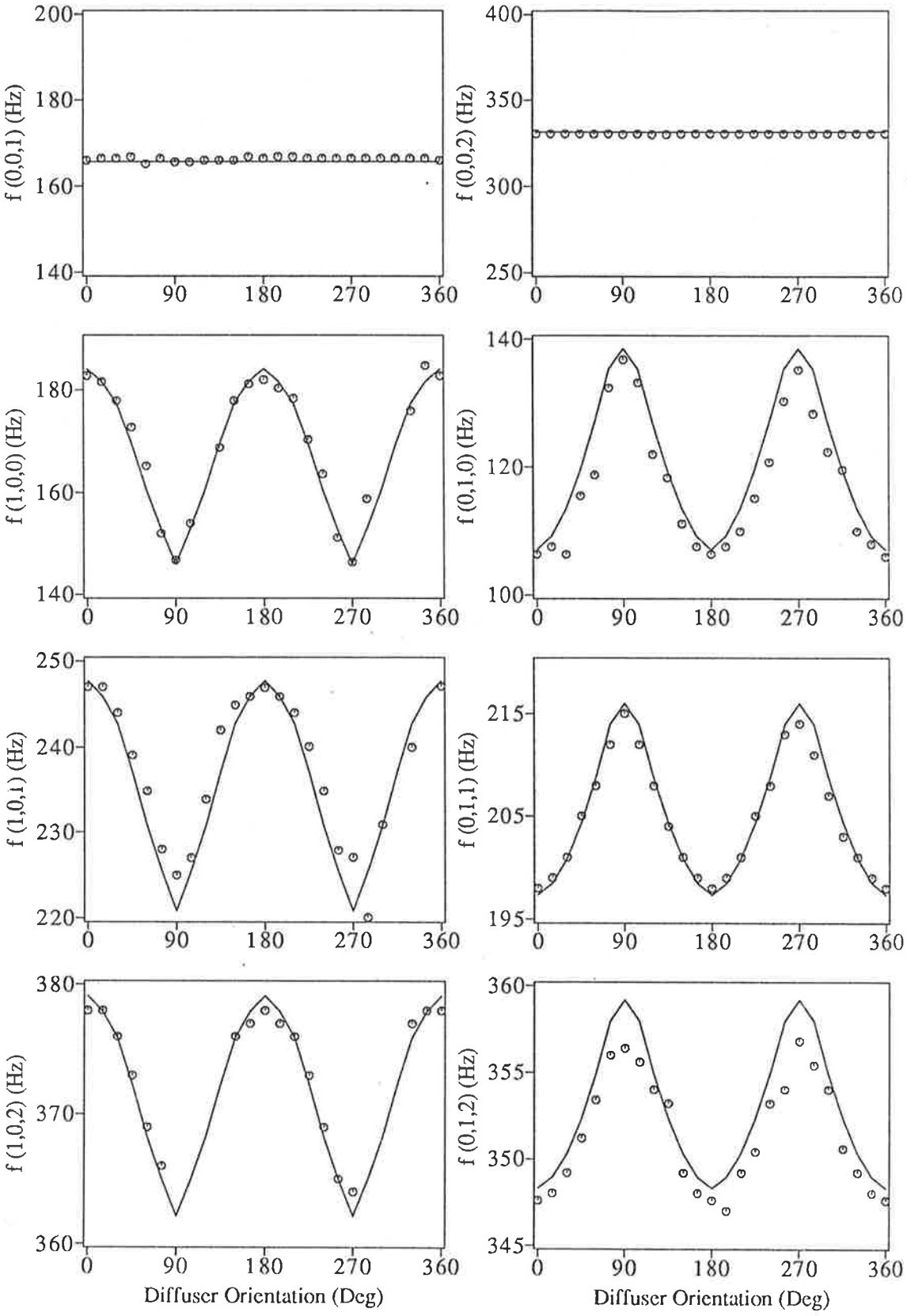

Figure 6.6: Calculated (——) and measured (o o o) resonance frequencies of the cavity modes as a function of the diffuser orientation.

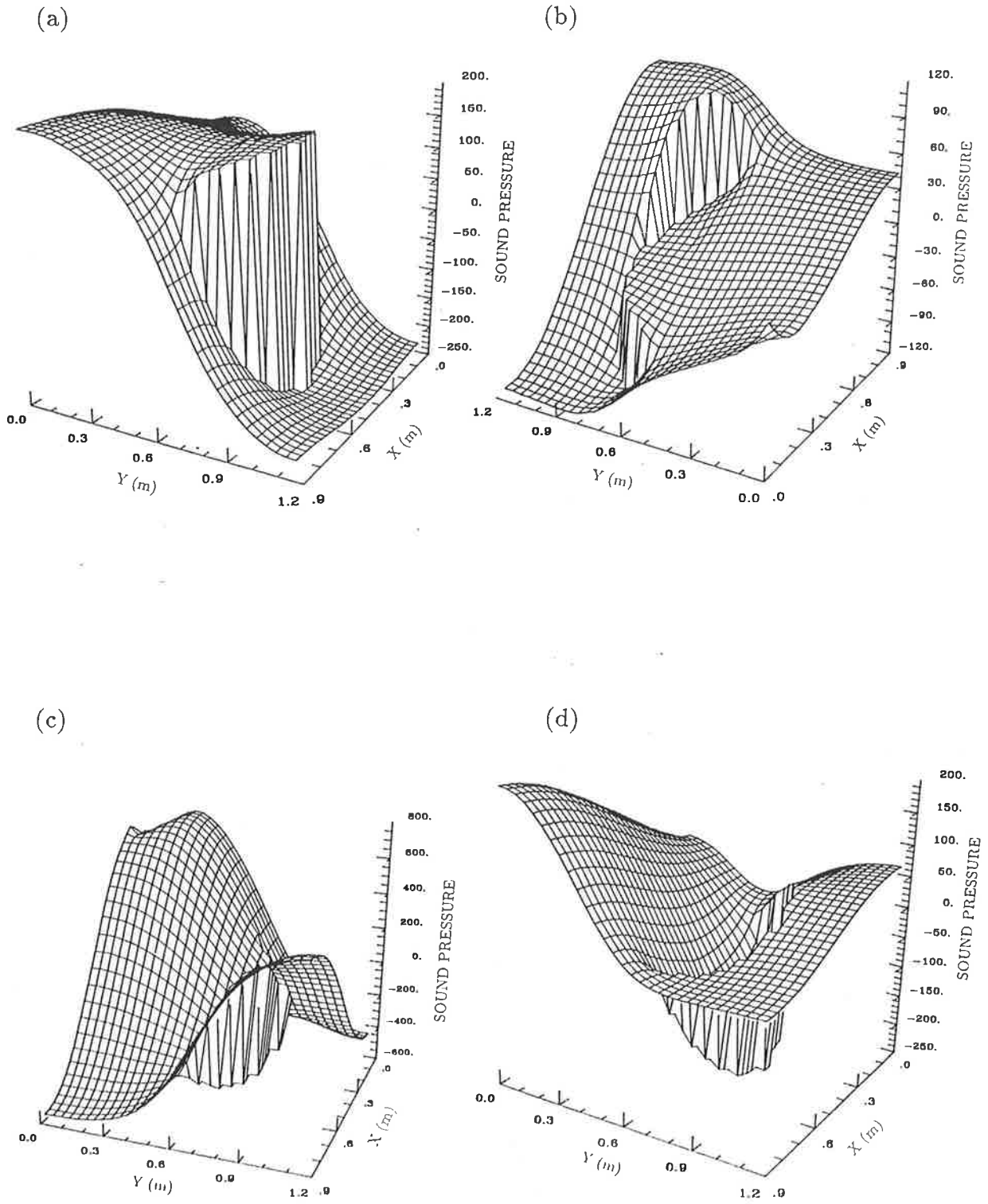

Figure 6.7: Two dimensional sound field distributions ($\theta = 0^o$).
(a) f = 107.1 Hz; (b) f =184.1 Hz; (c) f = 217.2 Hz; (c) f =251.1 Hz.

6.6 Discussion and conclusions

The work presented in this Chapter demonstrates that the presence of a semi-circular diffuser alters the resonance frequencies and the modal distributions of the sound field in a cavity. The resonance frequencies of the cavity modes were predicted by FEM as a function of diffuser orientation. An experiment in a three dimensional cavity with a semi-cylindrical diffuser was conducted to verify the numerical results. In practise, although the shapes of reverberation rooms and diffusers may vary, the basic effect of the diffuser on the sound field remains the same.

Although the boundaries of the cavity were assumed to be rigid in the calculation, it is expected that if the boundaries are modally reactive, the coupling between the altered cavity modes and the boundaries also depends upon the diffuser's properties. From the basic principles of the modal analysis (discussed in Chapters 3 and 4), the sound absorption of the boundaries will be determined by the altered resonance frequencies, the mode shapes and the boundary modal characteristics.

Figure 6.8 shows some modal decay times as a function of the diffuser orientation in a reverberation room (the diffuser and the reverberation room have been described in Chapter 2). The two curves for each room mode are obtained by placing panels in and withdrawing panels from the room to determine T'_{m60} and T_{m60} respectively. The panel absorbers have been described in Chapter 5. The difference of the damping factors of each room mode, k_{a1} and k_{a2}, with and without the panels respectively varies with diffuser positions. This difference is calculated by

$$(k_{a1} - k_{a2}) = 6.91(\frac{1}{T'_{m60}} - \frac{1}{T_{m60}}), \tag{6.4}$$

and is representative of the panel sound absorption property. Therefore this result shows that the variable diffuser orientation and associated variable coupling between the sound field in the room and the panels on the floor results in different sound absorptions of the panel absorbers.

If the diffuser is rotating, the motion of the diffuser should also be taken into consideration. At any particular diffuser position, there is a unique pattern of steady state acoustical modes. In this case the original modes decay and new modes become established. Therefore, if measurements are made with the diffuser in continuous motion, a measurement made at any instant will contain information from a mixture of decaying and growing acoustical modes.

From the characteristics of each individual cavity mode with a diffuser in a cavity, further numerical investigations into the coupling between the diffuser altered cavity modes and the boundaries, and the influence of diffuser motion upon the sound wave behavior may be carried out. These further investigations may present a quantitative comparison for the experimental results shown in Figure 6.8.

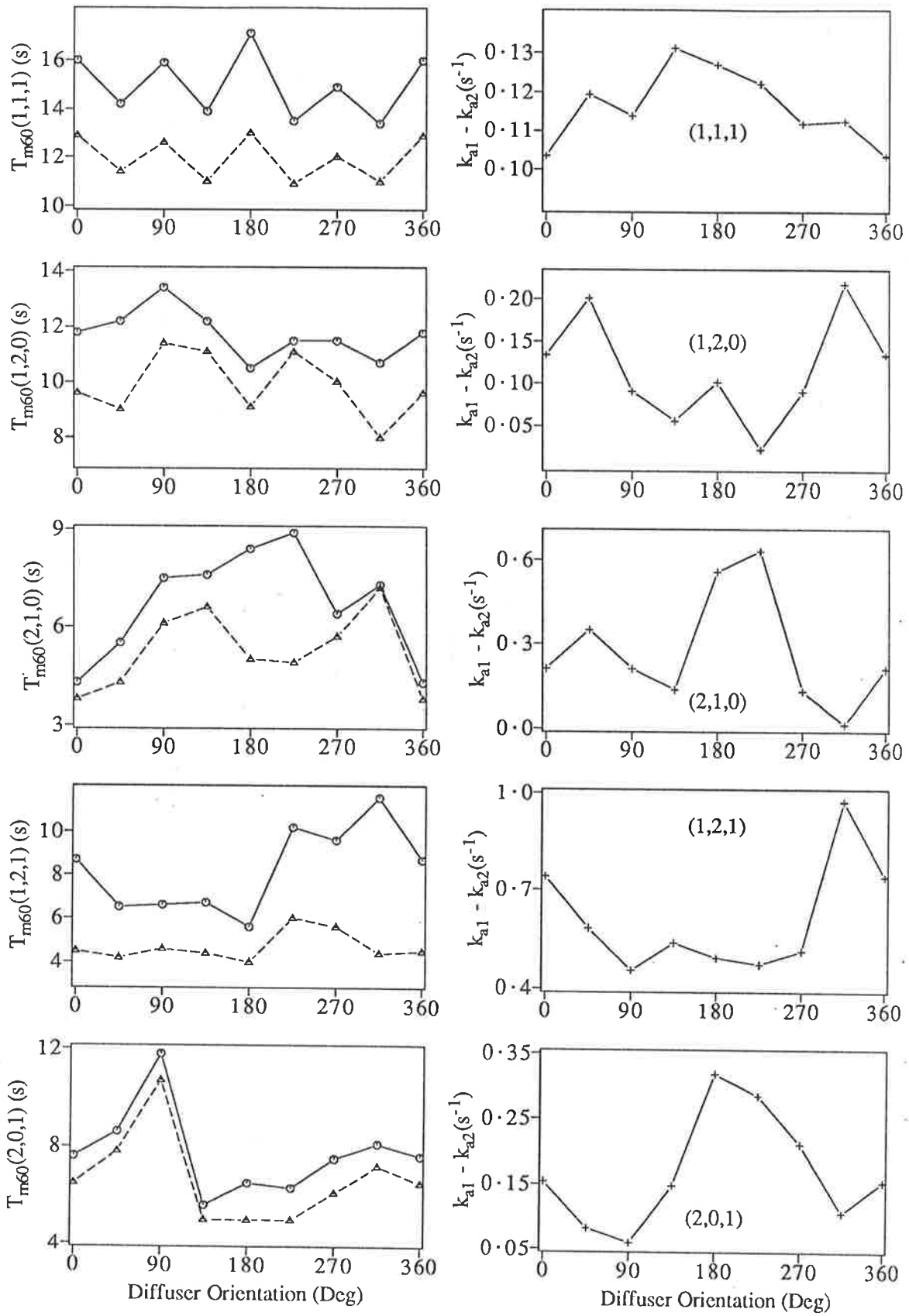

Figure 6.8: Measured 60 dB modal decay times as a function of diffuser orientation in a reverberation room with (- - -,T'_{m60}) panels and without (——,T_{m60}) panels. The plots on the right hand side indicate the difference in damping factors between these two cases (i.e. $k_{a1} - k_{a2} = 6.91(1/T'_{m60} - 1/T_{m60})$).

Appendix A

Mathematical derivations

A.1 Sound field part

In a room R, the free vibration of a sound field is described by the following equation in terms of the acoustical velocity potential Ψ

$$\nabla^2\Psi - \frac{1}{C_o^2}\frac{\partial^2\Psi}{\partial t^2} = 0. \tag{A.1}$$

The boundary conditions at the room internal surface A can be written as follows:

1. on locally reactive surface A_l:

$$\frac{\partial\Psi}{\partial n} = -\frac{\rho_o}{Z_A}\frac{\partial\Psi}{\partial t}, \tag{A.2}$$

   $\vec{n}$ is positive outwards.

2. on the panel internal surface A_f:

$$\frac{\partial\Psi}{\partial n} = \frac{\partial W}{\partial t}. \tag{A.3}$$

A.2 Green's function of the sound field

In a rigid wall room R_o, which has the same internal dimensions as R, the Nth eigenfunction Φ_N for the sound field in R_o satisfies following Equation:

$$\nabla^2\Phi_N + (\frac{\omega_{aN}}{C_o})^2\Phi_N = 0. \tag{A.4}$$

A point source at $\vec{r}_o$ ($\vec{r}_o$ is either in the cavity or at the boundaries of R_o) with angular frequency ω generates the field (Green's function) at the observation point $\vec{r}$ described by the following equation:

$$\nabla^2 G_A(\vec{r},\vec{r}_o;\omega) + k^2 G_A(\vec{r},\vec{r}_o;\omega) = \delta(\vec{r}-\vec{r}_o), \tag{A.5}$$

The equation can be solved by expressing G_A in terms of Φ_N (N=1,2,....). The Green's function obtained is as follows:

$$G_A(\vec{r},\vec{r}_o;\omega) = \sum_N \frac{C_o^2}{\Lambda_N} \frac{\Phi_N(\vec{r})\Phi_N(\vec{r}_o)}{(\omega^2-\omega_{aN}^2)}, \tag{A.6}$$

$$\Lambda_N = \int_V \Phi_N(\vec{r})\Phi_N(\vec{r})dv. \tag{A.7}$$

The Green's function G_A satisfies the boundary condition of R_o.

Multiplying both sides of the Eq.(A.1) by G_A, both sides of the Eq.(A.5) by Ψ, and subtracting the resulting equations, we obtain the following equation:

$$\Psi\delta(\vec{r}-\vec{r}_o) = \Psi\nabla^2 G_A - G_A\nabla^2\Psi. \tag{A.8}$$

Integrating Eq. (A.8) in R, and using Gauss's theorem to change the volume integral into a surface integral, the acoustical velocity potential $\Psi(\vec{r})$ can be written as:

$$\Psi(\vec{r}) = \int_A (\Psi\frac{\partial G_A}{\partial n} - G_A\frac{\partial\Psi}{\partial n})ds_o. \tag{A.9}$$

Applying the boundary conditions to this equation, we have

$$\begin{aligned}\Psi &= -\int_A G_A\frac{\partial\Psi}{\partial n}ds_o \\ &= -\int_{A_f}\frac{\partial W}{\partial t}G_A ds_o + i\frac{\omega}{C_o}\int_{A_l}\beta\Psi G_A ds_o,\end{aligned} \tag{A.10}$$

where $\beta = \frac{\rho_o C_o}{Z_A}$.

A.3 Eigenvalues and eigenfunctions of the cavity controlled modes

1. Multiplying both sides of the Eq.(A.4) by Ψ and of the Eq.(A.1) by Φ_N, subtracting the resulting equations and integrating the final equation in R and then using Gauss's theorem to substitute the boundary conditions, we obtain:

$$(\frac{\omega}{C_o})^2 = (\frac{\omega_{aN}}{C_o})^2 - \frac{\int_{A_f}\Phi_N\frac{\partial W}{\partial t}ds_o}{\int_V\Psi\Phi_N dv} + i\frac{\omega}{C_o}\frac{\int_{A_l}\beta\Psi\Phi_N ds_o}{\int_V\Psi\Phi_N dv}. \tag{A.11}$$

If Ψ is replaced by the Nth eigenfunction for R in Eq.(A.11), the equation gives the Nth eigenvalue squared.

2. Eq. (A.10) can be rewritten in another form by separating the Nth cavity mode from the rest of the modes:

$$\Psi = \left[i\frac{\omega}{C_o}\int_{A_l} \beta C_o^2 \frac{\Psi\Phi_N}{\Lambda_N(\omega^2-\omega_{aN}^2)}ds_o - \int_{A_f}\frac{\partial W}{\partial t}\frac{C_o^2\Phi_N}{\Lambda_N(\omega^2-\omega_{aN}^2)}ds_o\right]\Phi_N - \int_{A_f}\frac{\partial W}{\partial t}G'_A ds_o + i\frac{\omega}{C_o}\int_{A_l}\beta\Psi G'_A ds_o, \quad (A.12)$$

where $G'_A = \sum_{N'\neq N}\frac{C_o^2}{\Lambda_{N'}}\frac{\Phi_{N'}(\vec{r})\Phi_{N'}(\vec{r}_o)}{(\omega^2-\omega_{aN'}^2)}$. Normalizing the coefficient of the Φ_N, the Nth eigenvalue equation can be obtained as follows:

$$(\frac{\omega}{C_o})^2 = (\frac{\omega_{aN}}{C_o})^2 - \frac{\int_{A_f}\Phi_N\frac{\partial W}{\partial t}ds_o}{\int_V \Phi_N\Phi_N dv} + i\frac{\omega}{C_o}\frac{\int_A \beta\Psi\Phi_N ds_o}{\int_V\Phi_N\Phi_N dv}, \quad (A.13)$$

Therefore the sound field distribution of the Nth acoustical mode is

$$\Psi_N = \Phi_N - \int_{A_f}\frac{\partial W}{\partial t}G'_A ds_o + i\frac{\omega}{C_o}\int_{A_l}\beta\Psi G'_A ds_o \quad (A.14)$$

A.4 Panel vibration part

The displacement of the flexural waves in the panel is described by

$$\rho h\frac{\partial^2 W}{\partial t^2} + \frac{Eh^3}{12(1-\mu^2)}\nabla^4 W = \rho_o(\frac{\partial\Psi_E}{\partial t} - \frac{\partial\Psi}{\partial t}). \quad (A.15)$$

The Mth panel normal mode function S_M, which satisfies the simply supported boundary condition, is expressed by the following equation:

$$\frac{Eh^2}{12\rho(1-\mu^2)}\nabla^4 S_M - \omega_{pM}^2 S_M = 0, \quad (A.16)$$

where ω_{pM} is the corresponding eigenvalue.

For a point force on the panel surface at $\vec{x}_o$, the induced disturbance (Green's function of the panel) at $\vec{x}$ on the panel is described by:

$$\frac{Eh^2}{12\rho(1-\mu^2)}\nabla^4 G_P - \omega^2 G_P = \delta(\vec{x}-\vec{x}_o), \quad (A.17)$$

The solution of this equation for the simply supported boundary condition of the panel can be represented by the panel modes S_M (M=1,2,.....).

$$G_P(\vec{x},\vec{x}_o;\omega) = -\sum_M \frac{S_M(\vec{x})S_M(\vec{x}_o)}{\Lambda_M(\omega^2-\omega_{pM}^2)}, \quad (A.18)$$

$$\Lambda_M = \int_{A_f} S_M(\vec{x}) S_M(\vec{x}) ds. \tag{A.19}$$

In a way similar to the method used for the sound field calculation, we multiply the two sides of Eq.(A.17) by W and multiply the two sides of the Eq. (A.15) by G_P. The resulting equations are subtracted. Integrating the final equation on the panel surface, we have

$$W = -i\frac{\rho_o \omega}{\rho h} \int_{A_f} G_P(\vec{x}, \vec{x}_o; \omega)(\Psi - \Psi_E) ds_o + \frac{Eh^2}{12\rho(1-\mu^2)} \int_{A_f} (W\nabla^4 G_P - G_P \nabla^4 W) ds_o, \tag{A.20}$$

The second term on the right side of Eq.(A.20) vanishes, so

$$W = -i\frac{\rho_o \omega}{\rho h} \int_{A_f} G_P(\vec{x}, \vec{x}_o; \omega)(\Psi - \Psi_E) ds_o. \tag{A.21}$$

A.5 Eigenvalues and eigenfunctions of panel controlled modes

1. Multiplying both side of Eq. (A.16) with W and both side of Eq. (A.15) with S_M respectively, subtracting the resulting equations and integrating the final equation over A_f, the following solution is obtained:

$$\omega^2 = \omega_{pM}^2 + \frac{\rho_o}{\rho h} \frac{i\omega}{\int_{A_f} S_M W ds} \int_{A_f} S_M(\Psi - \Psi_E) ds. \tag{A.22}$$

   If W is replaced with the panel displacement part of the Mth eigenfunction, the equation provides the eigenvalue of the Mth acoustical mode.

2. Separating the Mth term in Eq.(A.21) from the rest and choosing a normalized coefficient for S_M, the panel vibration part of the eigenfunction for the Mth panel controlled mode and the corresponding eigenvalue can be written as

$$W_M = S_M - i\frac{\rho_o \omega}{\rho h} \int_{A_f} G'_P(\vec{x}, \vec{x}_o; \omega)(\Psi - \Psi_E) ds_o, \tag{A.23}$$

$$\omega^2 = \omega_{pM}^2 + \frac{\rho_o}{\rho h} \frac{i\omega}{\Lambda_M} \int_{A_f} S_M(\Psi - \Psi_E) ds, \tag{A.24}$$

   where $G'_P = -\sum_{M' \neq M} \frac{S_{M'}(\vec{x}) S_{M'}(\vec{x}_o)}{\Lambda_{M'}(\omega^2 - \omega_{pM'}^2)}$.

A.6 Approximate eigenvalue solutions

A.6.1 Eigenvalues for cavity controlled modes

From Eqs. (A.11)and (A.21) the squared eigenvalue for the Nth cavity controlled mode can be written as:

$$\xi_N^2 = k_{aN}^2 + i\frac{\int_{A_l}\beta\Psi\Phi_N ds}{\int_V \Psi\Phi_N dv}\xi_N + \frac{\rho_o C_o^2}{\rho h}\frac{\int_{A_f}\int_{A_f}[\Psi_E - \Psi]G_P\Phi_N ds_o ds}{\int_V \Psi\Phi_N dv}\xi_N^2 \tag{A.25}$$

By introducing the damping of the cavity and panel modes (see Chapter 3), the second term can be approximated by $2i\zeta_{aN}\xi_N$, and the effect of the damping on the system can be taken into account by replacing k_{aN}^2 in the sound field Green's function G_A by $(k_{aN}^2+2i\zeta_{aN}\xi_N)$ and k_{pM}^2 in the panel vibration Green's function G_P by $(k_{pM}^2 + 2i\zeta_{pM}\xi_N)$.

The third term on the right hand side of the Eq. (A.25) is the contribution of the panel internal damping and the panel radiation. By using Eq. (3.5) for Ψ_E and Eq. (A.14) for Ψ, the third term Δ_N can be written as

$$\Delta_N = \frac{C_o^2}{M_N^a}\sum_M \frac{B_{N,M}\int_{A_f}[\Psi - \Psi_E]S_M ds}{M_M^p[\xi_N^2 - (k_{pM}^2 + 2i\zeta_{pM}\xi_N)]}\xi_N^2, \tag{A.26}$$

where

$$\begin{aligned}\Psi - \Psi_E &= \Phi_N + i\xi_N\int_{A_l}\beta\Psi G_A' ds_o \\ &\quad - \int_{A_f}\frac{\partial W}{\partial t}[G_A' - \frac{1}{2\pi}\frac{\exp(-ikr)}{r}]ds_o,\end{aligned} \tag{A.27}$$

$M_N^a = \Lambda_N$ and $M_M^p = \dfrac{\rho h C_o^2}{\rho_o}\Lambda_M$.

To calculate the approximate panel displacement, the panel radiation influence is neglected. The panel displacement due to the sound field described by $(\Psi_N = \Phi_N)$ is

$$W \approx i\xi_N C_o \sum_M \frac{B_{N,M}S_M}{M_M^p[\xi_N^2 - (k_{pM}^2 + 2i\zeta_{pM}\xi_N)]}. \tag{A.28}$$

Substituting this expression into Eqs.(A.27) and (A.26), we obtain:

$$\begin{aligned}\Delta_N &\approx \frac{1}{M_N^a}U_{N,N}\xi_N^2 \\ &+ \frac{C_o^4}{M_N^a}\sum_M\sum_{M'}\frac{B_{N,M}B_{N,M'}\int_{A_f}\int_{A_f}S_{M'}[G_A' - \frac{1}{2\pi}\frac{\exp(-ikr)}{r}]S_M ds ds_o}{M_M^p M_{M'}^p[\xi_N^2 - (k_{pM}^2 + 2i\zeta_{pM}\xi_N)][\xi_N^2 - (k_{pM'}^2 + 2i\zeta_{pM'}\xi_N)]}\xi_N^4\end{aligned} \tag{A.29}$$

Neglecting cross panel mode coupling terms (i.e. those terms with $M' \neq M$), we then have Δ_N as a combination of a panel internal damping part Δ_N^{Pd} and a panel radiation part Δ_N^{Pr}

$$\Delta_N \approx \Delta_N^{Pd} + \Delta_N^{Pr}, \tag{A.30}$$

$$\Delta_N^{Pd} = \frac{1}{M_N^a} U_{N,N} \xi_N^2 + \sum_{N' \neq N} \frac{U_{N',N} U_{N,N'}}{M_N^a M_{N'}^a [\xi_N^2 - (k_{aN'}^2 + 2i\zeta_{aN'}\xi_N)]} \xi_N^4, \tag{A.31}$$

$$\Delta_N^{Pr} = -\frac{iA_f C_o^4}{4M_N^a} (\frac{\rho_o}{\rho h})^2 \sum_M \frac{B_{M,N}^2 [\sigma_{Im}(M,N) - i\sigma_{Re}(M,N)]}{(M_M^p)^2 [\xi_N^2 - (k_{pM}^2 + 2i\zeta_{pM}\xi_N)]^2} \xi^3, \tag{A.32}$$

where

$$U_{N,N} = \sum_M \frac{C_o^2 B_{N,M}^2}{M_M^p [\xi_N^2 - (k_{pM}^2 + 2i\zeta_{pM}\xi_N)]}, \tag{A.33}$$

$$U_{N',N} = \sum_M \frac{C_o^2 B_{N',M} B_{N,M}}{M_M^p [\xi_N^2 - (k_{pM}^2 + 2i\zeta_{pM}\xi_N)]}, \tag{A.34}$$

and $\sigma_{Im}(M,N)$ and $\sigma_{Re}(M,N)$ are defined in Eqs. (3.36) and (3.37).

Appendix B

A comparison of two decay terms

To estimate the magnitudes of the two decay terms in Eqs. (5.2) and (5.3), the following conditions are assumed:

1. $n_A \gg n_P$,

2. $\eta_A < \eta_P$.

The amplitudes of the first and second terms in Eqs. (5.2) and (5.3) are represented by A_{m1} and A_{m2} and the exponential terms are represented by E_{xp1} and E_{xp2}.

B.1 Decay of the sound field

1. The difference of the indices of the two exponential terms in Eq. (5.2) is

$$(s1 - s2)t = \omega[(\eta_A + \eta_{AP} - \eta_P - \eta_{PA})^2 + 4\eta_{AP}\eta_{PA}]^{1/2}t \ . \tag{B.1}$$

Due to the following relations:

$$\frac{\eta_{AP}}{\eta_{PA}} = \frac{n_P}{n_A}, \tag{B.2}$$

and above assumptions, we have

$$\eta_{AP} < \eta_{PA} \ , \tag{B.3}$$

and

$$\eta_A < \eta_P \ . \tag{B.4}$$

Therefore

$$(s1 - s2) > 0 \ , \tag{B.5}$$

and the exponential ratio

$$\frac{E_{xp1}}{E_{xp2}} = \exp[(s1 - s2)t] \ , \tag{B.6}$$

increases exponentially with time t.

2. The amplitude ratio of the first term to the second term in Eq. (5.2) is

$$\begin{aligned} \frac{A_{m1}}{A_{m2}} &= \frac{s1 + d1}{-(s2 + d1)} \\ &\geq \frac{n_A}{n_P} \frac{(\eta_P + \eta_{PA} - \eta_A - \eta_{AP})^2(\eta_P + \eta_{PA})}{\eta_{PA}^2(\eta_A + \eta_{AP})} \\ &\sim O(\frac{n_A}{n_P}) \ . \end{aligned} \tag{B.7}$$

The expression $O(\frac{n_A}{n_P})$ means to the order of $(\frac{n_A}{n_P})$. Eqs. (B.6) and (B.7) indicate that for the sound field decay, the first term in Eq. (5.2) dominates.

B.2 Decay of the panel vibration

1. The ratio of the first to the second exponential terms in Eq. (5.3) is the same as given by Eq. (B.6).

2. The amplitude ratio of the first term to the second term in Eq. (5.3) is

$$\begin{aligned} \frac{A_{m1}}{A_{m2}} &= \frac{s1 + d2}{-(s2 + d2)} \\ &\leq \frac{n_P}{n_A} \frac{\eta_{PA}^2(\eta_P + \eta_{PA})}{(\eta_P + \eta_{PA} - \eta_A - \eta_{AP})^2(\eta_A + \eta_{AP})} \\ &\sim O(\frac{n_P}{n_A}) \ . \end{aligned} \tag{B.8}$$

Eqs. (B.6) and (B.8) indicate that in the beginning the second term dominates because of the greater amplitude and the exponential term contribution is small but as time increases the exponential ratio of the first term to the second term increases exponentially and so the first term takes the dominate role in the decay.

Bibliography

[1] Anderson, G.L. (1973) "Application of a variational method to dissipative, non-conservative problems of elastic stability",
J. Sound Vib. **27**, 279-296 .

[2] AS (1971) "Methods of measurement of absorption",
Australian Standard 1045 .

[3] Benedetto, G., Brosto, E. and Spagnolo, R. (1981) "The effect of stationary diffusers in the measurement of sound absorption coefficients in a reverberation room: an experimental study",
Applied Acoustics **14**, 49-63 .

[4] Beranek, L.L., Johnson, F.R.,Schultz, T.J. and Watters, B.G. (1964) "Acoustics of Philharmonic Hall, New York, during Its First Season",
J. Acoust. Soc. Am. **36**, 1247-1262 .

[5] Bhatt, N.B. (1939) "Effect of an Absorbing Wall on the Decay of Normal Frequencies",
J. Acoust. Soc. Am. **11**, 67-73 .

[6] Bhattacharya, M.C. and Crocker, M.J. (1969/70) "Forced vibration of a panel and radiation of sound into a room",
Acustica, **22**, 275-294 .

[7] Bhattacharya, M.C. (1970) "The Transmission and Radiation of Acousto-Vibrational Energy",
Ph.D thesis. Department of Building Science, University of Liverpool .

[8] Bies, D.A. and Hansen, C.H. (1979) "Measurements of the radiation impedance presented to a source in a reverberation room containing a rotating diffuser",

J. Acoust. Soc. Am. **65**, 708-718 .

[9] Bliven, B.Jr. (1976) "Annals of Architecture",
New Yorker **8**, 51-135 .

[10] Bodlund, K. (1980) "Monotonic Curvature of Low Frequency Decay Records in Reverberation Chambers",
J. Sound and Vib. **73**(1), 19-29 .

[11] Brooks, J.E. and Maidanik, G. (1977) "Loss and coupling loss factors of two coupled dynamic systems",
J. Sound and Vib. **55**(3), 315-325 .

[12] Craggs, A. (1971) "The transient response of a coupled plate-acoustic system using plate and acoustic finite elements",
J. Sound Vib. **15**, 509-528 .

[13] Craggs, A. (1972) "The use of simple three-dimensional acoustic finite elements for determining the natural modes and frequencies of complex shaped enclosures",
J. Sound Vib. **23**, 331-339 .

[14] Crocker, M.J. and Price, A.J. (1969) "Sound transmission using statistical energy analysis",
J. Sound Vib. **9**, 469-486 .

[15] Dickinson, S.M. and Warburton, G.B. (1967) "Vibration of box-type structures",
J. Mech. Eng. Sc. **9**, 325-335 .

[16] Dowell, E.H. and Voss, H.M.(1963) "The effect of a cavity on panel vibration",
AIAA **1**, 476-477 .

[17] Dowell, E.H., Gorman, G.F. and Smith, D.A.(1977) "Acoustoelasticity : general theory, acoustic natural modes and forced response to sinusoidal excitation, including comparisons with experiment",
J. Sound Vib. **52**, 519-542 .

[18] Embleton T.F.W. (1971) In "Noise and Vibration Control". (ed. L.L. Beranek) Chap. **9**, McGraw-Hill Book Company .

[19] Eyring, C.F.(1930) "Reverberation time in 'dead' rooms",
J. Acoust. Soc. Am. **1**, 217-241 .

[20] Fahy, F.J. (1969) "Vibration of containing structures by sound in the contained fluid",
J. Sound Vib. **10**, 490-512 .

[21] Fahy, F.J., Majid, A. and Howlett, J.H.(1970) "Acoustic coupling between structure and liquids",
Annual Report. I.S.V.R.,University of Southampton. 76 .

[22] Fahy, F.J. (1985) "Sound and Structural Vibration: Radiation, Transmission and Response",
Academic Press Inc., Chap. **2**, 66-67 .

[23] Feshbach, H. (1944) "On the perturbation of boundary conditions",
Physical Review **65**, 307-318 .

[24] Ford, R.D. and McCormick, M.A.(1969) "Panel sound absorbers",
J. Sound Vib. **10**, 411-423 .

[25] Fuller, C.R. and Fahy, F.J.(1982) "Characteristics of wave propagation and energy distribution in cylindrical elastic shells filled with fluid",
J. Sound Vib. **81**, 501-518 .

[26] Fuller, C. R.(1986) "Analytical model for investigation of interior noise characteristics in aircraft with multiple propellers including synchrophasing",
J. Sound Vib. **109**, 141-156 .

[27] Gladwell, G.M.L. and Zimmermann, G.(1966) "On energy and complementary energy formulation of acoustic and structural vibration problems",
J. Sound Vib. **3**, 233-241 .

[28] Guy, R.W. and Bhattacharya, M.C. (1973) "The transmission of sound through a cavity backed finite plate",
J. Sound Vib. **27**, 207-223 .

[29] Guy, R.W. (1979a) "The steady state transmission of sound at normal and oblique incidence through a thin panel backed by a rectangular room — a multi-modal analysis",
Acustica, **43**, 295-304 .

[30] Guy, R.W. (1979b) "The response of a cavity backed panel to external airborne excitation: a general analysis",
J. Acoust. Soc. Am. **65**, 719-731 .

[31] Guy, R.W. (1980) "Pressure developed within a cavity backing a finite panel when subjected to external transient excitation",
J. Acoust. Soc. Am. **68**, 1736-1747 .

[32] Hansen, C.H. and Bies, D.A. (1980) "Near field measurement of the complex radiation impedance presented to a vibrating plate in a reverberation room containing a rotating diffuser",
J. Sound and Vib. **73**, 79-101 .

[33] Heckl, M. (1962) "Measurement of absorption coefficients on plates",
J. Acoust. Soc. Am. **34**, 803-808 .

[34] Hodgson, M.(1983) "Measurement of the Influence of Fitting and Roof Pitch on the Sound Field in Panel-Roof Factories",
Appl. Acoust. **16**, 369-391 .

[35] Hunt, F.V. (1939a) "The sound absorption coefficient problem",
J. Acoust. Soc. Am. **11**, 38-40 .

[36] Hunt, F.V., Beranek, L.L. and Maa, D.Y.(1939) "Analysis of Sound Decay in Rectangular Rooms",
J. Acoust. Soc. Am. **11**, 80-94.

[37] Hunt, F.V.(1939b) "Investigation of Room Acoustics by Steady-State Transmission Measurements. I.",
J. Acoust. Soc. Am. **10**, 216-227 .

[38] Jacobsen, F.(1982) "Decay Rates and Wall Absorption at Low Frequencies",
J. Sound and Vib. **81**(3), 405-412 .

[39] Junger, M. C. and Feit, D. (1986) "Sound, Structures and Their Interaction",
MIT, Cambridge, MA, 2nd ed.

[40] Khilman, T.(1967) "Sound radiation into a rectangular room. Applications to airborne sound transmission in buildings",
Acustica, **18**, 11-20 .

[41] Kiesewetter, N. (1986) "Impedance and Resonances of a Plate before and Enclosed Air Volume",
Acustica, **61**, 214-217 .

[42] Knudsen, V.O.(1932) "Resonance in small rooms",
J. Acoust. Soc. Am. **4**, 20-37 .

[43] Knudsen, V.O., Delsasso, L.P. and Leonard, R.W.(1967) "Reverberation-Room —— Effects of Various Boundary Conditions",
J. Acoust. Soc. Am. **42**, 953-965 .

[44] Knudsen, V.O. and Harris, C.M. (1978) "Acoustical Designing in Architecture",
Acoust. Soc. Am. fourth printing, 349 .

[45] Kuhl, W. and Kaiser, H.(1952) "Absorption of structure-borne sound in building materials without and with sand-filled cavities",
Acustica. **2**, 179-188 .

[46] Leppington, F.G., Broadbent, E.G.,Heron, F.R.S., and K.H. (1982) "The acoustic radiation efficiency of rectangular panels",
Proc. R. Soc. Lond. A **382**, 245-271 .

[47] Louisell, W.H. (1960) "Coupled mode and parametric electronics",
(John Wiley and Sons, Inc. New York), 15 .

[48] Lyon, R.H. and Maidanik, G. (1962) "Power flow between linearly coupled oscillators",
J. Acoust. Soc. Am. **34**, 623-639 .

[49] Lyon, R.H. (1963) "Noise Reduction of Rectangular Enclosures with One Flexible Wall",
J. Acoust. Soc. Am. **35**, 1791-1797 .

[50] Lyon, R.H. (1975) "Statistical Energy Analysis of Dynamical System: Theory and Applications",
Cambridge, Massachusetts and London, England: The MIT Press, Chap. **3**, 92 .

[51] Lubman, D. (1971) "Spacial averaging in sound power measurements",
J. Sound Vib. **16**, 43-58 .

[52] Lyamshev, L.M.(1983) "diffusion of sound by a periodically moving plate",
Sov. Phys. Dokl. **28**(3) 274-276 .

[53] Maidanik, G. (1962) "Response of Ribbed Panels to Reverberant Acoustic Fields", J. Acoust. Soc. Am. **34**, 809-926 .

[54] Maidanik, G. (1977) "Some Elements in Statistical Energy Analysis", J. Sound Vib. **52**, 171-191 .

[55] Millington, G. (1932) "A modified formula for reverberation", J. Acoust. Soc. Am. **4**, 69 .

[56] Morris, R.M., Nixon, G.M. and Parkinson, J.S. (1938) "Variations in absorption coefficients as obtained by the reverberation chamber method", J. Acoust. Soc. Am. **9**, 234-243 .

[57] Morse, P.M. (1939) "Some Aspects of the Theory of Room Acoustics", J. Acoust. Soc. Am. **11**, 56-66 .

[58] Morse, P.M. and Bolt, R.H.(1944) "Sound Waves in Rooms", Rev. Modern Physics. **16**, 69-105 .

[59] Morse, P.M.(1948a) "Vibration and Sound", (McGraw-Hill Inc.: New York.) 2nd ed., Chap.**8**, 388 .

[60] Morse, P.M.(1948b) Ibid, Chap. **8**, 403 .

[61] Morse, P.M.(1948c) Ibid, Chap. **8**, 394 .

[62] Morse, P.M. and Feshbach, H. (1953) "Methods of Theoretical Physics", McGraw-Hill Book Company 1435-1440 .

[63] Morse, P.M. and Ingard, K.U. (1968a) "Theoretical Acoustics", (McGraw-Hill Book Co., New York,) Chap. **6**, 259-270 .

[64] Morse, P.M. and Ingard, K.U. (1968b) Ibid Chap. **3**, 67 .

[65] Morse, P.M. and Ingard, K.U. (1968c) Ibid Chap. **3**, 65 .

[66] Munro, T.J. (1982) "Alternative Models of the Sound Field in a Reverberation Room". M. Eng. Thesis. Department of Mechanical Engineering, University of Adelaide, Adelaide, South Australia.

[67] Naryannan, S. and Shanbhag, R. L.(1981a) "Sound Transmission through Elastically Supported Sandwich Panels into a Rectangular Enclosure",
J. Sound and Vib. **77**(2), 251-270 .

[68] Naryannan, S. and Shanbhag, R. L.(1981b) "Acoustoelasticity of a Damped Sandwich Panel Backed by a Cavity",
J. Sound and Vib. **78**(4), 453-473 .

[69] Nefske, D.J., Wolf, JR., J.A. and Howell, L.J.(1982) "Structural-acoustic finite element analysis of the automobile passenger compartment",
J. Sound Vib. **80**, 247-266 .

[70] Norris, R.F. (1932) "A deviation of the reverberation formula",
Appendix II in Architectural Acoustics by V. O. Knudsen (John Wiley and Sons, Inc., New York).

[71] Ochs, J. and Snowdon, J. (1975) "Transmissibility across simply supported thin plates, 1. Rectangular and square plates with and without damping layers",
J. Acoust. Soc. Am. **58**, 832-840 .

[72] Pan, J. and Bies, D.A. (1988) "An experimental investigation into the interaction between a sound field and its boundaries",
J. Acoust. Soc. Am. **83**, 1436-1444 .

[73] Parkin, P.H. and Purkis, H.J. (1951) "Sound absorption of wood panels for the royal festival hall",
Acustica, **1**, 81-82 .

[74] Pope, L.D. and Wilby, J.F. (1977) "Band-limited power flow into enclosures",
J. Acoust. Soc. Am. **62**, 906-911 .

[75] Pope, L.D. Rennison, D.C., Willis, C.M. and Mayes, W.R. (1982) "Development and validation of preliminary analytical models for aircraft interior noise prediction",
J. Sound Vib. **82**, 541-575 .

[76] Pope, L.D. Wilby, E.G., Willis, C.M. and Mayes, W.R. (1983) "Aircraft interior noise models: sidewall trim stiffened structures and cabin acoustics with floor partition",
J. Sound Vib. **89**, 371-417 .

[77] Pretlove, A.J. (1965a) "Free vibrations of a rectangular panel backed by a closed rectangular cavity",
J. Sound Vib. **2**, 197-209 .

[78] Pretlove, A.J. (1965b) "Note on the virtual mass for a panel in an infinite baffle",
J. Acoust. Soc. Am. **38** , 266-270 .

[79] Pretlove, A.J. (1966) "Forced vibrations of a rectangular panel backed by a closed rectangular cavity",
J. Sound Vib. **3**, 252-261 .

[80] Pretlove, A.J. (1969) "Acousto-elastic effect in the response of large windows to sonic bangs",
J. sound Vib. **9**, 487-500 .

[81] Rayleigh, J.W. S. (1896) "Theory of sound",
(MacMillan, London,) 2nd ed., Vol. **2**, 107 .

[82] Rogers, R. (1939) "The absorption of sound by vibrating plates backed with an air space",
J. Acoust. Soc. Am. **10**, 280-287 .

[83] Sabine, P.E. and Ramer, L.G.(1948) "Absorption-frequency characteristics of plywood panels",
J. Acoust. Soc. Am. **20**, 267-262 .

[84] Sabine, W.C. (1922) "Collected Papers on Acoustics",
(Harvard University Press), 44 .

[85] Sestieri, A., Vescovo, D. D. and Lucibello, P.(1984) "Structural-acoustic couplings in complex shaped cavities",
J. Sound Vib. **96**, 219-233 .

[86] Schultz, T.J. (1971) "Diffusion in Reverberation Rooms",
J. Sound Vib. **16**, 17-28 .

[87] Smith, P.W. Jr. (1962) "Response and radiation of structural modes excited by sound ", J. Acoust. Soc. Am. **34**, 640-647 .

[88] Snowdon, J.C. (1970) "Forced vibration of internally damped circular plates with supported and free boundaries", J. Acoust. Soc. Am. **47**, 882-891 .

[89] Snowdon, J.C. (1974) "Forced vibration of internally damped rectangular and square plates with simply supported boundaries", J. Acoust. Soc. Am. **56**, 1177-1184 .

[90] Sun, J.C., Sun, H.B.,Chow, L.C. and Richards, E.J. (1986a) "Prediction of total loss factors of structures Part II: Loss factors of sand-filled structure", J. Sound Vib. **104**, 243-257 .

[91] Sun, H.B.,Sun, J.C. and Richards, E.J. (1986b) "Prediction of total loss factors of structures Part III: Effective loss factors in quasi-transient condition", J. Sound Vib. **106**, 465-479 .

[92] Sung, S. H. and Nefske, D.J. (1984) "A coupled structural-acoustic finite element model for vehicle interior noise analysis", Tran. ASME. (J.Vib.Acoust.,Stress,and Rel in Design) **106**, 314-318 .

[93] Swift, P.B. and Bies, D.A. (1978) "Vibrational energy distribution in coupled plates", Conference on Machinery, Vibration and noise, Adelaide, 29-30 May, 53-57 .

[94] Tichy, J. and Baade, P.K.(1975) "Effect of rotating diffuser and sampling techniques on sound-pressure averaging in reverberation rooms", J. Acoust. Soc. Am. **56**, 137-143 .

[95] Vér, I.L. and Curtis, I.H. (1971) In "Noise and Vibration Control". (ed. L.L. Beranek) Chap. **11**, McGraw-Hill Book Company .

[96] Vyalyshev, A.I., Tartakovskii, B.D. and Éfrussi,M.M.(1977) "Coupling of Sound and Vibration Fields in the Compensation of Radiation from a Plate at Subcritical Frequencies", Akust. Zh. **23**, 475-477 . [English transl.: Soc. Phys. Acoust. **23**, 268-269 (1977)].

[97] Wallace, C.E. (1972) "Radiation resistance of a rectangular panel",
J. Acoust. Soc. Am. **51**, 946-952 .

[98] "IMSL Library" (1985) —— FORTRAN subroutines for mathematics and statistics,
IMSL, Inc.

[99] "IMSL TWODEPEP" (1985),
IMSL, Inc.